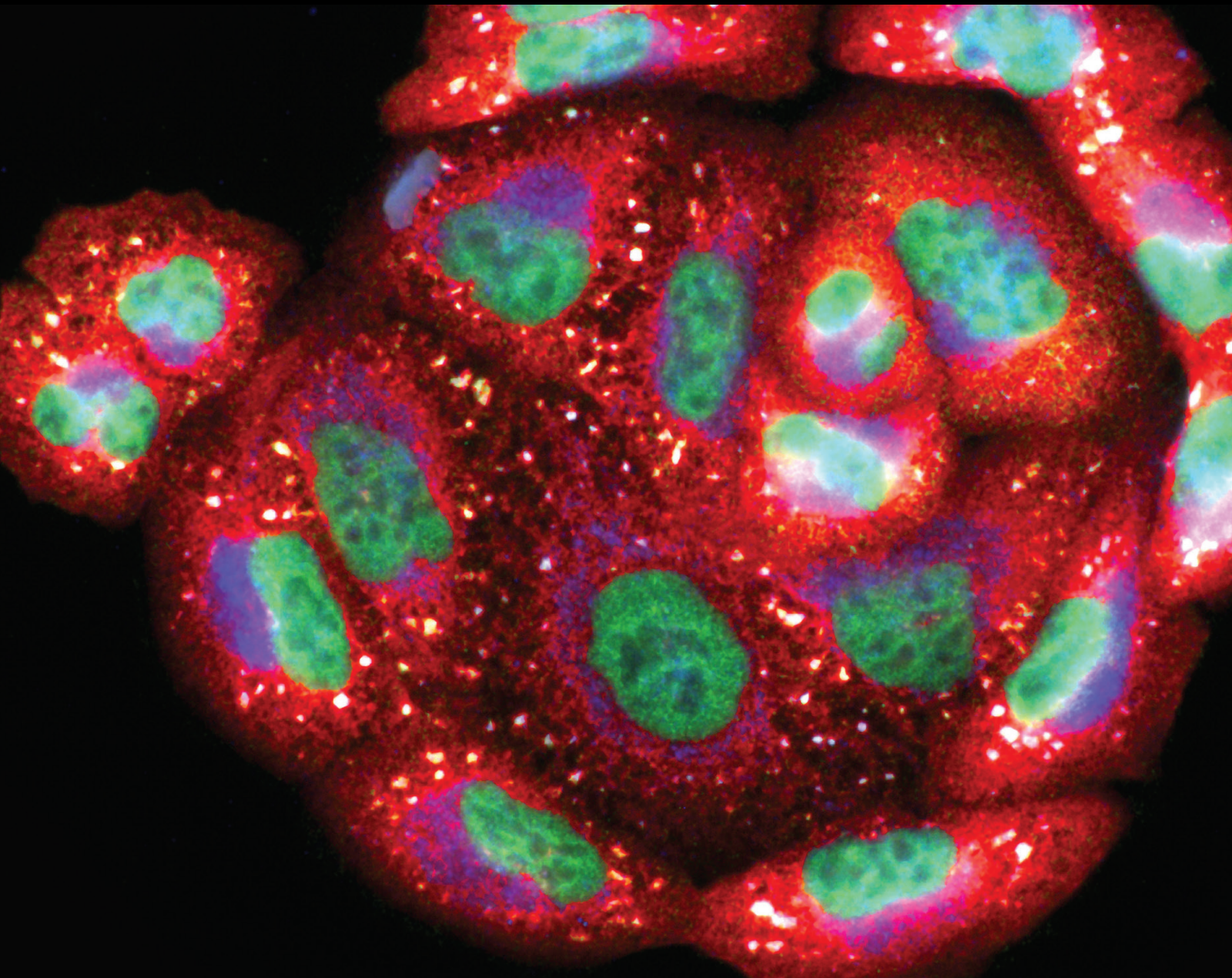


New Therapeutics to Prevent Sepsis-Induced Cardiac Dysfunctions

Lead Guest Editor: Luc Demaison

Guest Editors: Christian Jung and Salvatore Pepe





New Therapeutics to Prevent Sepsis-Induced Cardiac Dysfunctions

Oxidative Medicine and Cellular Longevity

New Therapeutics to Prevent Sepsis- Induced Cardiac Dysfunctions

Lead Guest Editor: Luc Demaison

Guest Editors: Christian Jung and Salvatore Pepe



Copyright © 2021 Hindawi Limited. All rights reserved.

This is a special issue published in "Oxidative Medicine and Cellular Longevity" All articles are open access articles distributed under the Creative Commons Attribution License, which permits unrestricted use, distribution, and reproduction in any medium, provided the original work is properly cited.

Chief Editor

Jeannette Vasquez-Vivar, USA

Associate Editors

Amjad Islam Aqib, Pakistan
Angel Catalá , Argentina
Cinzia Domenicotti , Italy
Janusz Gebicki , Australia
Aldrin V. Gomes , USA
Vladimir Jakovljevic , Serbia
Thomas Kietzmann , Finland
Juan C. Mayo , Spain
Ryuichi Morishita , Japan
Claudia Penna , Italy
Sachchida Nand Rai , India
Paola Rizzo , Italy
Mithun Sinha , USA
Daniele Vergara , Italy
Victor M. Victor , Spain

Academic Editors

Ammar AL-Farga , Saudi Arabia
Mohd Adnan , Saudi Arabia
Ivanov Alexander , Russia
Fabio Altieri , Italy
Daniel Dias Rufino Arcanjo , Brazil
Peter Backx, Canada
Amira Badr , Egypt
Damian Bailey, United Kingdom
Rengasamy Balakrishnan , Republic of Korea
Jiaolin Bao, China
Ji C. Bihl , USA
Hareram Birla, India
Abdelhakim Bouyahya, Morocco
Ralf Braun , Austria
Laura Bravo , Spain
Matt Brody , USA
Amadou Camara , USA
Marcio Carcho , Portugal
Peter Celec , Slovakia
Giselle Cerchiaro , Brazil
Arpita Chatterjee , USA
Shao-Yu Chen , USA
Yujie Chen, China
Deepak Chhangani , USA
Ferdinando Chiaradonna , Italy

Zhao Zhong Chong, USA
Fabio Ciccarone, Italy
Alin Ciobica , Romania
Ana Cipak Gasparovic , Croatia
Giuseppe Cirillo , Italy
Maria R. Ciriolo , Italy
Massimo Collino , Italy
Manuela Corte-Real , Portugal
Manuela Curcio, Italy
Domenico D'Arca , Italy
Francesca Danesi , Italy
Claudio De Lucia , USA
Damião De Sousa , Brazil
Enrico Desideri, Italy
Francesca Diomede , Italy
Raul Dominguez-Perles, Spain
Joël R. Drevet , France
Grégory Durand , France
Alessandra Durazzo , Italy
Javier Egea , Spain
Pablo A. Evelson , Argentina
Mohd Farhan, USA
Ioannis G. Fatouros , Greece
Gianna Ferretti , Italy
Swaran J. S. Flora , India
Maurizio Forte , Italy
Teresa I. Fortoul, Mexico
Anna Fracassi , USA
Rodrigo Franco , USA
Juan Gambini , Spain
Gerardo García-Rivas , Mexico
Husam Ghanim, USA
Jayeeta Ghose , USA
Rajeshwary Ghosh , USA
Lucia Gimeno-Mallench, Spain
Anna M. Giudetti , Italy
Daniela Giustarini , Italy
José Rodrigo Godoy, USA
Saeid Golbidi , Canada
Guohua Gong , China
Tilman Grune, Germany
Solomon Habtemariam , United Kingdom
Eva-Maria Hanschmann , Germany
Md Saquib Hasnain , India
Md Hassan , India

Tim Hofer , Norway
John D. Horowitz, Australia
Silvana Hrelia , Italy
Dragan Hrnčić, Serbia
Zebo Huang , China
Zhao Huang , China
Tariq Hussain , Pakistan
Stephan Immenschuh , Germany
Norsharina Ismail, Malaysia
Franco J. L. , Brazil
Sedat Kacar , USA
Andleeb Khan , Saudi Arabia
Kum Kum Khanna, Australia
Neelam Khaper , Canada
Ramoji Kosuru , USA
Demetrios Kouretas , Greece
Andrey V. Kozlov , Austria
Chan-Yen Kuo, Taiwan
Gaocai Li , China
Guoping Li , USA
Jin-Long Li , China
Qiangqiang Li , China
Xin-Feng Li , China
Jialiang Liang , China
Adam Lightfoot, United Kingdom
Christopher Horst Lillig , Germany
Paloma B. Liton , USA
Ana Lloret , Spain
Lorenzo Loffredo , Italy
Camilo López-Alarcón , Chile
Daniel Lopez-Malo , Spain
Massimo Lucarini , Italy
Hai-Chun Ma, China
Nageswara Madamanchi , USA
Kenneth Maiese , USA
Marco Malaguti , Italy
Steven McAnulty, USA
Antonio Desmond McCarthy , Argentina
Sonia Medina-Escudero , Spain
Pedro Mena , Italy
V́ctor M. Mendoza-Núñez , Mexico
Lidija Milkovic , Croatia
Alexandra Miller, USA
Sara Missaglia , Italy

Premysl Mladenka , Czech Republic
Sandra Moreno , Italy
Trevor A. Mori , Australia
Fabiana Morroni , Italy
Ange Mouithys-Mickalad, Belgium
Iordanis Mourouzis , Greece
Ryoji Nagai , Japan
Amit Kumar Nayak , India
Abderrahim Nemmar , United Arab Emirates
Xing Niu , China
Cristina Nocella, Italy
Susana Novella , Spain
Hassan Obied , Australia
Pál Pacher, USA
Pasquale Pagliaro , Italy
Dilipkumar Pal , India
Valentina Pallottini , Italy
Swapnil Pandey , USA
Mayur Parmar , USA
Vassilis Paschalis , Greece
Keshav Raj Paudel, Australia
Ilaria Peluso , Italy
Tiziana Persichini , Italy
Shazib Pervaiz , Singapore
Abdul Rehman Phull, Republic of Korea
Vincent Pialoux , France
Alessandro Poggi , Italy
Zsolt Radak , Hungary
Dario C. Ramirez , Argentina
Erika Ramos-Tovar , Mexico
Sid D. Ray , USA
Muneeb Rehman , Saudi Arabia
Hamid Reza Rezvani , France
Alessandra Ricelli, Italy
Francisco J. Romero , Spain
Joan Roselló-Catafau, Spain
Subhadeep Roy , India
Josep V. Rubert , The Netherlands
Sumbal Saba , Brazil
Kunihiro Sakuma, Japan
Gabriele Saretzki , United Kingdom
Luciano Saso , Italy
Nadja Schroder , Brazil

Anwen Shao , China
Iman Sherif, Egypt
Salah A Sheweita, Saudi Arabia
Xiaolei Shi, China
Manjari Singh, India
Giulia Sita , Italy
Ramachandran Srinivasan , India
Adrian Sturza , Romania
Kuo-hui Su , United Kingdom
Eisa Tahmasbpour Marzouni , Iran
Hailiang Tang, China
Carla Tatone , Italy
Shane Thomas , Australia
Carlo Gabriele Tocchetti , Italy
Angela Trovato Salinaro, Italy
Rosa Tundis , Italy
Kai Wang , China
Min-qi Wang , China
Natalie Ward , Australia
Grzegorz Wegrzyn, Poland
Philip Wenzel , Germany
Guangzhen Wu , China
Jianbo Xiao , Spain
Qiongming Xu , China
Liang-Jun Yan , USA
Guillermo Zalba , Spain
Jia Zhang , China
Junmin Zhang , China
Junli Zhao , USA
Chen-he Zhou , China
Yong Zhou , China
Mario Zoratti , Italy

Contents

The Secretome Deregulations in a Rat Model of Endotoxemic Shock

A. Blangy-Letheule, A. Persello , S. Michelland, V. Cunin, F. Souab, V. Aillerie, J. Dhot, A. Erraud, J. Montnach , M. Seve , S. Bourgoïn-Voillard , B. Rozec , M. De Waard , and B. Lauzier 
Research Article (13 pages), Article ID 6650464, Volume 2021 (2021)

Effect of Verapamil, an L-Type Calcium Channel Inhibitor, on Caveolin-3 Expression in Septic Mouse Hearts

Bruna A. C. Rattis , Ana C. Freitas , Jordana F. Oliveira , João L. A. Calandrini-Lima , Maria J. Figueiredo , Danilo F. Soave , Simone G. Ramos , and Mara R. N. Celes 
Research Article (8 pages), Article ID 6667074, Volume 2021 (2021)

Anti-inflammatory Effects of *S. cumini* Seed Extract on Gelatinase-B (MMP-9) Regulation against Hyperglycemic Cardiomyocyte Stress

Neha Atale , Chandra Bhushan Mishra , Shrey Kohli, Raj Kumar Mongre , Amresh Prakash , Sweta Kumari, Umesh C. S. Yadav , Raok Jeon , and Vibha Rani 
Research Article (14 pages), Article ID 8839479, Volume 2021 (2021)

New Approaches to Identify Sepsis Biomarkers: The Importance of Model and Sample Source for Mass Spectrometry

Angélique Blangy-Letheule, Antoine Persello, Bertrand Rozec , Michel De Waard , and Benjamin Lauzier 
Review Article (10 pages), Article ID 6681073, Volume 2020 (2020)

Uncovering the Molecular Mechanism of the Qiang-Xin 1 Formula on Sepsis-Induced Cardiac Dysfunction Based on Systems Pharmacology

Shasha He , Jingxia Zhao , Xiaolong Xu , Xuran Cui , Ning Wang, Xuyang Han , Yuhong Guo , and Qingquan Liu 
Research Article (26 pages), Article ID 3815185, Volume 2020 (2020)

Research Article

The Secretome Deregulations in a Rat Model of Endotoxemic Shock

A. Blangy-Letheule,¹ A. Persello ^{1,2} S. Michelland,^{3,4,5} V. Cunin,^{3,4} F. Souab,¹ V. Aillerie,¹ J. Dhot,¹ A. Erraud,¹ J. Montnach ¹ M. Seve ^{3,4} S. Bourgoin-Voillard ^{3,4,6} B. Rozec ¹ M. De Waard ^{1,7} and B. Lauzier ¹

¹Université de Nantes, CHU Nantes, CNRS, Inserm, L'Institut du Thorax, F-44000 Nantes, France

²InFlectis BioScience, Nantes, France

³Univ. Grenoble Alpes, LBFA and BEeSy, Inserm, U1055, PROMETHEE Proteomic Platform, Saint-Martin-d'Hères, France

⁴CHU Grenoble Alpes, Institut de Biologie et de Pathologie, PROMETHEE Proteomic Platform, Grenoble, France

⁵University of Grenoble Alpes, CNRS, Grenoble INP, TIMC, PROMETHEE Proteomic Platform, 38000 Grenoble, France

⁶University of Paris-Est Créteil (UPEC), Inserm U955, Equipe 21, UMR_S955, APHP, Hôpital H. Mondor-A. Chenevier, Centre d'Investigation Clinique Biothérapie, Créteil, France

⁷LabEx Ion Channels, Science and Therapeutics, F-06560 Valbonne, France

Correspondence should be addressed to B. Lauzier; benjamin.lauzier@univ-nantes.fr

Received 15 November 2020; Accepted 13 June 2021; Published 26 July 2021

Academic Editor: Christian Jung

Copyright © 2021 A. Blangy-Letheule et al. This is an open access article distributed under the Creative Commons Attribution License, which permits unrestricted use, distribution, and reproduction in any medium, provided the original work is properly cited.

Introduction. Septic shock is a systemic inflammatory response syndrome associated with organ failures. Earlier clinical diagnosis would be of benefit to a decrease in the mortality rate. However, there is currently a lack of predictive biomarkers. The secretome is the set of proteins secreted by a cell, tissue, or organism at a given time and under certain conditions. The plasma secretome is easily accessible from biological fluids and represents a good opportunity to discover new biomarkers that can be studied with nontargeted “omic” strategies. **Aims.** To identify relevant deregulated proteins (DEP) in the secretome of a rat endotoxemic shock model. **Methods.** Endotoxemic shock was induced in rats by intravenous injection of lipopolysaccharides (LPS, *S. enterica typhi*, 0.5 mg/kg) and compared to controls (Ringer Lactate, *iv*). Under isoflurane anesthesia, carotid cannulation allowed mean arterial blood pressure (MAP) and heart rate (HR) monitoring and blood sampling at different time points (T0 and T50 or T0 and T90, with EDTA and protease inhibitor). Samples were prepared for large-scale tandem mass spectrometry (MS-MS) based on a label-free quantification to allow identification of the proteins deregulated upon endotoxemic conditions. A Gene Ontology (GO) analysis defined several clusters of biological processes (BP) in which the DEP are involved. **Results.** Ninety minutes after shock induction, the LPS group presents a reduction in MAP (-45%, $p < 0.05$) and increased lactate levels (+27.5%, $p < 0.05$) compared to the control group. Proteomic analyses revealed 10 and 33 DEP in the LPS group, respectively, at 50 and 90 minutes after LPS injection. At these time points, GO-BP showed alterations in pathways involved in oxidative stress response and coagulation. **Conclusion.** This study proposes an approach to identify relevant DEP in septic shock and brings new insights into the understanding of the secretome adaptations upon sepsis.

1. Introduction

Septic shock is responsible for one death every 2.8 seconds worldwide [1]. In 50% of cases, septic shock causes myocardial dysfunction resulting in over 60% excess global mortality [2, 3]. The dynamics of septic shock consist of a compensa-

tion phase followed by decompensation. The kinetics of the different phases of the pathology varies according to the patient, resulting in a variation in the kinetics of organ dysfunctions from one patient to another. Limiting the development of cardiovascular dysfunctions and optimizing care would increase the patient's chances of survival. Septic shock

is multifactorial and presents a large heterogeneity between patients. This point explains the variable kinetics of pathology development and makes it difficult to investigate causal mechanisms [4]. The early use of sensitive and specific biomarkers of septic shock clinical evolution would facilitate rapid diagnosis and early management of patients. Such biomarkers must be easily accessible and quickly analyzable for clinical use. Unfortunately, due to the complexity of the pathology, such biomarkers are not currently available for clinicians [5]. The use of animal models allows investigators to considerably limit the heterogeneity between individuals, while, at the same time, improving access to samples before shock initiation and throughout the progression of the pathology. The *in vivo* administration of lipopolysaccharides (LPS), which triggers endotoxemic shock, is one of the most common and simple ways to model shock in animals [6].

In this context, the study of the secretome, defined as the set of proteins secreted by a cell, tissue, or organism at a given time and under certain conditions, is a relevant approach [7]. Changes in plasmatic secretome composition may reflect a pathological state [8]. Indeed, injection of plasma from patients diagnosed with septic shock in a healthy mouse constituted the first proof of concept in 2011 that the secretome could provide information on this pathology. This approach demonstrated the presence of circulating blood factors causing the physiopathology of septic shock [9]. The proteins that are deregulated in the secretome of septic shock patients could potentially be used as biomarkers of the septic shock prognosis. The objective of this study is to identify early biomarkers of septic shock by studying sepsis prior to and at the acute stage of the decompensation phase. For this purpose, the plasma secretome in a rat model of endotoxemic shock was studied at two time points using a large-scale nontargeted mass spectrometry (MS) approach. The design of this study made it possible to follow each subject before shock induction and then at two important time points of the development of the pathology. Through this approach, we identified deregulated proteins (DEP) of the acute stage of shock that is associated with the deregulation of numerous biological processes such as coagulation or the response to oxidative stress.

2. Methods

2.1. Animals. Twelve-week-old male Wistar rats were housed under standard conditions of temperature (21–24°C), humidity (40–60%), and a 12-hour light/dark cycle. Food and water were available *ad libitum*. Experiments were approved by the ethics committee in charge of animal experimentation, the committee of the Pays de la Loire (12760-2017121810244298), and were performed in accordance with the French law on animal welfare, EU Directive 2010/63/EU for animal experiments, and the National Institutes of Health (NIH).

2.2. Endotoxemic Rat Model. Endotoxemia was induced by intravenous injection of 0.05 mg·kg⁻¹ of purified LPS obtained from *Salmonella enterica* serotype *typhimurium* (batch 078M4021V, Sigma, St. Louis, USA) suspended in Ringer Lactate (RL, B. Braun, France) as previously described [10]. Rats were randomly distributed into four groups: the

control group, having received an injection of RL, and LPS groups followed during 50 minutes (CT50 and LPS50, respectively) or during 90 minutes (CT90 and LPS90, respectively), with 6 animals per group. In each group, animals are their own control meaning that each group comprised a T0 time point and either a T50 or a T90 time point (Figure 1).

2.3. Monitoring. Animals were anesthetized with 2% volume of isoflurane and 0.6 L·min⁻¹ O₂ to limit hemodynamic effects of anesthesia. Arterial blood pressure measurements were performed through the left carotid artery to calculate the mean arterial blood pressure (MAP) and heart rate (HR). Briefly, the right carotid artery was isolated and ligated at the distal end, and a PE-50 catheter containing Ringer Lactate was inserted. Pressure signal and HR were continuously recorded, displayed, and stored by the IOX[®] software (EMKA Technologies, Paris, France).

2.4. Blood Analyses and Plasma Preparation. A volume of 500 µL or 5 mL of arterial blood was, respectively, collected at T0 and at the terminal endpoint (50 or 90 minutes) through the carotid catheter. At T0, vascular filling with RL was performed to compensate for the volume collected. Blood samples were placed in 2 mL EDTA tubes (Sarstedt AG & Co. KG, Numbrecht, Germany) containing protease inhibitors (Complete ULTRA Tablet, Mini, Protease Inhibitor Cocktail, MERCK laboratory). Lactate concentration was measured from 10 µL of venous blood using Nova StatStrip (Nova Biomedical, Rungis, France). For terminal sampling, blood gases, electrolytes, and metabolites (BGEM) were measured from 90 µL of arterial blood using a BGEM card (Siemens Healthcare[™], Ottawa, Canada) and analyzed by the ePOC analyzer (Siemens Healthcare[™], Ottawa, Canada). Plasma was obtained by blood centrifugation (10 minutes, 1,300 g) at room temperature (RT) and frozen in liquid nitrogen. Thereafter, samples were stored at -80°C.

2.5. Sample Preparation for Label-Free Mass Spectrometry Analyses. Plasmatic protein concentration was determined by colorimetry using the BCA method (BiCinchoninic acid Assay, Thermo Fisher Scientific, Walt-man, Massachusetts, United States). The absorbance was measured at 560 nm using a Varioskan reader (Thermo Fisher Scientific, Walt-man, Massachusetts, USA). Plasmatic samples were enriched for low abundance proteins using ProteoMiner[™] kits (Bio-Rad, Hercules, USA), in accordance with the manufacturer's instructions. The plasma volume loaded on the ProteoMiner[™] column contained 10 mg of total proteins per column. In order to remove salts, the eluate was loaded in 2 kDa dialysis cassette (Slide-A-Lyzer, Thermo Fisher Scientific, United States) in a 50 mM ammonium bicarbonate dialysis buffer (pH = 7.7 ± 0.1, batch BCBZ3540, Sigma-Aldrich, St. Louis, USA). The concentration of proteins present in the dialysate was determined as previously described. Aliquots were finally prepared in order to obtain 25 µg of proteins and stored at -80°C prior to the mass spectrometry analysis. Prior to mass spectrometry, 25 µg of proteins of each sample was reduced with Dithiothreitol (DTT, Sigma-Aldrich) at 56°C for 1 h, alkylated with iodoacetamide (Sigma-Aldrich) at 37°C for 30 min in the dark, and

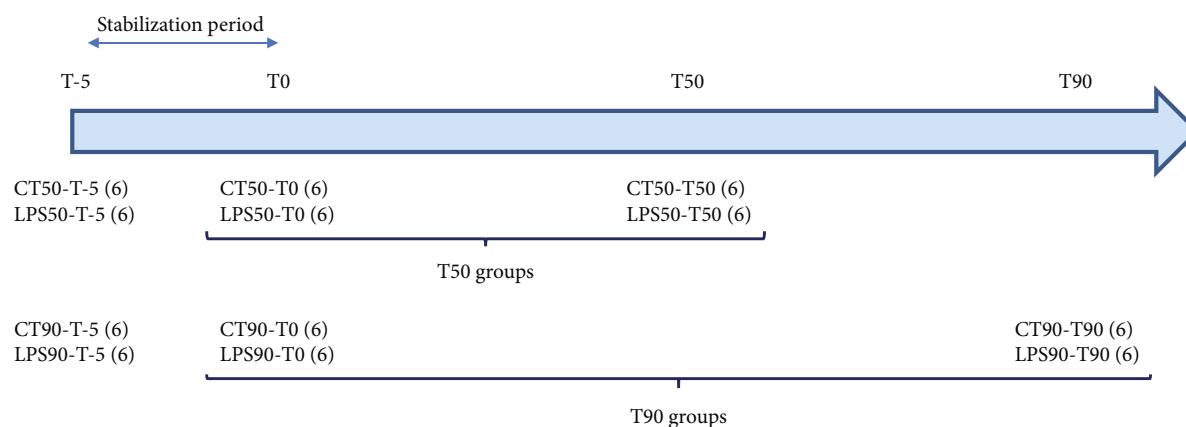


FIGURE 1: Group repartition for the 12-week-old Wistar rats. The period between T-5 and T0 corresponds to stabilization. T0 is the control before solvent or LPS injection and therefore concerns the same rats 50 or 90 minutes after injection. Each group consists of 6 rats (6).

digested at 37°C overnight simultaneously with both trypsin and Lys-C enzymes (Trypsin/Lys-C Mix, Mass Spec Grade, Promega, France) using an enzyme/protein ratio of 3:100. Each sample was spiked with 700 fmol of enolase digest from *Saccharomyces cerevisiae* (Waters, Milford, United Kingdom). Resulting peptides were desalted with C18 spin columns with a peptide binding capacity of 30 µg (Pierce C18 Spin Columns, Thermo Fisher Scientific, Walt-man, Massachusetts, United States). Two micrograms of each sample was mixed to prepare a Quality Control (QC) sample. Samples were dried by using a speed vacuum (Eppendorf) and stored at -20°C until label-free high-mass resolution/accuracy mass spectrometry analyses.

2.6. Liquid Chromatography and High-Resolution Accurate-Mass (HRAM) Mass Spectrometry Analyses. Protein quantitation was performed according to a label-free quantitative proteomic approach based on a high-resolution accurate-mass (HRAM) mass spectrometry analysis. For this purpose, samples (including QC to verify the stability of the signal) were analyzed by an UHPLC-MS (HRAM) system, a Vanquish Flex Binary UHPLC system (Thermo Fisher Scientific, France) coupled with a Q Exactive Plus mass spectrometer (Thermo Fisher Scientific, France) equipped with an electrospray ionization source operating in a positive mode and an Orbitrap mass analyzer. Peptides resuspended in buffer A (2% ACN, 0.1% FA) were loaded on the Vanquish UPLC equipped with a Viper Fingertight Fittings Column Protection (Viper Inline Filter, Titanium, av. Frit presize 0.5 µm) and a C18 column (ACCL RSLC120 C18, 2.2 µm, 120 Å, 2.1 mm × 250 mm). A binary gradient of 120 min of buffer A (99.9% H₂O, 0.1% FA) and buffer B (99.9% ACN, 0.1% FA) at a flow rate of 0.4 mL/min and at 60°C set up as follows: 0–2 min, 1–3% B; 2–55 min, 3–15% B; 55–95 min, 15–38% B; 95–105 min, 38–95% B; 105–109 min, 95% B; 109–110 min, 95–1% B; and 110–120 min, 1% B was applied to separate peptides. MS analyses were performed upon a full MS mode with a resolution of 70,000, a maximum IT of 17 ms within a scan range of 200–2,000 *m/z*, and a lock-mass ion at *m/z* 445.120024 of polycyclodimethylsiloxane from the ambient air. The external calibration was done with a CalMix

calibrant (Pierce, Thermo Fisher Scientific, Walt-man, Massachusetts, United States) in positive mode by considering ±5 ppm of mass tolerance. MS/MS analyses were performed by using a data-dependent acquisition based on HCD (higher-energy collisional dissociation) activation mode with an isolation window of 4 u, a resolution of 17,500, an automatic gain control target of 2.10⁵, and a maximum IT of 200 ms on the 10 most intense ions. A dynamic exclusion of 10 s was applied. Each sample was analyzed in duplicate. The data were acquired with Thermo Scientific™ XCalibur 2017 v.4.1.31.9. software.

2.7. Data Analyses. The identification of proteins was achieved thanks to PEAKS®X Studio 10.0 software [11] and the UniProtKB database of *Rattus norvegicus* (UP000002494, Release 2020_01) uploaded with the enolase protein from *Saccharomyces cerevisiae* (P00924). The following criteria were applied for the protein identification: a fixed modification of carbamidomethylation, variable modifications of oxidation (HW), oxidation (M), acetylation (protein N-term), 2 missed cleavages, at least 2 unique peptides, a tolerance MS of 5 ppm, a tolerance MS/MS of 0.01 Da, a peptide FDR of 1%, and a protein-10Log_p of 20. The identification was done by using PEAKS DE Novo, PEAKS database, and SPIDER tools. The label-free protein quantitation was done by considering a retention time shift tolerance of 3 min and the enolase 1 protein from *Saccharomyces cerevisiae* (P00924) as an internal standard for the signal normalization. The quantity of proteins after LPS injection was compared in each group of six biological replicates with paired controls as detailed in the previous section. LPS and RL administration in Wistar rats allowed the study of (i) changes in the secretome 50 min postinjection (group CT50-T0 vs. CT50-T50 and group LPS50-T0 vs. LPS50-T50) and (ii) secretome adaptations 90 min LPS postinjection (group CT90-T0 vs. group CT90-T90 and group LPS90-T0 vs. LPS90-T90). A total of 48 samples, with technical duplicates for each of them, were therefore analyzed. The protein quantitation was performed only on proteins in which at least two peptides were quantified within a chromatography retention time range between 0

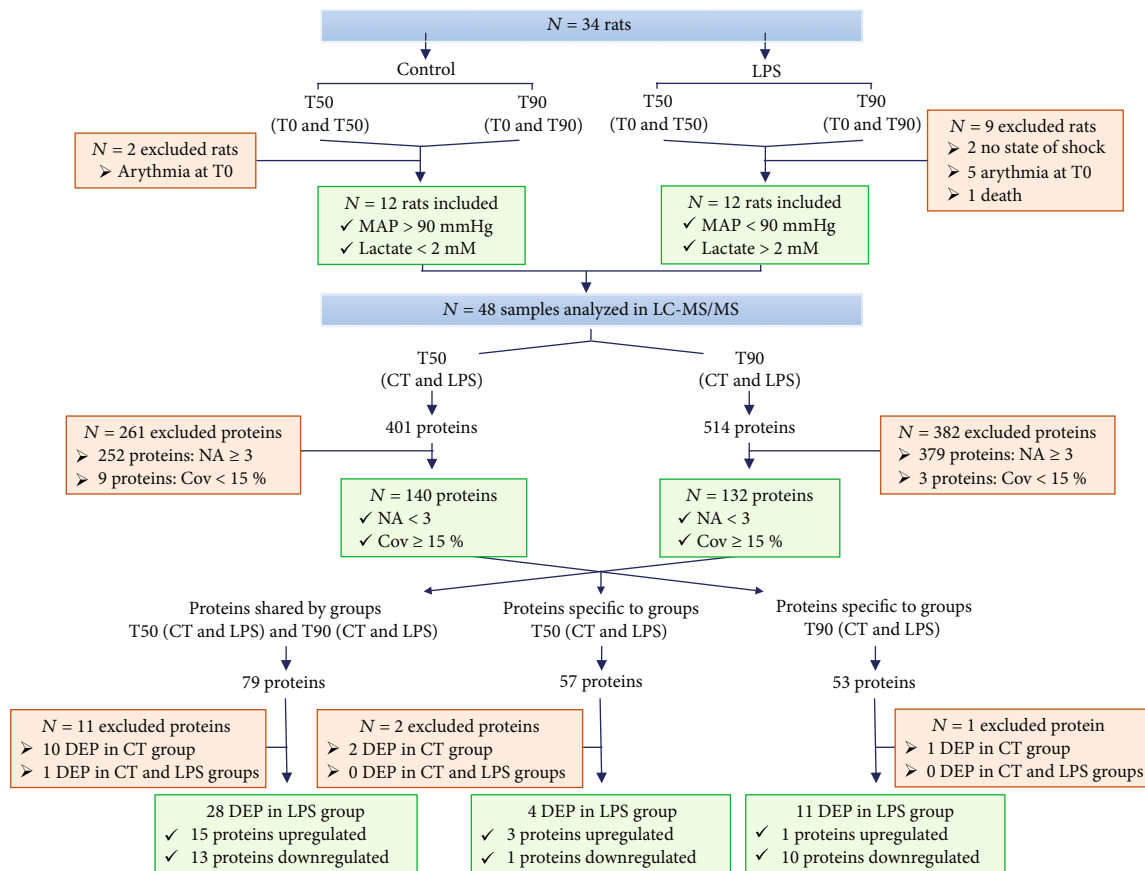


FIGURE 2: Flow chart of inclusion and exclusion procedure used to obtain a list of deregulated protein. The animals were divided into 4 groups (CT50, LPS50, CT90, and LPS90). Physiological parameters made it possible to include 24 rats in the study. For each rat, 2 time points were studied (T0 and T50 or T0 and T90) and were analyzed by mass spectrometry ($N = 48$ samples), and proteomic results were analyzed by RStudio software. Proteins with a maximum of 2 missing data (NA) per sample and a coverage (Cov) greater than 15% were selected. A total of 140 proteins in group T50 and 132 proteins in group T90 were included. The deregulated proteins (DEP) present in the controls were excluded from the study.

and 120 min with a score quality ≥ 6 . This approach led to the identification of 401 proteins in the T50 group and 514 proteins in the T90 group.

Proteins with missing values (indicated by the NA symbol) in at least 3 samples per group and less than 15% of coverage were withdrawn (Figure 2). The quantified proteins were considered deregulated only if they have a fold change higher than 2 ($\text{Log}_2\text{FC} \geq 1$) or lower than -2 ($\text{Log}_2\text{FC} \leq -1$) in at least 4 samples over the 6 in each group. 14 deregulated proteins in the control groups were excluded from the study (Figure 2).

The clustering of the DEP was analyzed using the STRING protein database for Gene Ontology (GO) analyses. The results of the analyses include biological process (BP) and cellular component (CC).

2.8. Western Blot Analyses. Western blotting experiments were performed on plasma samples using an antibody directed against Gpx3 (13647-1-AP, Manchester, United Kingdom, Proteintech). Briefly, proteins were quantified using a BCA protein assay kit. 50 mg of each sample was separated on an SDS-PAGE gel and transferred to a nitrocellulose membrane. The membranes were blocked with 5% milk in TBS

1x-Tween 0.5x (TBS-T) and then incubated with primary antibody (Gpx3, 1 : 400) overnight at 4°C. After 4 washes with TBS-T, the membranes were incubated with an HRP-conjugated secondary antibody (anti-rabbit, 1:10 000, sc-2054, Santa Cruz Biotechnology). Analyses were performed using Image Lab software (Bio-Rad, California, United States). A ratio to the stain-free intensity was calculated.

2.9. Statistical Analyses. Hemodynamic results were expressed as the mean \pm SEM of N different rats. For hemodynamic parameters, lactatemia, and creatinemia, data were analyzed by a two-way ANOVA test with Bonferroni post hoc test.

Analyses of Western blots were expressed in relation to the average of the protein quantification (stain-free) and then reduced to the average of the control samples (CT50-T0, CT90-T0, LPS-T0, and LPS-T90). Data were analyzed with a two-way-ANOVA test with repeated measures and a Bonferroni post hoc test.

A value of $p < 0.05$ was considered significant. All statistical calculations and graphs (except those performed with R software) were performed using GraphPad PRISM 8 software (8.4.2 version).

2.10. Data Availability. The proteomic data were deposited to the ProteomeXchange Consortium with the MassIVE identifier MSV000087803 (<http://massive.ucsd.edu>) and ProteomeXchange identifier PXD027255 (<http://www.proteomexchange.org>).

3. Results

3.1. Animal Model

3.1.1. Effect of Endotoxemic Shock on Hemodynamic Parameters. Continuous hemodynamic monitoring showed no significant changes neither in HR nor in MAP during the 5 min of stabilization (from T-5 to T0). MAP and HR remained stable in the control group at 90.0 ± 10.0 mmHg and 390.0 ± 10.0 bpm during the whole procedure. Injection of LPS (T0) induce any modification in HR (400.0 ± 10.0 bpm) (Figure 3(a)), whereas it was followed by an early decrease in MAP (Ctrl: 95.6 ± 2.9 mmHg vs. LPS: 80.6 ± 3.7 mmHg, $p < 0.05$, Figure 3(b)) with a return to basal values after 10 min. From 50 min after LPS injection to the end of the procedure, MAP decreased significantly (from 91.4 ± 3.4 mmHg at 50 min to 60.5 mmHg ± 6.9 mmHg at 90 min, $p < 0.001$, Figure 3(b)).

3.1.2. Effect of Endotoxemic Shock on Plasmatic Biomarkers. Arterial creatinine and venous lactate concentrations were measured in the Ctrl and LPS groups at T50 and T90 and T0, T50, and T90, respectively (Figure 4). No change in creatinemia was observed at T50 between the Ctrl and LPS groups. However, creatinemia in the LPS T90 groups increases significantly when compared to time-matched Ctrl (Ctrl T90: 0.26 ± 0.04 mg/dL; LPS T90: 1.07 ± 0.16 mg/dL, $p < 0.01$, Figure 4(a)) indicating an alteration in renal function. Lactatemia remained in the normal range in Ctrl throughout the protocol while significantly increasing in the LPS T90 group (LPS T0: 1.02 ± 0.09 mmol/L vs. LPS T90: 3.04 ± 0.90 mmol/L, $p < 0.001$; LPS T50: 1.63 ± 0.10 mmol/L vs. LPS T90: 3.04 ± 0.90 mmol/L, $p < 0.05$; and Ctrl T90: 0.82 ± 0.17 mmol/L vs. LPS T90: 3.04 ± 0.90 mmol/L, $p < 0.001$, Figure 4(b)). These results suggest a compensated state 50 min after LPS administration, followed by the onset of hypotension, which is probably a cause of the hypoperfusion and tissue distress detected during the decompensation phase at 90 min after LPS administration.

3.2. Identification of Deregulated Proteins in the Secretome during Sepsis. Over the 48 samples included in the study, 401 and 514 proteins were quantified by LC-MS/MS analyses in the T50 (CT and LPS) and T90 (CT and LPS) groups, respectively (Figure 2). Cleaning raw data by protein coverage $> 15\%$ and number of missing data (NA) per group led to the identification of 140 proteins at T50 and 132 proteins at T90 (Figure 2). DEP in the control groups (14) were excluded from this study. Three levels of analyses were then performed (1) the study of proteins identified in LPS samples, both in the T50 and T90 groups; (2) the study of proteins identified only in the T50 group; and (3) the study of proteins identified only in the T90 group (Figure 2).

3.2.1. Study of the Evolution of the Level of Proteins Identified in the T50 and T90 Groups. Seventy-nine proteins were found to be common in the T50 and T90 groups (CT and LPS) (Figure 2 and Supplementary Table 2). The study of levels of these proteins over time showed a variation in their expression profile between the CT and LPS groups (Supplementary Figure S1-2).

Among these 79 proteins, to analyze common or deregulated proteins, T50 or T90 was compared to their T0. Among the LPS groups, 15 proteins were upregulated (5 proteins at T50 groups and 10 proteins at T90). Finally, 13 proteins were found downregulated: 1 at T50 and 12 at T90 (Table 1).

The analyses of Gene Ontology highlighted functional annotations of the selected proteins. The analyses of the GO cellular component (CC) showed that the proteins identified are plasma proteins (Supplementary Table 1). Fifty minutes after LPS administration, upregulated proteins belong to tissue remodeling, immune system, and starvation (Figure 5(a)), whereas downregulated ones belong to response to oxidative stress (Figure 5(b)). Ninety minutes after LPS administration, upregulated proteins belong to carboxypeptidase activity, cytolysis, tissue remodeling, and coagulation (Figure 5(c)), whereas downregulated ones belong to lipid metabolism, membrane organization, and response to corticoid (Figure 5(d)).

3.2.2. Identification of Proteins Specific to the T50 Groups. Analyses of the proteins specific to T50 (CT and LPS) identified 57 proteins that are present at T50 but not at T90 (Figure 2 and Supplementary Table 3). The study of protein expression over time revealed a variation in the protein profile between the control and LPS groups (Supplementary Figure 3). Among the 57 proteins identified, 3 are upregulated and 1 protein is downregulated 50 minutes after LPS administration (Table 2). Either upregulated or downregulated proteins specific to the T50 group are implicated in immune response (Figure 6).

3.2.3. Identification of Proteins Specific to the T90 Groups. Analyses of the proteins specific to T90 (CT and LPS) identified 53 proteins that are present at T90 but not at T50 (Figure 2 and Supplementary S4). The study of protein expression over time revealed a variation in the protein expression profile between the control and LPS groups (Figure S4). Among the 53 proteins identified, 11 proteins were found to be specifically deregulated in the LPS group between T0 and T90. Among the deregulated proteins in the LPS group, 1 protein is upregulated and 10 are downregulated (Table 3).

Upregulated proteins specific to the T90 group are implicated in glucose metabolism, whereas downregulated ones are implicated in lipid metabolism, negative regulation of endopeptidase activity, and coagulation (Figure 7).

3.3. Validation of Gpx3 Downregulation by Western Blotting. The antioxidant enzyme Gpx3 plays a critical role in the protection of tissues and organs from oxidative damage. Plasmatic expression levels of Gpx3 were assessed by Western blotting. No modification in plasmatic levels of Gpx3 were observed between groups at T0 and T50. Ninety minutes

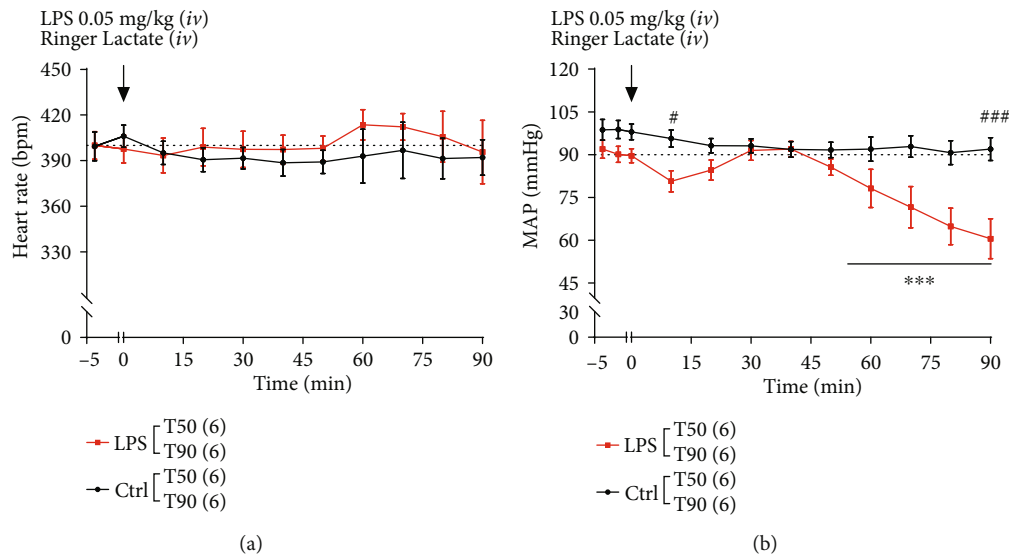


FIGURE 3: Effect of lipopolysaccharide (LPS) administration on heart rate (HR) and mean arterial blood pressure (MAP). Black and red squares represent the control and LPS rats, respectively. The dotted line represents the threshold considered physiological. The T50 and T90 groups are pooled for both control and LPS conditions ($n = 12$ in the control group and $n = 12$ in the LPS group). Only the T90 group is monitored after 50 minutes ($n = 6$ for the T90 control group and $n = 6$ for the T90 LPS group). Values represent the mean \pm SEM of 6 rats per group. (a) Heart rate and (b) MAP were evaluated during 50 or 90 min after LPS injection and were expressed in beats per min (bpm) and mmHg, respectively. The symbol # represents a comparison at a given time between the CT and LPS groups, and the symbol * represents a comparison over time for the LPS group. # $p < 0.01$, ### $p < 0.001$, and *** $p < 0.001$ two-way ANOVA test with Bonferroni post hoc test.

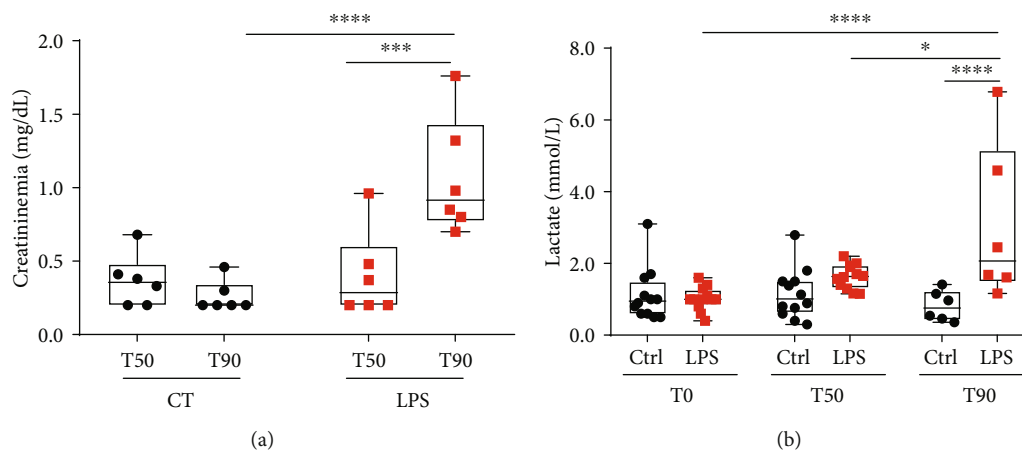


FIGURE 4: Variation of creatininemia (mg/dL) and lactatemia (mmol/L) throughout the development of endotoxemic shock. Black circles and red squares represent the control and LPS rats, respectively. (a) Arterial creatinine was measured at 50 or 90 minutes after shock induction; (b) venous lactates were measured at 0 and 50 or 0 and 90 min. Box & whiskers represent measures. (a, b) Were analyzed with a two-way ANOVA test with Bonferroni post hoc test. * $p < 0.05$, *** $p < 0.001$, and **** $p < 0.0001$.

after shock induction, Gpx3 expression levels in the plasma were decreased by 2-fold in the LPS group compared to T0 (LPST90-T0: 1.00 ± 0.16 ; LPST90-T90: 0.53 ± 0.19) (Figure 8).

4. Discussion

Our study is aimed at identifying the secretome adaptations of a rat model of septic shock. For this purpose, a proteomic analysis was performed in the secretome of control rats and

rats in endotoxemic shock 50 (T50) or 90 (T90) minutes after LPS administration. Thus, this study integrates the notion of pathology progression at 2 time points. The T50 point represents a compensated system, whereas the T90 point represents an acute phase of decompensation. Three levels of analyses have been carried out: first the study of proteins identified in both T50 and T90 groups (CT and LPS), next the study of proteins only identified in the T50 group (CT and LPS), and finally the study of proteins only identified in the T90 group (CT and LPS). All these studies demonstrate

TABLE 1: Proteins with a Log₂foldchange (Log₂FC) greater than 1 are highlighted in bold, and proteins with a Log₂FC less than -1 are not in bold.

UniProt accession number	Protein	Gene name	Protein reference described	Log ₂ FC Median (min; max)	n/6
LPS T50					
P06765	Platelet factor 4*	<i>Pf4</i>	[12]	3.31 (1.02; 5.20)	5/6
D3ZFH5	Inter-alpha-trypsin inhibitor heavy chain 2	<i>Itih2</i>	—	1.25 (1.08; 2.34)	
P26644	Beta-2-glycoprotein 1*	<i>ApoH</i> <i>B2GPI</i>	[13]	1.45 (1.03; 1.55)	4/6
O55004	Ribonuclease 4	<i>RNase 4</i>	—	1.78 (1.70; 2.90)	
P00697	Lysozyme C-1*	<i>Lyz1</i>	[14]	1.77 (1.70; 2.63)	
P23764	Glutathione peroxidase 3*	<i>Gpx3</i>	[15]	-2.58 (-1.45; -4.75)	4/6
LPS T90					
P17475	Alpha-1-antiproteinase*	<i>Serpina1</i>	[16]	3.73 (2.97; 5.65)	5/6
Q99PS8	Histidine-rich glycoprotein*	<i>Hrg</i>	[17]	2.39 (1.37; 3.89)	
D3ZFH5	Inter-alpha-trypsin inhibitor heavy chain 2	<i>Itih2</i>	—	1.92 (1.58; 3.82)	
Q9QUH3	Apolipoprotein A-V*	<i>Apoa5</i>	[18]	1.44 (1.00; 2.24)	
P24594	Insulin-like growth factor-binding protein 5	<i>Igfbp5</i>	—	2.14 (1.02; 3.79)	
P08650	Complement C5*	<i>C5</i>	—	5.27 (3.28; 6.21)	4/6
O55004	Ribonuclease 4	<i>Rnase4</i>	—	1.68 (1.28; 2.32)	
D3ZTE0	Coagulation factor XII*	<i>F12</i>	[19]	1.42 (1.32; 1.73)	
P00697	Lysozyme C-1*	<i>Lyz1</i>	[14]	2.86 (1.25; 3.81)	
Q6IRK9	Carboxypeptidase Q	<i>Cpq</i>	—	1.94 (1.05; 3.34)	
P04638	Apolipoprotein A-II*	<i>Apoa2</i>	[20]	-1.96 (-1.19; -5.20)	
P55797	Apolipoprotein C-IV	<i>Apoc4</i>	—	-1.88 (-1.37; -2.91)	
P20767	Ig lambda-2 chain C region	<i>N/A</i>	—	2.39 (-1.50; -3.30)	
Q8R2H5	Phosphatidylinositol-glycan-specific phospholipase D*	<i>Gpld1</i>	[21]	-1.48 (-1.02; -2.72)	5/6
P14630	Apolipoprotein M*	<i>Apom</i>	[22]	-2.94 (-1.46; -4.82)	
P23764	Glutathione peroxidase 3*	<i>Gpx3</i>	[15]	-2.05 (-1.48; -3.44)	
Q68FP1	Gelsolin*	<i>Gsn</i>	[23]	-2.05 (-1.67; -4.47)	
P06759	Apolipoprotein C-III	<i>Apoc3</i>	—	-2.60 (-1.08; -3.66)	
P55159	Serum paraoxonase/arylesterase 1*	<i>Pon1</i>	[24]	-2.15 (-1.17; -2.49)	
P02651	Apolipoprotein A-IV	<i>Apoa4</i>	—	-1.54 (-1.04; -2.61)	4/6
P35859	Insulin-like growth factor-binding protein complex acid labile subunit	<i>Igfals</i>	—	-2.49 (-2.20; -2.90)	
P10960	Prosaposin*	<i>Psap</i>	[25]	-2.57 (-1.53; -3.90)	

N represent the number of rats in which the protein has been found to be deregulated over the 6 rats. Proteins with an asterisk have already been described by other reports in the context of sepsis and septic shock.

the deregulation of plasma levels of 11 proteins at 50 min and 33 proteins at 90 min after LPS administration.

4.1. Model of Endotoxemic Shock. In this study, we compared, at 2 different times, the evolution of protein expression during the progression of septic shock. For this, a rat model of endotoxemic shock, previously described, was chosen [32]. The endotoxemic shock model was preferred because the use of LPS allows a better control of the kinetics of the development of pathology. In this way, the sampling should lead to more homogeneous interindividual results. In this study,

90 min after the injection of LPS, the animals developed a clinical picture similar to sepsis with systemic arterial hypotension leading to an increase in plasma creatinine and lactate, which characterize organ dysfunction and altered metabolism [33]. These results show that this model of early endotoxemic shock reproduces several characteristics of septic shock. However, interestingly, the heart rate did not change after the injection of LPS. This could be explained by the strain of LPS used. Nevertheless, according to the definition of Singer and collaborators, animals can be considered in septic shock [3, 34]. The secretome of rats

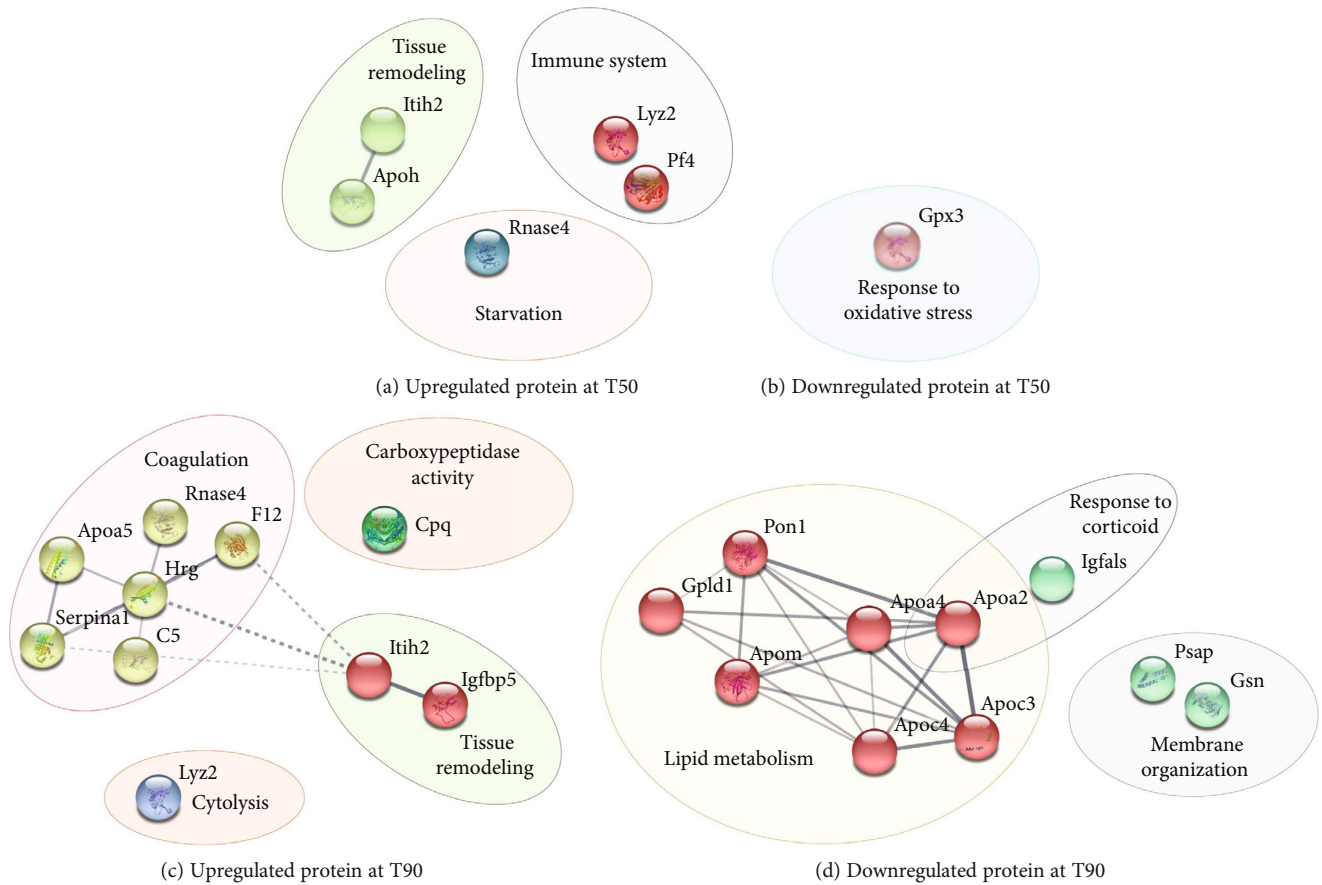


FIGURE 5: Protein-protein interaction network of (a) up and (b) downregulated proteins in the LPS T50 group and (c) up and (d) downregulated proteins in the LPS T90 groups. The study of proteins identified both in T50 (CT and LPS) and T90 (CT and LPS). The analyses using Gene Ontology (GO) databases revealed the most modified biological processes following the injection of LPS. STRING protein database was used to clustered deregulated proteins. The continuous lines represent protein interactions within the cluster, and the discontinuous lines represent protein interactions between different clusters.

TABLE 2: Proteins with a $\text{Log}_2\text{foldchange}$ (Log_2FC) greater than 1 are highlighted in bold, and proteins with a Log_2FC less than -1 are not in bold.

UniProt accession number	Protein	Gene name	Protein reference described	Log_2FC (range)	<i>n</i> / <i>6</i>
Q5FVN3	Ccl9-like protein*	<i>Ccl9</i>	[26]	3.69 (1.38; 4.98)	
Q05820	Putative lysozyme C-2	<i>Lyz2</i>	—	1.67 (1.30; 2.64)	4/6
Q63556	Serine protease inhibitor A3M	<i>Serpina3m</i>	—	1.10 (1.30; 2.63)	
Q5BK77	Chemerin*	<i>Rarres2</i>	[27]	-2.24 (-1.36; -2.98)	5/6

N represent the number of rats in which the protein has been found to be deregulated over the 6 rats. Proteins with an asterisk have already been described in the context of sepsis and septic shock.

developing such a shock was studied by proteomic analysis based on nontargeted mass spectrometry. Analyses of the GOs of the plasma secretome showed that the state of shock leads to an alteration of several biological processes.

4.2. Proteomic Analyses of the Secretome

4.2.1. Altered Protein Expression at T50. Fifty minutes after shock induction, DEP were identified while the physiological

parameters show any signs of tissue suffering or hypoperfusion. At this time, affected biological processes are associated with the immune system, starvation, and response to oxidative stress. Our study, using a model of shock triggered by LPS injection, demonstrated an increase in beta-2-glycoprotein 1 (B2GPI), also known as apolipoprotein H, which is a potential regulator of complement. A recent study proposed that B2GPI may be able to mediate the anti-inflammatory effects of LPS by shunting it away from

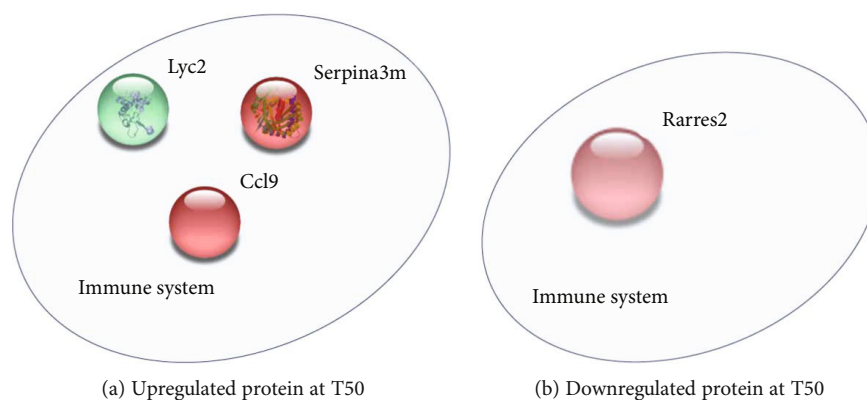


FIGURE 6: The network of (a) upregulated proteins and (b) downregulated protein in the LPS T50-specific group. The study of proteins identified in T50 (CT and LPS) and not in T90 (CT and LPS). The analyses using Gene Ontology (GO) databases reveal the most modified biological processes (BP) following the injection of LPS. STRING protein database was used to clustered deregulated proteins.

TABLE 3: Proteins with a $\text{Log}_2\text{foldchange}$ (Log_2FC) greater than 1 are highlighted in bold, and proteins with a Log_2FC less than -1 are not in bold.

UniProt accession number	Protein	Gene name	Protein reference described	Log_2FC (range)	n/6
Q5GAM5	Angiogenin ribonuclease 2	Ang2	—	1.79 (1.32; 3.47)	4/6
Q6MG90	C4a anaphylatoxin	<i>C4a</i>	—	-3.22 (-1.42; -6.85)	
D3ZQ25	Fibulin-1	<i>Fbln1</i>	—	-2.37 (1.24; 5.70)	
Q5M890	Apolipoprotein N	<i>Apon</i>	—	-4.55 (-1.46; -5.61)	6/6
Q5M8C3	Serine (or cysteine) proteinase inhibitor, clade A (alpha-1 antiproteinase, antitrypsin), member 4	<i>Serpina4</i>	—	-1.59 (-1.11; -2.75)	
Q64240	Protein AMBP*	<i>Ambp</i>	[28]	-3.25 (-1.09; -5.11)	
B1H260	Coagulation factor XIII B chain	<i>F13b</i>	—	-3.86 (-1.07; -5.12)	5/6
F1LZ11	Ig-like domain-containing protein	<i>N/A</i>	—	-1.72 (-1.00; -3.56)	
A0A0G2JXI1	Coagulation factor V*	<i>F5</i>	[29]	-2.23 (-1.76; -4.25)	
P08649	Complement C4*	<i>C4</i>	[30]	-3.14 (-1.16; -4.59)	4/6
P07151	Beta-2-microglobulin*	<i>B2m</i>	[31]	-1.51 (-1.32; -2.36)	

N represent the number of rats in which the protein has been found to be deregulated over the 6 rats. Proteins with an asterisk have already been described in the context of sepsis and septic shock.

TLR4 activation [35]. This neutralization of LPS could be an effective means to limit the toxic consequences of severe Gram-negative infections. A study performed on patients admitted to the hospital following sepsis showed a decrease in B2GPI within 48 hours of patient admission [13]. A study performed in a mouse model 6 and 24 hours after induction of endotoxemic shock highlighted that the decrease in total B2GPI levels is thought to be due to the functional utilization of B2GPI as part of the protective response of the immune system [36]. Overall, these data suggest that LPS may trigger an increase in plasma B2GPI levels during the early phase of endotoxemic shock that would later on be consumed which would explain the decrease of B2GPI described in the literature. These results suggest that decreased B2GPI could be a biomarker of the early phase of sepsis.

4.2.2. Altered Protein Expression at T90. Ninety minutes after shock induction, this study identified deregulated proteins involved in biological processes associated with coagulation and lipid metabolism. This study demonstrated the deregulation of apolipoprotein (Apo) expression which is related to the metabolism of high-density lipoproteins (HDL). In this study, analyses of the secretome in the LPS group at 90 minutes show a decrease in Apo N, Apo M, Apo C-III, Apo C-IV, Apo A-IV, and Apo A-II and an increase in Apo AV. Among these proteins, some are not yet described, such as Apo C-III and Apo C-IV, while others have already been identified in sepsis. These data reinforce the interest of our study. Khovidhunkit and colleagues described a decrease in hepatic mRNA levels of Apo A-II and an increase in Apo A-V mRNA 8 hours after endotoxin injection. These changes in hepatic mRNA levels lead to a decrease of Apo A-II and an

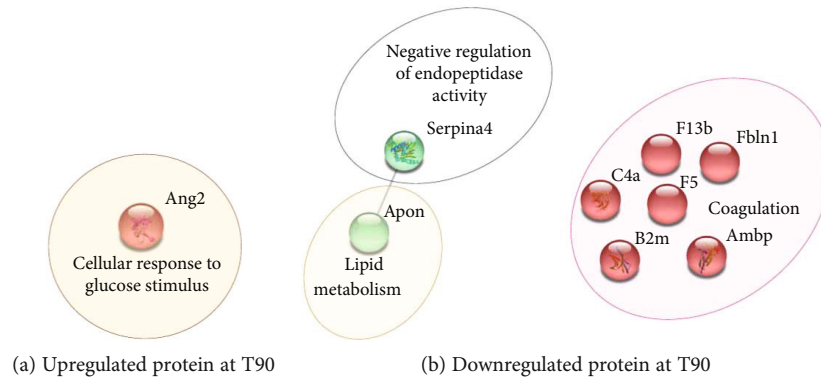


FIGURE 7: The network of (a) upregulated and (b) downregulated proteins in the LPS T90-specific group. The analyses using Gene Ontology (GO) databases revealed the most modified biological processes (BP) following the injection of LPS. STRING protein database was used to clustered deregulated proteins. The continuous line represents protein interactions within the cluster.

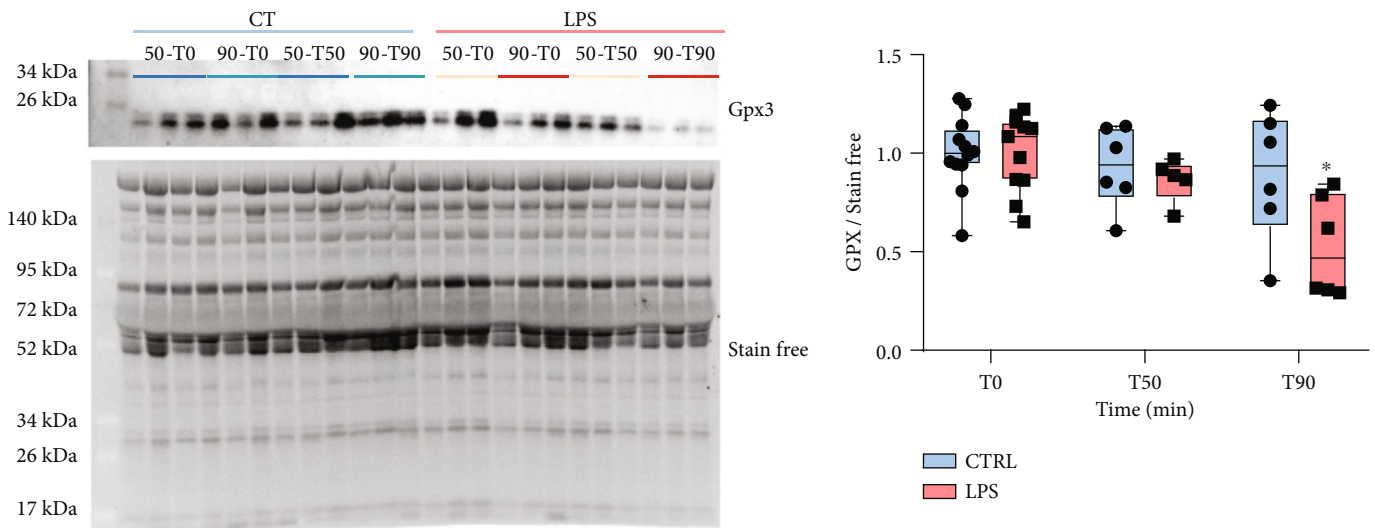


FIGURE 8: Measure in plasma level expression of glutathione peroxidase 3 (Gpx3) throughout the development of the shock. Quantification of Gpx3 levels was normalized to stain-free. Results are expressed as a mean \pm SEM. * $p < 0.05$: two-way ANOVA with repeated measures and a Bonferroni post hoc test.

increase of Apo A-V in HDL particles [20]. Interestingly, a recent study suggests, in septic pediatric patients, the prognostic value of Apo A-V based on an observation of an increase in Apo A-V levels in the serum at the admission and a decrease in patients who did not survive. Moreover, they highlighted a significant association between low levels of Apo A-V and sepsis-induced acute kidney injuries [18]. These results and those provided in this study suggest that Apo A-V could be a biomarker of septic shock. On the other hand, although studies have shown that Apo A-II is an important predictor of cardiovascular disease risk, its role in lipid metabolism is less clear and requires further research [37]. Interestingly, Apo A-II and Apo M have been described as being decreased in patients developing severe forms of COVID-19 which may be at the origin of septic shock [38].

4.2.3. Altered Protein Expression at T50 and T90. Interestingly, among the deregulated proteins identified in both

T50 and T90 groups, the majority of DEP identified at T50 were found to be downregulated at T90. Our study shows a decrease in the plasma expression of glutathione peroxidase 3 (Gpx3). Some studies support the major role of reactive oxygen species (ROS) in the pathogenesis of sepsis and its contribution to the progression to multiple organ dysfunction [39]. Indeed, oxidative stress caused by inflammatory response can lead to lipid peroxidation, DNA damage, and altered mitochondrial function promoting organ dysfunction. The metabolism of glutathione is an essential mechanism of antioxidant defense. The main function of Gpx3 is to catalyze the reduction of hydrogen peroxide, organic peroxides, and lipid peroxides by converting reduced glutathione into oxidized glutathione. Considering the acute oxidative stress observed in sepsis patients, it is interesting to observe that Gpx3 bioactivity is inversely associated with the severity of sepsis and associated mortality [40, 15]. Thus, although understanding of the mechanisms of regulation of

Gpx3 expression and its pathophysiological role in sepsis is limited, Gpx3 could be a promising biomarker for assessing oxidative stress.

4.3. Limitations of the Study. The use of an endotoxemic rat model to mimic septic shock raises concern regarding the extrapolation to human. A rat model based on LPS injection does not reflect exactly the complexity of human pathophysiological responses particularly because it is based on the use of a single bacterial strain. Septic shock can be induced by several bacterial strains or even by nonbacterial pathogens. The changes in the secretome observed in this study may in part differ with the infectious agent causing the pathology, which needs to be further investigated [41]. However, it is currently the only model to follow sepsis kinetic over time in a reproducible manner. A second limitation of this study is based on the study of the plasma secretome, which requires the use of selective depletion techniques. The plasma secretome is made up of a vast dynamic range of compound concentrations. This makes analysis of proteins of low abundance particularly difficult and hinders the identification of biomarkers using mass spectrometry. A selective depletion technique, called ProteoMiner[®], was used in this study to detect the low abundance protein signal in a complex protein sample by reducing the dynamic concentration range of the proteins. Although necessary, this approach may remove low abundance or low molecular weight proteins because of a weak or rare interaction between the sample proteins and the hexapeptides in this ProteoMiner[®]. A third limitation of this study is the validation of the DEP obtained from the proteomic analysis. Indeed, the Western blot analysis was complicated by the lack of sensitivity of this approach and by the fact that most of the antibodies tested lack specificity with the proteins identified in this study.

5. Conclusion

This preliminary study found several deregulated proteins at 50 and 90 minutes after LPS injection. Gene Ontology study showed that the expression of proteins associated with the response to oxidative stress, the immune system, the coagulation, or the lipid metabolism is particularly deregulated during the development of sepsis. Other studies have also reported the deregulation of these different biological processes, which reinforces the results of our work. However, this study identified proteins, such as Apo A-II or Apo C-IV, which were not described previously in sepsis phenotype. Subsequently, the proteins identified as being deregulated in this study will have to be (i) validated by the use of more complex models for a better recapitulation of what happens at the clinical level and (ii) tested on cellular models in order to understand the role they could play in the pathophysiology of shock.

Data Availability

The proteomic data were deposited to the ProteomeXchange Consortium with the MassIVE identifier MSV000081840 (<http://massive.ucsd.edu>) and ProteomeXchange identifier PXD008530 (<http://www.proteomexchange.org>).

Conflicts of Interest

The authors declare no conflict of interest.

Authors' Contributions

M. De Waard and B. Lauzier codirected this work. A. Blangy-Letheule and A. Persello participated equally to this work. A. Blangy-Letheule and A. Persello equally contributed to data acquisition, analyses, and interpretation and participated to the article writing. S. Michelland, V. Cunin, M. Seve, and S. Bourgoïn-Voillard contributed to the experiments, performed the proteomic data acquisition/analyses, and participated to the writing of the manuscript. V. Aillerie, A. Erraud, F. Souab, and J. Dhot contributed to the experiments and the acquisition and interpretation of the data. J. Montnach contributed to the analysis of proteomic data. B. Rozec, M. De Waard, and B. Lauzier managed the project and contributed to experimental design and correcting the manuscript for intellectual content and gave final approval of the version to be submitted.

Acknowledgments

We thank Dr. A. LeGouellec and the Platform group of GExiM, University Grenoble Alpes, for the access to Q Exactive Plus (Thermo Fisher) mass spectrometer supported by IDEX and Auvergne Rhone Alpes Grants. We thank the IBISA core facility Therassay for its assistance and their technical support. We thank the Experimental Therapeutic Unit (UTE) of IRS-UN for its assistance and technical support. We want to thank the Région Pays de la Loire and the European FEDER for their financial support to M. De Waard. This work was supported by an Agence Nationale de la Recherche Grant to the LabEx Ion Channels, Science and Therapeutics (ANR-11-LABX-0015). The postdoctoral fellowship of J. Montnach is provided by the ANR-15-CE14-0004-02 grant. ANR heroism, association Sauve ton Coeur. This work was supported by Astrid, Agence Nationale de la Recherche, and Génavie.

Supplementary Materials

Supplementary Figure 1 represents the variation in fold change of each protein, common to the T90 and T50 groups, identified in the control and LPS group 50 minutes after shock induction. Supplementary Figure 2 represents the variation of the fold change of each protein, common to the T90 and T50 groups, identified in the control and LPS group 90 minutes after shock induction. Supplementary Figure 3 represents the variation in fold change of each protein, specific to the T50 group, identified in the control and LPS group 50 minutes after shock induction. Supplementary Figure 4 represents the variation in fold change of each protein, specific to the T90 group, identified in the control and LPS group 90 minutes after shock induction. Supplementary Table 1 corresponds to the results of Gene Ontology (GO) analysis which highlighted the most modified cellular components (CC) following the injection of LPS. Supplementary Table 2 includes all quantified proteins and unique peptides as well as measured coverage and calculated Log₂foldchange for

proteins common to the T50 and T90 groups. Supplementary Table 3 includes all quantified proteins, unique peptides, and the measured coverage and calculated Log₂foldchange for T50-specific proteins. Supplementary Table 4 includes all quantified proteins, unique peptides, and the measured coverage and calculated Log₂foldchange for T90-specific proteins. (*Supplementary Materials*)

References

- [1] CoMO, "World sepsis day - why every second counts. CoMO," 2019, <https://www.comomeningitis.org/post/world-sepsis-day-why-every-second-counts>.
- [2] M. M. Parker, J. H. Shelhamer, S. L. Bacharach et al., "Profound but reversible myocardial depression in patients with septic shock," *Annals of Internal Medicine*, vol. 100, no. 4, pp. 483–490, 1984.
- [3] M. Singer, C. S. Deutschman, C. W. Seymour et al., "The third international consensus definitions for sepsis and septic shock (sepsis-3)," *JAMA*, vol. 315, no. 8, pp. 801–810, 2016.
- [4] J. A. Nemzek, K. M. S. Hugunin, and M. R. Opp, "Modeling sepsis in the laboratory: merging sound science with animal well-being," *Comparative Medicine*, vol. 58, no. 2, pp. 120–128, 2008.
- [5] A. Teggert, H. Datta, and Z. Ali, "Biomarkers for point-of-care diagnosis of sepsis," *Micromachines*, vol. 11, no. 3, p. 286, 2020.
- [6] A. J. Lewis, C. W. Seymour, and M. R. Rosengart, "Current murine models of sepsis," *Surgical Infections*, vol. 17, no. 4, pp. 385–393, 2016.
- [7] J. Chenu, S. Michelland, and M. Seve, "Secretome: definitions and biomedical interest," *La Revue de Médecine Interne*, vol. 29, no. 7, pp. 606–608, 2008.
- [8] F. J. Vizoso, N. Eiro, S. Cid, J. Schneider, and R. Perez-Fernandez, "Mesenchymal stem cell secretome: toward cell-free therapeutic strategies in regenerative medicine," *International Journal of Molecular Sciences*, vol. 18, no. 9, p. 1852, 2017.
- [9] H. W. H. van Hees, W.-J. M. Schellekens, M. Linkels et al., "Plasma from septic shock patients induces loss of muscle protein," *Critical Care*, vol. 15, no. 5, 2011.
- [10] D. Roul, B. Rozec, G. André et al., "Increased B₂-adrenergic vasorelaxation at the early phase of endotoxemic shock in rats," *Vascular Pharmacology*, vol. 72, pp. 181–189, 2015.
- [11] B. Ma, K. Zhang, C. Hendrie et al., "PEAKS: powerful software for peptide de novo sequencing by tandem mass spectrometry," *Rapid Communications in Mass Spectrometry*, vol. 17, no. 20, pp. 2337–2342, 2003.
- [12] J. Tang, Y. Sun, W. K. K. Wu et al., "Propofol lowers serum PF4 level and partially corrects hypercoagulopathy in endotoxemic rats," *Biochimica et Biophysica Acta (BBA) - Proteins and Proteomics*, vol. 1804, no. 9, pp. 1895–1901, 2010.
- [13] I. T. Schrijver, H. Kemperman, M. Roest, J. Kesecioglu, and D. W. de Lange, "Beta-2-glycoprotein I as a biomarker for sepsis in critically ill patients in the intensive care unit: a prospective cohort study," *Critical Care*, vol. 24, no. 1, p. 341, 2020.
- [14] J. Gotes, K. Kasian, H. Jacobs, Z.-Q. Cheng, and S. Mink, "Lysozyme, a mediator of sepsis that deposits in the systemic vasculature and kidney as a possible mechanism of acute organ dysfunction," *Shock*, vol. 41, no. 3, pp. 256–265, 2014.
- [15] W.-J. Lee, Y.-L. Chen, Y.-W. Chu, and D.-S. Chien, "Comparison of glutathione peroxidase-3 protein expression and enzyme bioactivity in normal subjects and patients with sepsis," *Clinica Chimica Acta*, vol. 489, pp. 177–182, 2019.
- [16] N. Blaurock-Möller, M. Gröger, F. Siwczak et al., "CAAP48, a new sepsis biomarker, induces hepatic dysfunction in an in vitro liver-on-chip model," *Frontiers in Immunology*, vol. 10, 2019.
- [17] H. Wake, Y. Takahashi, Y. Yoshii et al., "Histidine-rich glycoprotein possesses antioxidant activity through self-oxidation and inhibition of hydroxyl radical production via chelating divalent metal ions in Fenton's reaction," *Free Radical Research*, vol. 54, no. 8-9, pp. 649–661, 2020.
- [18] C. Wang, Y. Cui, H. Miao et al., "Apolipoprotein A-V is a novel diagnostic and prognostic predictor in pediatric patients with sepsis: a prospective pilot study in PICU," *Mediators of Inflammation*, vol. 2020, 9 pages, 2020.
- [19] A. Mavrommatis, T. Theodoridis, A. Orfanidou, C. Roussos, V. Christopoulou-Kokkinou, and S. Zakynthinos, "Coagulation system and platelets are fully activated in uncomplicated sepsis," *Critical Care Medicine*, vol. 28, no. 2, pp. 451–457, 2000.
- [20] W. Khovidhunkit, P. N. Duchateau, K. F. Medzihradsky et al., "Apolipoproteins A-IV and A-V are acute-phase proteins in mouse HDL," *Atherosclerosis*, vol. 176, no. 1, pp. 37–44, 2004.
- [21] H. Rhode, E. Lopatta, M. Schulze et al., "Glycosylphosphatidylinositol-specific phospholipase D in blood serum: is the liver the only source of the enzyme?," *Clinica Chimica Acta*, vol. 281, no. 1-2, pp. 127–145, 1999.
- [22] S. B. Kumaraswamy, A. Linder, P. Åkesson, and B. Dahlbäck, "Decreased plasma concentrations of apolipoprotein M in sepsis and systemic inflammatory response syndromes," *Critical Care*, vol. 16, no. 2, 2012.
- [23] Z. Horváth-Szalai, P. Kustán, B. Szirmay et al., "Predictive value of serum gelsolin and Gc globulin in sepsis - a pilot study," *Clinical Chemistry and Laboratory Medicine*, vol. 56, no. 8, pp. 1373–1382, 2018.
- [24] I. Bednarz-Misa, M. Mierzchala-Pasierb, P. Lesnik et al., "Cardiovascular insufficiency, abdominal sepsis, and patients' age are associated with decreased paraoxonase-1 (PON1) activity in critically ill patients with multiple organ dysfunction syndrome (MODS)," *Disease Markers*, vol. 2019, 12 pages, 2019.
- [25] J. Yamaguchi, M. Nagase, Y. Yamamoto et al., "Increased oxidative stress and renal injury in patients with sepsis," *Journal of Clinical Biochemistry and Nutrition*, vol. 63, no. 2, pp. 137–143, 2018.
- [26] V. Nunez, D. Alameda, D. Rico et al., "Retinoid X receptor controls innate inflammatory responses through the up-regulation of chemokine expression," *Proceedings of the National Academy of Sciences of the United States of America*, vol. 107, no. 23, pp. 10626–10631, 2010.
- [27] P. Horn, U. B. Metzger, R. Steidl et al., "Chemerin in peritoneal sepsis and its associations with glucose metabolism and prognosis: a translational cross-sectional study," *Critical Care*, vol. 20, no. 1, 2016.
- [28] S. Ramadan, T. Li, W. Yang et al., "Chemical synthesis and anti-inflammatory activity of bikunin associated chondroitin sulfate 24-mer," *ACS Central Science*, vol. 6, no. 6, pp. 913–920, 2020.
- [29] Y. Wang, O. Ö. Braun, S. Zhang, L. Luo, E. Norström, and H. Thorlacius, "Dynamic changes in thrombin generation in abdominal sepsis in mice," *Shock*, vol. 42, no. 4, pp. 343–349, 2014.

- [30] D. Lendak, D. Mihajlovic, G. Mitic et al., "Complement component consumption in sepsis correlates better with hemostatic system parameters than with inflammatory biomarkers," *Thrombosis Research*, vol. 170, pp. 126–132, 2018.
- [31] R. Gao, G. Li, R. Yang, H. Yuan, and S. Zhang, "Hippocampal β 2-microglobulin mediates sepsis-induced cognitive impairment," *Molecular Medicine Reports*, vol. 17, no. 6, pp. 7813–7820, 2018.
- [32] M. Ferron, J. Cadiet, A. Persello et al., "O -GlcNAc stimulation: a new metabolic approach to treat septic shock," *Scientific Reports*, vol. 9, no. 1, 2019.
- [33] L. Gattinoni, F. Vasques, L. Camporota et al., "Understanding lactatemia in human sepsis. Potential impact for early management," *American Journal of Respiratory and Critical Care Medicine*, vol. 200, no. 5, pp. 582–589, 2019.
- [34] F. Brognara, J. A. Castania, D. P. M. Dias, A. Kanashiro, and H. C. Salgado, "Time course of hemodynamic responses to different doses of lipopolysaccharide in unanesthetized male rats," *Frontiers in Physiology*, vol. 10, 2019.
- [35] S. Zhou, G. Chen, M. Qi et al., "Gram negative bacterial inflammation ameliorated by the plasma protein beta 2-glycoprotein I," *Scientific Reports*, vol. 6, no. 1, 2016.
- [36] F. El-Assaad, M. Qi, A. K. Gordon et al., "Beta 2-glycoprotein I protects mice against gram-negative septicaemia in a sexually dimorphic manner," *Scientific Reports*, vol. 7, no. 1, p. 8201, 2017.
- [37] D. Nedelkov, "Mass spectrometric studies of apolipoprotein proteoforms and their role in lipid metabolism and type 2 diabetes," *Proteomes*, vol. 5, no. 4, p. 27, 2017.
- [38] B. Shen, X. Yi, Y. Sun et al., "Proteomic and metabolomic characterization of COVID-19 patient sera," *Cell*, vol. 182, no. 1, pp. 59–72.e15, 2020.
- [39] V. Molina, B. von Dessauer, R. Rodrigo, and C. Carvajal, "Oxidative stress biomarkers in pediatric sepsis: a prospective observational pilot study," *Redox Report*, vol. 22, no. 6, pp. 330–337, 2017.
- [40] W. Manzanares, A. Biestro, F. Galusso et al., "Serum selenium and glutathione peroxidase-3 activity: biomarkers of systemic inflammation in the critically ill?," *Intensive Care Medicine*, vol. 35, no. 5, pp. 882–889, 2009.
- [41] A. Blangy-Letheule, A. Persello, B. Rozec, M. De Waard, and B. Lauzier, "New approaches to identify sepsis biomarkers: the importance of model and sample source for mass spectrometry," *Oxidative Medicine and Cellular Longevity*, vol. 2020, Article ID 6681073, 10 pages, 2020.

Research Article

Effect of Verapamil, an L-Type Calcium Channel Inhibitor, on Caveolin-3 Expression in Septic Mouse Hearts

Bruna A. C. Rattis ^{1,2} **Ana C. Freitas** ¹ **Jordana F. Oliveira** ²
João L. A. Calandrini-Lima ² **Maria J. Figueiredo** ¹ **Danilo F. Soave** ³
Simone G. Ramos ¹ and **Mara R. N. Celes** ^{1,2}

¹Department of Pathology, Faculty of Medicine of Ribeirão Preto, University of São Paulo, Ribeirão Preto, São Paulo, Brazil

²Department of Bioscience and Technology, Institute of Tropical Pathology and Public Health, Federal University of Goiás, Goiânia, Goiás, Brazil

³Department of Morphofunctional, Faculty of Medicine of Goianesia (FAMEGO), University of Rio Verde (UniRV), Goianesia, Goiás, Brazil

Correspondence should be addressed to Mara R. N. Celes; mrubia_celes@ufg.br

Received 20 November 2020; Revised 4 March 2021; Accepted 23 March 2021; Published 9 April 2021

Academic Editor: Luc Demaison

Copyright © 2021 Bruna A. C. Rattis et al. This is an open access article distributed under the Creative Commons Attribution License, which permits unrestricted use, distribution, and reproduction in any medium, provided the original work is properly cited.

Sepsis-induced myocardial dysfunction considerably increases mortality risk in patients with sepsis. Previous studies from our group have shown that sepsis alters the expression of structural proteins in cardiac cells, resulting in cardiomyocyte degeneration and impaired communication between cardiac cells. Caveolin-3 (CAV3) is a structural protein present in caveolae, located in the membrane of cardiac muscle cells, which regulates physiological processes such as calcium homeostasis. In sepsis, there is a disruption of calcium homeostasis, which increases the concentration of intracellular calcium, which can lead to the activation of potent cellular enzymes/proteases which cause severe cellular injury and death. The purpose of the present study was to test the hypotheses that sepsis induces CAV3 overexpression in the heart, and the regulation of L-type calcium channels directly relates to the regulation of CAV3 expression. Severe sepsis increases the expression of CAV3 in the heart, as immunostaining in our study showed CAV3 presence in the cardiomyocyte membrane and cytoplasm, in comparison with our control groups (without sepsis) that showed CAV3 presence predominantly in the plasma membrane. The administration of verapamil, an L-type calcium channel inhibitor, resulted in a decrease in mortality rates of septic mice. This effect was accompanied by a reduction in the expression of CAV3 and attenuation of cardiac lesions in septic mice treated with verapamil. Our results indicate that CAV3 has a vital role in cardiac dysfunction development in sepsis and that the regulation of L-type calcium channels may be related to its expression.

1. Introduction

Sepsis is a potentially fatal organ dysfunction, characterized by an unregulated response of a host to an infection [1]. Despite significant advances in diagnosis and therapeutic approaches in recent years, sepsis remains the major cause of death in intensive care units (ICUs). A robust study from Rudd et al. showed that there are about 48.9 million cases of sepsis each year, causing 11 million deaths worldwide [2]. A study estimated that about 200,000 deaths are caused

by sepsis in Brazilian ICUs each year [3]. Sepsis patients are often affected by sepsis-induced myocardial dysfunction (SIMD), which is associated with worse prognoses and higher mortality rates when compared to patients with sepsis without SIMD [4–9]. These patients may present global biventricular dysfunction (systolic or diastolic) with reduced contractility, left ventricular dilation, and decreased response to resuscitation with fluids and catecholamines [9].

Previous results from our research group demonstrated that structural changes in cardiac cells elucidate the

physiopathology of SIMD [10]. During experimental sepsis, loss and reduction of structural protein expressions were implicated with compromised functioning of cardiac cells [10]. The reduction of connexin-43 and N-cadherin resulted in the loss of structural integrity of intercalated discs, hindering communication between myocardial cells [11]. Subsequently, cardiomyocyte degeneration and lysis of actin and myosin filaments, all caused by sepsis, were associated with reduced expression of dystrophin [12].

Dystrophin proteins act as critical components of the dystrophin-glycoprotein complex (DGC), establishing connections between the intracellular cardiac contractile machinery and the extracellular matrix. Furthermore, DGC performs three essential basic functions: stabilization of the membrane during contraction cycles, transduction of contractile force, and the organization of membrane specializations [13]. In addition to dystrophin, evidence indicates that CAV3 is localized to the sarcolemma, where it associates with the DGC [14, 15]. CAV3 is part of the caveolin group (caveolins-1, 2, and 3); caveolins-1 (CAV1) and 2 are expressed in most cell types, including adipocytes, smooth muscle cells, endothelial cells, epithelial cells, and fibroblasts whereas caveolin-3 is expressed in striated and cardiac muscle tissue [16]. These groups are concentrated in regions rich in cholesterol and sphingolipids called lipids rafts, forming the caveolae [16, 17]. The caveolae are vesicular invaginations of the plasma membrane, responsible for regulating endocytosis, exocytosis, signal transduction, mechanoprotection, cholesterol, and calcium homeostasis [16, 18, 19].

Caveolae are associated with several ion channels in cardiomyocytes, such as long-lived and voltage-dependent L-type Ca^{2+} channels (LTCCs) [19, 20]. CAV3 is colocalized with the $\alpha 1$ isoform of LTCCs in cardiomyocytes in the *Cav β* region [19, 21, 22]. Caveolae can modulate the process of excitation-contraction of cardiac cells, regulating the calcium transient and response to β -adrenergic stimulation. In addition, the loss of caveolae decreases the amplitude of the transient $[\text{Ca}^{2+}]_i$, reducing the contraction [19, 23, 24].

The loss of calcium homeostasis is harmful to the cell. The intracellular increase of this ion activates proteases, nucleases, and ATPases that lead to cell death. In vitro studies have shown a significant increase in the concentration of free intracellular calcium $[\text{Ca}^{2+}]_i$ in cardiomyocytes exposed to the serum of septic mice [25]. The role of CAV3 in septic cardiomyocytes and its relationship to calcium are still unclear. Thus, the present study is aimed at evaluating the expression of caveolin-3 in the heart of septic mice associated with verapamil treatment, an L-type calcium channel antagonist.

2. Materials and Methods

2.1. Experimental Animals. Male C57BL/6 mice, weighing 22–24 g, were maintained at ambient room temperature ($22 \pm 2^\circ\text{C}$) under a 12/12-hour light-dark cycle. They were housed at the Animal Facility of the Department of Pathology of the Faculty of Medicine of Ribeirão Preto and given standard mouse feed and water *ad libitum*. The animal protocol was approved by the Committee on Animal Research of the Faculty of Medicine of Ribeirão Preto, University of

São Paulo, Brazil (Protocol no. 083/2012). All efforts were made to minimize animal suffering.

2.2. Polymicrobial Sepsis (Cecal Ligation and Puncture (CLP) Model). A modified CLP model was used to induce polymicrobial sepsis [25]. The mice were quickly anesthetized with 2.0% isoflurane, vaporized in medical oxygen (O_2), via a face mask. The abdomen was shaved, and a midline incision was performed. The cecum was isolated and ligated with 6–0 silk thread below the ileocecal valve without causing bowel obstruction. The cecum was then punctured with an 18-gauge needle to induce severe septic injury (SSI). Bowel content was gently extruded through the puncture, and the cecum was then replaced to its original position. The abdomen was then sutured. Sham-operated animals (controls) underwent the same procedures, except for cecal ligation and puncturing. To prevent dehydration, all mice received subcutaneous doses of saline (50 mL/kg of body weight) immediately and 12 hours after the surgical procedure. For pain relief, sodium dipyrone solution (10 mg/100 g body weight, i.p.) was administered at the start of the surgery and 6–12 hours after surgery. Mice were monitored daily for signs of disease, such as piloerection, hunched gait, lethargy, and eye discharge. Mice displaying severe signs of distress (labored breathing, nonresponsiveness to cage tapping, failure of grooming, and severe eye discharge) were humanely euthanized by injecting a mixture of ketamine (90–120 mg/kg) and xylazine (10 mg/kg), followed by cervical dislocation.

2.3. Experimental Groups and Drug. For the experiments, male C57BL/6 mice were arbitrarily allocated into four groups: (1) sham, (2) SSI, (3) sham+verapamil (SH+VP), and (4) SSI+verapamil (SSI+VP). The verapamil hydrochloride (5 mg/kg body weight, Sigma-Aldrich Co., St. Louis, USA) was diluted in sterile 0.9% NaCl saline (100 μL total volume/animal) and injected intraperitoneally (i.p.) two hours after CLP surgery (SSI+VP) or the sham operation (SH+VP). Untreated control (sham) and untreated septic mice (SSI) received an equivalent volume of saline. The survival rates were monitored every 12 hours for five days after surgery using 10 animals per group (sham, SSI, SH+VP, and SSI+VP, $n = 10$ per group).

2.4. Histopathology. For the histopathology analyses, mice were euthanized with 100 μL of a 10:1 mixture of ketamine (90–120 mg/kg) and xylazine (10 mg/kg), respectively. The thoracic cavity was opened, and the heart was removed 24 hours after surgery ($n = 6$ animals/group SSI/SSI+VP and $n = 4$ animals/group sham/SH+VP). Hearts were longitudinally sectioned into two halves; one-half of the heart was fixed in phosphate-buffered 10% formalin and embedded in Histo-resin (Leica Instruments, Heidelberg, Germany) for high-resolution light microscopy. The 2 μm thick sections were stained with toluidine blue, and left ventricles were analyzed. Another half of the hearts were frozen at -80°C for the immunoblotting procedure.

2.5. Immunohistochemistry. For the immunostaining of CAV3, immunohistochemistry was performed. The slides

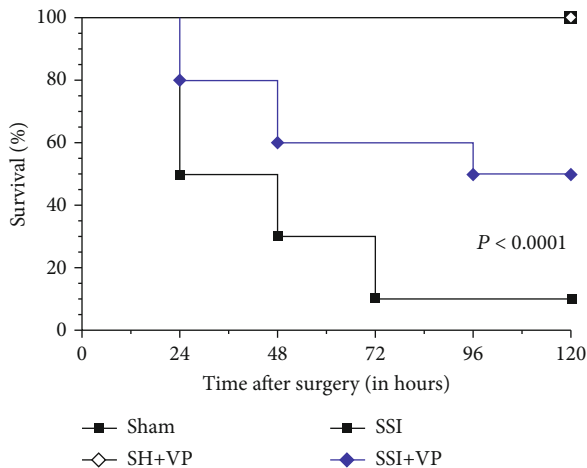


FIGURE 1: Survival curve of the mice subjected to cecal ligation and puncture (CLP) sepsis. Groups of 10 mice were submitted to sham operation (sham) or severe septic injury (SSI) and were treated with verapamil (SH+VP, SSI+VP). The survival rate was determined daily up to 120 hours after surgery. Statistical analysis was performed using the Kaplan-Meier with a Mantel-Cox (log-rank) test. Survival curves obtained with verapamil treatment (SSI+VP) were significantly different ($P < 0.001$) as compared to the sepsis group (SSI).

were deparaffinized in an oven (55°C for 30 minutes) and a xylene bath. The cuts were then hydrated in decreasing alcohol concentrations of 100%, 90%, and 70%. Subsequently, the slides were placed in warm distilled water and underwent antigenic recovery in citrate buffer (pH 6.0) at 95°C . Consecutively, the slides went to the inactivation stage of endogenous peroxidase with 3% hydrogen peroxide solution (H_2O_2) for three minutes. The slides were then incubated with 2% BSA for 25 minutes. After, sections were incubated with primary antibody (anti-caveolin-3; BD Transduction Laboratories) diluted at the concentration of 1:1000 in blocking buffer overnight (18 hours) at 4°C , in a humidified chamber. Subsequently, the sections were incubated with biotinylated secondary anti-mouse antibody (LSAB[®]+ Kit, K0675, Dako Corporation, Carpinteria, United States) for 20 minutes and then with streptavidin peroxidase solution for 20 minutes (LSAB[®]+ Kit, K0675, Dako Corporation). The reaction was developed from the chromogenic solution of diaminobenzidine (DAB) (3,3'-diaminobenzidine, Sigma) and prepared with 1 mL of substrate (hydrogen peroxide (H_2O_2) 3%) for one minute. The cuts were washed briefly in distilled water. In this process, the slides were counterstained for 30 seconds in hematoxylin and placed in a container for washing with running water for eight minutes. The cuts underwent dehydration in alcohol of 70%, 95%, and 100% and in xylene. Finally, the slides were mounted with the coverslip using the Entellan mounting medium. A 0.01 M phosphate-buffered saline solution (PBS) with pH 7.2-7.4 was used to wash the cuts.

2.6. Western Blotting. To determine the amount of CAV3 in the hearts of sham ($n = 4$), SSI ($n = 6$), SH+VP ($n = 4$), and SSI+VP ($n = 6$) mice, homogenates of left ventricles were

submitted to immunoblotting 6, 12, and 24 hours after the CLP or sham procedure. Hearts of mice were homogenized in the modified RIPA buffer lysis (Tris HCl 0.05°M (pH $^{\circ}$ 7.4); NaCl 0.15°M ; EDTA 0.001°M (pH $^{\circ}$ 8.0); SDS 0.1%) supplemented with a protease inhibitor cocktail (Sigma-Aldrich) and the phosphatase inhibitors (Na_3VO_4 0.001°M ; NaF 0.025°M ; $\text{Na}_4\text{P}_2\text{O}_7$ 0.0005°M). This buffer does not separate cytosolic protein from plasma membrane protein. Equal concentrations ($50^{\circ}\mu\text{g/well}$) of total proteins (homogenate) were resolved on 10% SDS-Page gels and transferred to a PVDF membrane (Amersham Pharmacia Biotech, Amersham, UK). The membranes were blocked with 5% albumin for two hours and incubated overnight at 4°C with the primary antibodies: anti-caveolin-3 (mouse monoclonal antibody, 1 : 10000; BD Transduction Laboratories) and anti-GAPDH (rabbit monoclonal antibody, 1 : 1000; Cell Signaling Technology). Then, the blots were washed and incubated with HRP-conjugated secondary antibodies for one hour at room temperature. Membranes were washed, developed using ECL (Amersham Pharmacia Biotech), and viewed with ChemiDoc XRS (BioRad). Image analysis was performed using the public domain ImageJ program (developed at the National Institutes of Health and available at <http://rbs.info.nih.gov/nih-image/>) with the “Gel Analysis” function. Analysis results are represented by the values of each band; each value is proportional to the integrated density value (IDV) of the specific band, which corresponds to the arbitrary unit (AU). GAPDH was used to determine equivalent loading conditions.

2.7. Statistical Analysis. Data were analyzed using the GraphPad Prism 5 statistics program (GraphPad Software Inc., San Diego, United States). Data were expressed as means \pm standard deviation (S.D.). Statistically significant differences between groups for western blot analysis were measured by one-way analysis of variance (ANOVA) followed by post hoc Tukey’s multiple comparison test (parametric data). Statistical analysis of survival curves was performed using the Kaplan-Meier with a Mantel-Cox (log-rank) test. $P < 0.05$ was considered statistically significant. All P values are demonstrated in the graphics.

3. Results

3.1. Sepsis Survival Rates. Figure 1 shows the survival rate of mice submitted to the sham operation (sham) and SSI until 120 hours after surgery. The sham (sham) and sham-treated (SH+VP) animals showed full recovery from anesthesia and maintained 100% survival until the end of the observation. The SSI mice showed a 50% survival rate 24 hours after injury, decreasing to a 10% survival rate 72 hours after surgery. Rates then remained steady until 120 hours after surgery. In contrast, the treated septic mice (SSI+VP) showed a survival rate of around 80% in 24 hours, decreasing to 50% at 96 hours. Rates then remained stable until the end of observation at 120 hours.

3.2. Effect of Verapamil Administration on Cardiac Lesions. Histopathological analyses of the heart showed that severe

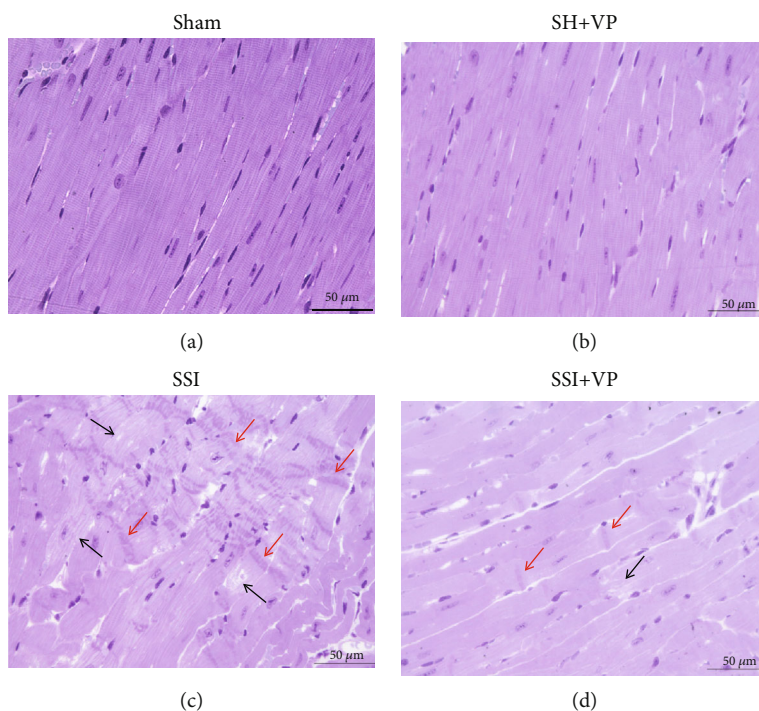


FIGURE 2: Histopathology of myocardial tissue from mice subjected to cecal ligation and puncture (CLP) sepsis. The sham-operated mice (sham and SH+VP) showed no changes (a, b). The SSI group (c) had evident disorientation of the myofibrils with the formation of contracture bands (red arrows) and myocytolysis (black arrows) as compared to the SSI+VP group (d), 24 hours after surgery. Scale bars indicate 50 μm .

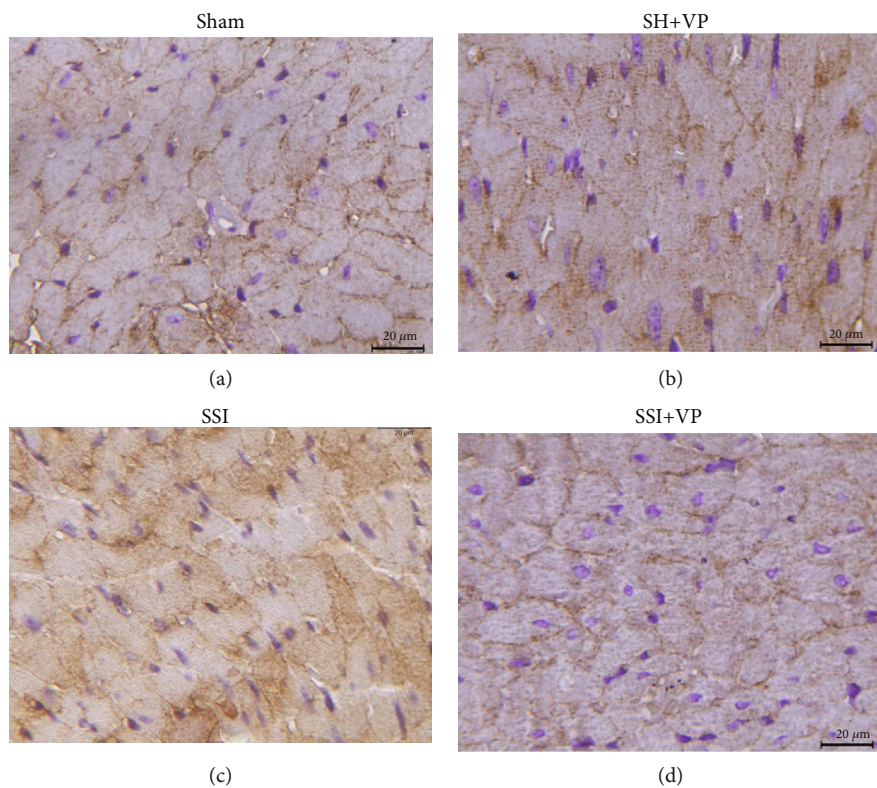


FIGURE 3: Immunolocalization of caveolin-3 in cardiac tissue 24 hours after sepsis induction. (a, b) Show the immunostaining of CAV3 on cardiomyocytes (sham and SH+VP) bounded by the plasma membrane. (c) Represents the scattered staining of CAV3 in the cytoplasm and cell membrane of septic cardiomyocytes (SSI group). (d) The septic mice treated with verapamil (SSI+VP) showed immunostaining of CAV3 more related to that observed in the control groups (sham and SH+VP). Scale bars indicate 50 μm .

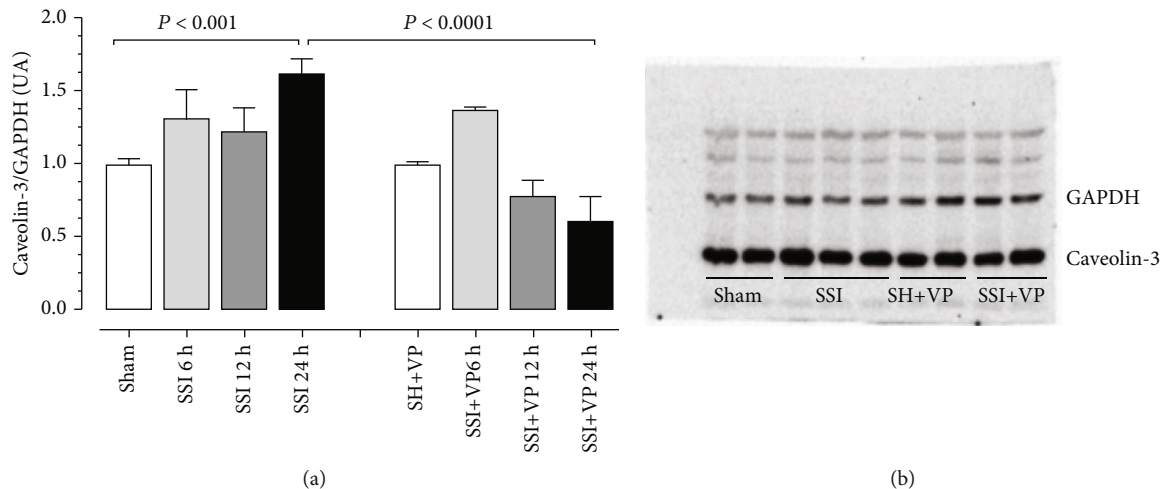


FIGURE 4: Western blot analysis of CAV3. (a) The amounts of CAV3 in the sham ($n = 4$) and SH+VP ($n = 4$) groups were measured 24 hours after sham operation. The amounts of CAV3 in the SSI ($n = 6$) and SSI+VP ($n = 6$) groups were measured 6, 12, and 24 hours after CLP surgery and expressed in arbitrary units (AUs). GAPDH was used to determine equivalent loading conditions. Note that the expression of CAV3 was significantly increased in the SSI group 24 hours after CLP as compared to SSI+VP and sham group mice. Statistical analysis was performed by one-way ANOVA followed by Tukey's test. Data were expressed as the mean \pm SD; $P < 0.0001$ (SSI vs. SSI+VP) and $P < 0.001$ (SSI vs. sham). (b) The autoradiograph resulting from western blot analysis of representative protein levels for CAV3 and GAPDH of mouse hearts, subjected to sham operation (sham, SH+VP) or sepsis induction (SSI, SSI+VP) 24 hours after surgery.

sepsis resulted in extensive lesions in the myocardium (Figure 2). After 24 hours of sepsis induction, the cardiac tissue septic group (SSI) presented regions of myofibril disorientation with the formation of contraction bands, necrosis, and an apparent rupture of the sarcolemma. However, septic mice treated with verapamil (SSI+VP) had more preserved cardiomyocytes and less cellular changes than the untreated septic group (SSI). The sham-operated mice (sham and SH+VP) showed no changes.

3.3. Effect of Verapamil Administration on Caveolin-3 Distribution in the Heart. Figure 3 shows the distribution of CAV3 in the cardiac cells 24 hours after sepsis induction. In the cardiomyocytes of the control groups (sham and SH+VP), CAV3 was delimited in the plasma membrane of the cells. The untreated septic group (SSI) presented immunostaining of CAV3 scattered throughout the cytoplasm (not membrane-bound fraction) and plasma membrane of the heart cells. In contrast, when treated with verapamil, the septic mice (SSI+VP group) showed immunostaining of CAV3 closer to that observed in the control groups (sham and SH+VP).

3.4. Effects of Verapamil Administration on Caveolin-3 Expression in the Heart. Figure 4 shows the quantitative analysis of CAV3 protein levels in the myocardium of controls (sham, SH+VP) and animals subjected to severe sepsis (SSI) and treated with verapamil (SSI+VP) 6, 12, and 24 hours after surgery. The results showed a significant increase in the levels of CAV3 expression only 24 hours after the severe sepsis induction (SSI) when compared to the values observed in the hearts of the control group (sham). For the slight increase in the levels of CAV3, 6 and 12 hours after CLP surgery, there was no statistical difference among the groups.

Additionally, septic mice treated with verapamil (SSI+VP) showed significantly reduced levels of CAV3 24 hours after CLP surgery when compared to untreated septic animals (SSI).

4. Discussion

In this study, we demonstrated for the first time that CAV3 is overexpressed in the hearts of septic mice, and the treatment with verapamil influenced the reduction of CAV3 in septic mouse hearts. Additionally, reduced expression of CAV3 led to a reduction of sepsis-induced cardiac injuries and a decreased mortality rate.

Septic patients frequently develop hypocalcemia [26]. However, calcium is essential in several physiological processes, such as excitation-contraction of cardiac cells. Thus, parenteral calcium administration could potentially generate positive results in these hypocalcemic patients [27]. Calcium supplementation in septic patients and animals has been shown to increase mortality rates and lead to organ failure [28, 29]. Interestingly, intracellular calcium concentrations are increased in sepsis; this has been associated with pathophysiological changes [30]. The displacement of calcium into the cells may be largely responsible for hypocalcemia. Although parenteral calcium administration appears to be the solution, it can contribute to organ dysfunction [26, 29].

A previous study from our research group showed an increase in $[Ca^{2+}]_i$ in cultured neonatal cardiomyocytes treated with septic animal serum [31]. Calcium overload by CLP has also been demonstrated in the heart, brain, liver, and spleen cells of septic rats [32]. The hypotheses for this increase in $[Ca^{2+}]_i$ involve failures in the channels that regulate the entry of Ca^{2+} , microruptures in the plasma

membrane, and the excessive release of Ca^{2+} by the sarcoplasmic reticulum [31, 33, 34].

However, one hypocalcemia hypothesis suggests that sepsis-induced failures in calcium channels cause an increased influx of Ca^{2+} into cells [32]. This hypothesis is supported by the fact that the administration of a calcium channel blocker results in a better prognosis and a reduction in mortality rates of septic patients [35]. These data corroborate with experimental findings; the administration of verapamil in septic animals resulted in a reduction of mortality, attenuation of cardiac lesions, reduction of intracellular calcium concentration, and attenuation of hypocalcemia [31, 32, 36]. The data from the present study also supports this hypothesis, as septic animals treated with verapamil survived longer than septic animals without treatment.

The increase in $[\text{Ca}^{2+}]_i$ activates proteases inside the cell, such as calpain. In sepsis, calpain expression in cardiomyocytes increases, with a concomitant reduction in dystrophin-glycoprotein complex (DGC) proteins [37]. The disturbance of this complex, the consequent reduction in dystrophin, and the contraction process make the cell more susceptible to mechanical stress in the plasma membrane, resulting in its rupture [38, 39]. The consequences of dystrophin reduction can be seen in Duchenne Muscular Dystrophy (DMD). DMD patients can develop cardiomyopathy with cardiac cell loss. This leads to greater vulnerability to pressure overload and can result in dilated cardiomyopathy [40]. Experimental models of DMD have shown that the loss of dystrophin causes a progressive increase in the expression of CAV3 in the plasma membrane, cytoplasm, and caveolae in muscle cells [41]. Consistent with these results, we observed that CAV3 was overexpressed in mouse hearts with sepsis, demonstrating its presence in the plasma membrane and cytoplasm through immunostaining. As previously demonstrated, this occurred even with the activation of proteases such as calpain. This indicates that CAV3 does not undergo the process of degradation mediated by calpain, as observed with dystrophin [37].

A study using the lung of septic mice (induced by the CLP model) demonstrated a reduction of CAV1, which was reported as a host cytoprotective factor to regulate the number of available caveolae that can be used by pathogens as an escape mechanism from lysosomal degradation [42]. Surprisingly, human lung endothelial cells challenged with LPS exhibited a concentration- and time-dependent increased expression of CAV1 mRNA and protein. This effect has been found to be dependent on NF- κ B activation and thereby contributes to the mechanism of microvascular permeability in sepsis [43].

The cause of CAV3 overexpression in sepsis is still unknown. Studies that induced overexpression of CAV3 in transgenic mice showed severe cardiomyocyte degeneration with reduced cardiac function, in addition to skeletal muscle damage and negative regulation of DGC; such findings are similar to those found in DMD [44, 45]. However, CAV3 knockout mice developed progressive cardiomyopathy and an incorrect DGC complex location [46]. It is surprising to see reduced CAV3 expressions in pathological cardiac conditions, such as myocardial infarction, heart failure, and hyper-

trophy [20, 47]. Our study demonstrates that cardiac changes induced by sepsis provide a different response regarding the expression of CAV3, as septic animals showed a significant increase in CAV3 levels.

There are strong indications that CAV3 regulates calcium homeostasis in cardiac cells, an important relationship in maintaining cellular physiology. One study showed the absence of slow Ca^{2+} waves in cells absent from CAV3, and this also occurred when the interaction of CAV3 with G protein was interrupted [48]. On the other hand, the induced overexpression of CAV3 interrupted the hypertrophic signaling caused by pressure overload through the inhibition of the type T calcium channel current and the suppression of the Ca^{2+} -dependent calcineurin-NFAT pathway [20].

5. Conclusions

Our results indicate that sepsis leads to increased expression of CAV3 in the heart, and the treatment with verapamil can directly or indirectly modulate its expression resulting in a reduction of mortality rates and cardiac injuries.

Data Availability

The data used to support the findings of this study are available from the corresponding authors upon request.

Conflicts of Interest

The authors declare that there is no conflict of interest regarding the publication of this paper.

Authors' Contributions

Conceptualization was handled by MRNC, BACR, ACSF, MJF, and SGR. Data curation was worked on by BACR and ACSF. Formal analysis was made by BACR, ACSF, LBM, DFS, and MRNC. Funding acquisition and resources were secured by MRNC and SGR. Investigation was taken care of by BACR, ACSF, JFO, JLLCA, MJF, and MRNC. Methodology was managed by BACR, ACSF, JFO, and JLLCA. The project was administrated by MRNC. Supervision was conducted by MRNC, SGR, LBM, and DFS. Validation was handled by BACR, ACSF, MJF, DFS, and MRNC. Visualization was made by MRNC, SGR, BACR, ACSF, and DFS. Writing (original draft) was conducted by BACR and MRNC. Writing (review and editing) was taken care of by MRNC, SGR, BACR, and DFS.

Acknowledgments

We would like to thank Lígia Grecco V.B. Santoro, Gisleine F. França, and Elaine M. Floriano for their valuable help and technical assistance during the preparation of the manuscript. This work was supported by grants from Fundação de Amparo à Pesquisa do Estado de Goiás (FAPEG) (2017/1026700006-8), Fundação de Amparo à Pesquisa do Estado de São Paulo (FAPESP) (07/58843-2), and Conselho Nacional de Desenvolvimento Científico e Tecnológico

(CNPq) (481457/2013-5, 303308/2013-3, and 134468/2017-1).

References

- [1] M. Singer, C. S. Deutschman, C. W. Seymour et al., “The third international consensus definitions for sepsis and septic shock (sepsis-3),” *JAMA*, vol. 315, no. 8, pp. 801–810, 2016.
- [2] K. E. Rudd, S. C. Johnson, K. M. Agesa et al., “Global, regional, and national sepsis incidence and mortality, 1990–2017: analysis for the Global Burden of Disease Study,” *Lancet*, vol. 395, no. 10219, pp. 200–211, 2020.
- [3] F. R. Machado, A. B. Cavalcanti, F. A. Bozza et al., “The epidemiology of sepsis in Brazilian intensive care units (the Sepsis PREvalence Assessment Database, SPREAD): an observational study,” *The Lancet Infectious Diseases*, vol. 17, no. 11, pp. 1180–1189, 2017.
- [4] A. Burton and M. D. Waisbren, “Bacteremia due to Gram-negative bacilli other than the Salmonella,” *A.M.A. Archives of Internal Medicine*, vol. 88, no. 4, p. 467, 1951.
- [5] J. E. Parrillo, “Septic shock in humans,” *Annals of Internal Medicine*, vol. 113, no. 3, pp. 227–242, 1990.
- [6] M. W. Merx and C. Weber, “Sepsis and the heart,” *Circulation*, vol. 116, no. 7, pp. 793–802, 2007.
- [7] V. C. de Souza Dantas and E. L. V. Costa, “A look at the diastolic function in severe sepsis and septic shock,” *Revista Brasileira de terapia intensiva*, vol. 27, pp. 307–308, 2015.
- [8] M. M. Wei Cheng, Y. Long, H. Wang, M. M. Wen Han, J. Zhang, and N. Cui, “Role of the mTOR signalling pathway in human sepsis-induced myocardial dysfunction,” *Canadian Journal of Cardiology*, vol. 35, no. 7, pp. 875–883, 2019.
- [9] M. L. Heureux, M. Sternberg, L. Brath, J. Turlington, and M. G. Kashouris, “Sepsis-induced cardiomyopathy: a comprehensive review,” *Current Cardiology Reports*, vol. 22, no. 5, p. 35, 2020.
- [10] M. R. N. Celes, C. M. Prado, and M. A. Rossi, “Sepsis: going to the heart of the matter,” *Pathobiology*, vol. 80, no. 2, pp. 70–86, 2013.
- [11] M. R. N. Celes, D. Torres-Dueñas, J. C. Alves-Filho, D. B. Duarte, F. Q. Cunha, and M. A. Rossi, “Reduction of gap and adherens junction proteins and intercalated disc structural remodeling in the hearts of mice submitted to severe cecal ligation and puncture sepsis,” *Critical Care Medicine*, vol. 35, no. 9, pp. 2176–2185, 2007.
- [12] M. R. N. Celes, D. Torres-Dueñas, L. M. Malvestio et al., “Disruption of sarcolemmal dystrophin and β_2 -dystroglycan may be a potential mechanism for myocardial dysfunction in severe sepsis,” *Laboratory Investigation*, vol. 90, no. 4, pp. 531–542, 2010.
- [13] K. A. Lapidus, R. Kakkar, and E. M. McNally, “The dystrophin glycoprotein complex: signaling strength and integrity for the sarcolemma,” *Circulation Research*, vol. 94, no. 8, pp. 1023–1031, 2004.
- [14] B. Van Deurs, K. Roepstorff, A. M. Hommelgaard, and K. Sandvig, “Caveolae: anchored, multifunctional platforms in the lipid ocean,” *Trends in Cell Biology*, vol. 13, no. 2, pp. 92–100, 2003.
- [15] K. E. Davies and K. J. Nowak, “Molecular mechanisms of muscular dystrophies: old and new players,” *Nature Reviews. Molecular Cell Biology*, vol. 7, no. 10, pp. 762–773, 2006.
- [16] C. M. Thomas and E. J. Smart, “Caveolae structure and function,” *Journal of Cellular and Molecular Medicine*, vol. 12, no. 3, pp. 796–809, 2008.
- [17] A. R. Busija, H. H. Patel, and P. A. Insel, “Caveolins and caveolae in the trafficking, maturation, and degradation of caveolae: implications for cell physiology,” *American Journal of Physiology. Cell Physiology*, vol. 312, no. 4, pp. C459–C477, 2017.
- [18] R. G. W. Anderson, “Potocytosis of small molecules and ions by caveolae,” *Trends in Cell Biology*, vol. 3, no. 3, pp. 69–72, 1993.
- [19] K. Balijepalli, “Caveolae, ion channels and cardiac arrhythmias,” *Progress in Biophysics and Molecular Biology*, vol. 98, no. 2–3, pp. 149–160, 2008.
- [20] Y. S. Markandeya, L. J. Phelan, M. T. Woon et al., “Caveolin-3 overexpression attenuates cardiac hypertrophy via inhibition of T-type Ca^{2+} current modulated by protein kinase $C\alpha$ in cardiomyocytes,” *Journal of Biological Chemistry*, vol. 290, no. 36, pp. 22085–22100, 2015.
- [21] H. Abriel, J.-S. Rougier, and J. Jalife, “Ion channel macromolecular complexes in cardiomyocytes: roles in sudden cardiac death,” *Circulation Research*, vol. 116, no. 12, pp. 1971–1988, 2015.
- [22] J. S. Rougier and H. Abriel, “Cardiac voltage-gated calcium channel macromolecular complexes,” *Biochimica et Biophysica Acta (BBA) - Molecular Cell Research*, vol. 1863, no. 7, pp. 1806–1812, 2016.
- [23] S. Calaghan and E. White, “Caveolae modulate excitation-contraction coupling and β_2 -adrenergic signalling in adult rat ventricular myocytes,” *Cardiovascular Research*, vol. 69, no. 4, pp. 816–824, 2006.
- [24] A. Barbuti, B. Terragni, C. Brioschi, and D. DiFrancesco, “Localization of f-channels to caveolae mediates specific β_2 -adrenergic receptor modulation of rate in sinoatrial myocytes,” *Journal of Molecular and Cellular Cardiology*, vol. 42, no. 1, pp. 71–78, 2007.
- [25] K. A. Wichterman, A. E. Baue, and I. H. Chaudry, “Sepsis and septic shock—a review of laboratory models and a proposal,” *The Journal of Surgical Research*, vol. 29, no. 2, pp. 189–201, 1980.
- [26] T. Steele, R. Kolamunnage-Dona, C. Downey, C. H. Toh, and I. Welters, “Assessment and clinical course of hypocalcemia in critical illness,” *Critical Care*, vol. 17, no. 3, p. R106, 2013.
- [27] R. M. Forsythe, C. B. Wessel, T. R. Billiar, D. C. Angus, and M. R. Rosengart, “Parenteral calcium for intensive care unit patients,” *Cochrane Database of Systematic Reviews*, vol. 4, 2008.
- [28] D. I. A. N. A. S. MALCOLM, G. A. R. Y. P. ZALOGA, and J. O. H. N. W. HOLADAV, “Calcium administration increases the mortality of endotoxic shock in rats,” *Critical Care Medicine*, vol. 17, no. 9, pp. 900–903, 1989.
- [29] R. D. Collage, G. M. Howell, X. Zhang et al., “Calcium supplementation during sepsis exacerbates organ failure and mortality via calcium/calmodulin-dependent protein kinase signaling,” *Critical Care Medicine*, vol. 41, no. 11, pp. e352–e360, 2013.
- [30] S. K. Song, I. E. Karl, J. J. Ackerman, and R. S. Hotchkiss, “Increased intracellular Ca^{2+} : a critical link in the pathophysiology of sepsis?,” *Proceedings of the National Academy of Sciences of the United States of America*, vol. 90, no. 9, pp. 3933–3937, 1993.
- [31] M. R. N. Celes, L. M. Malvestio, S. O. Suadicani et al., “Disruption of calcium homeostasis in cardiomyocytes underlies

- cardiac structural and functional changes in severe sepsis,” *PLoS One*, vol. 8, no. 7, p. e68809, 2013.
- [32] W. He, L. Huang, H. Luo, Y. Zang, Y. An, and W. Zhang, “Hypocalcemia in sepsis: analysis of the subcellular distribution of Ca²⁺ in septic rats and LPS/TNF- α -treated HUVECs,” *Journal of Infection in Developing Countries*, vol. 14, no. 8, pp. 908–917, 2020.
- [33] M. Fanchaouy, E. Polakova, C. Jung, J. Ogrodnik, N. Shirokova, and E. Niggli, “Pathways of abnormal stress-induced Ca²⁺ influx into dystrophic *_mdx_* cardiomyocytes,” *Cell Calcium*, vol. 46, no. 2, pp. 114–121, 2009.
- [34] M. Sepúlveda, L. A. Gonano, M. Viotti et al., “Calcium/calmodulin protein kinase II-dependent ryanodine receptor phosphorylation mediates cardiac contractile dysfunction associated with sepsis,” *Critical Care Medicine*, vol. 45, no. 4, pp. e399–e408, 2017.
- [35] C. C. Lee, M. T. G. Lee, W. C. Lee et al., “Preadmission use of calcium channel blocking agents is associated with improved outcomes in patients with sepsis,” *Critical Care Medicine*, vol. 45, no. 9, pp. 1500–1508, 2017.
- [36] E. Wyska, “Pretreatment with R(+)-verapamil significantly reduces mortality and cytokine expression in murine model of septic shock,” *International Immunopharmacology*, vol. 9, no. 4, pp. 478–490, 2009.
- [37] A. C. S. Freitas, M. J. Figueiredo, E. C. Campos et al., “Activation of both the calpain and ubiquitin-proteasome systems contributes to septic cardiomyopathy through dystrophin loss/disruption and mTOR inhibition,” *PLoS One*, vol. 11, no. 11, p. e0166839, 2016.
- [38] N. W. Andrews, P. E. Almeida, and M. Corrotte, “Damage control: Cellular mechanisms of plasma membrane repair,” *Trends in Cell Biology*, vol. 24, no. 12, pp. 734–742, 2014.
- [39] T. A. Meyers and D. W. Townsend, “Cardiac pathophysiology and the future of cardiac therapies in duchenne muscular dystrophy,” *International Journal of Molecular Sciences*, vol. 20, no. 17, p. 4098, 2019.
- [40] M. T. Tayeb, “Deletion mutations in Duchenne muscular dystrophy (DMD) in Western Saudi children,” *Saudi Journal of Biological Sciences*, vol. 17, no. 3, pp. 237–240, 2010.
- [41] S. Repetto, M. Bado, P. Broda et al., “Increased number of caveolae and caveolin-3 overexpression in Duchenne muscular dystrophy,” *Biochemical and Biophysical Research Communications*, vol. 261, no. 3, pp. 547–550, 1999.
- [42] A. Kataki, I. Karagiannidis, N. Memos et al., “Host’s endogenous caveolin-1 expression is downregulated in the lung during sepsis to promote cytoprotection,” *Shock*, vol. 50, no. 2, pp. 199–208, 2018.
- [43] C. Tiruppathi, J. Shimizu, K. Miyawaki-Shimizu et al., “Role of NF- κ B-dependent Caveolin-1 Expression in the Mechanism of Increased Endothelial Permeability Induced by Lipopolysaccharide,” *Journal of Biological Chemistry*, vol. 283, no. 7, pp. 4210–4218, 2008.
- [44] F. Galbiati, D. Volonte, J. B. Chu et al., “Transgenic overexpression of caveolin-3 in skeletal muscle fibers induces a Duchenne-like muscular dystrophy phenotype,” *Proceedings of the National Academy of Sciences of the United States of America*, vol. 97, no. 17, pp. 9689–9694, 2000.
- [45] B. Aravamudan, D. Volonte, R. Ramani et al., “Transgenic overexpression of caveolin-3 in the heart induces a cardiomyopathic phenotype,” *Human Molecular Genetics*, vol. 12, no. 21, pp. 2777–2788, 2003.
- [46] S. E. Woodman, D. S. Park, A. W. Cohen et al., “Caveolin-3 Knock-out Mice Develop a Progressive Cardiomyopathy and Show Hyperactivation of the p42/44 MAPK Cascade,” *Journal of Biological Chemistry*, vol. 277, no. 41, pp. 38988–38997, 2002.
- [47] E. C. Feiner, P. Chung, J. F. Jasmin et al., “Left ventricular dysfunction in murine models of heart failure and in failing human heart is associated with a selective decrease in the expression of caveolin-3,” *Journal of Biological Chemistry*, vol. 17, no. 3, pp. 253–263, 2011.
- [48] Y. Guo, U. Golebiewska, and S. Scarlata, “Modulation of Ca²⁺ Activity in Cardiomyocytes through Caveolae-G α_q Interactions,” *Biophysical Journal*, vol. 100, no. 7, pp. 1599–1607, 2011.

Research Article

Anti-inflammatory Effects of *S. cumini* Seed Extract on Gelatinase-B (MMP-9) Regulation against Hyperglycemic Cardiomyocyte Stress

Neha Atale ¹, Chandra Bhushan Mishra ², Shrey Kohli,³ Raj Kumar Mongre ²,
Amresh Prakash ⁴, Sweta Kumari,⁵ Umesh C. S. Yadav ⁶, Raok Jeon ²,
and Vibha Rani ¹

¹Department of Biotechnology, Jaypee Institute of Information Technology, A-10, Sector-62, Noida, 201307 Uttar Pradesh, India

²College of Pharmacy, Sookmyung Women's University, Hyochangwon-gil 52, Yongsan-13 Gu, Seoul 140-742, Republic of Korea

³Institute for Laboratory Medicine, Clinical Chemistry and Molecular Diagnostics, University of Leipzig (Medical Faculty), Leibnizstr. 27, 04103 Leipzig, Germany

⁴Amity Institute of Integrative Sciences and Health, Amity University, Gurgaon 122413, Haryana, India

⁵Division of Biochemistry, Indian Agricultural Research Institute (IARI), Pusa Campus, 110012, New Delhi, India

⁶School of Life Sciences, Central University of Gujarat, Sector-30, Gandhinagar, 382030 Gujarat, India

Correspondence should be addressed to Raok Jeon; rjeon@sookmyung.ac.kr and Vibha Rani; vibha.rani@jiit.ac.in

Received 5 September 2020; Revised 4 December 2020; Accepted 16 February 2021; Published 4 March 2021

Academic Editor: Christian Jung

Copyright © 2021 Neha Atale et al. This is an open access article distributed under the Creative Commons Attribution License, which permits unrestricted use, distribution, and reproduction in any medium, provided the original work is properly cited.

Black berry (*Syzygium cumini*) fruit is useful in curing diabetic complications; however, its role in diabetes-induced cardiomyopathy is not yet known. In this study, we investigated the regulation of gelatinase-B (MMP-9) by *S. cumini* methanol seed extract (MSE) in diabetic cardiomyopathy using real-time PCR, RT-PCR, immunocytochemistry, gel diffusion assay, and substrate zymography. The regulatory effects of MSE on NF- κ B, TNF- α , and IL-6 were also examined. Identification and estimation of polyphenol constituents present in *S. cumini* extract were carried out using reverse-phase HPLC. Further, *in silico* docking studies of identified polyphenols with gelatinase-B were performed to elucidate molecular level interaction in the active site of gelatinase-B. Docking studies showed strong interaction of *S. cumini* polyphenols with gelatinase-B. Our findings indicate that MSE significantly suppresses gelatinase-B expression and activity in high-glucose- (HG-) stimulated cardiomyopathy. Further, HG-induced activation of NF- κ B, TNF- α , and IL-6 was also remarkably reduced by MSE. Our results suggest that *S. cumini* MSE may be useful as an effective functional food and dietary supplement to regulate HG-induced cardiac stress through gelatinase.

1. Introduction

Syzygium cumini, a seasonal perishable berry, commonly known as malabar plum, belongs to the family Myrtaceae. The plant is native to Asia and Oceanic regions, mainly India, China, and New Zealand. It is also grown in East Africa, South America, and tropical parts of the USA [1, 2]. The purple fruits of jamun are used for the processing of chips, vinegar, jams, smoothies, and squashes and hold a significant position in the functional food industry. Besides the fruits, other parts of the plant also have been found useful in treat-

ing chronic diseases including diabetes-related complications [3, 4]. The plant of *S. cumini*, especially its fruit, is considered a functional food, as it consists of plenty of polyphenols such as gallic acid, quercetin, β -sitosterol, eicosane, diphenic acid, ellagic acid, isoquercetin, and myricetin, which may facilitate healthy benefits against diabetes-induced detrimental changes and also reduce the risk of neurological and cardiovascular diseases (CVDs) [5]. These molecules are known for their anti-inflammatory, antihyperlipidemic, antioxidative, free radical scavenging, and antidiabetic potential [6]. Further studies have shown that *S. cumini* seed extracts function

as a chemopreventive agent against DNA damages and also have antimutagenic as well as antigenotoxic effects [7].

Cardiac stress has become a leading cause of morbidity and mortality among people with type 2 diabetes. Diabetic individuals have two to four times greater risks of cardiac arrest than nondiabetic people [8, 9]. The alarming rate of diabetes incidences and its impact on the heart make diabetic cardiomyopathy a challenging health condition worldwide. However, the effect of *S. cumini* seed polyphenolic constituents on diabetes-induced cardiac stress is not known. Thus, it is important to study the effect of MSE against diabetes-induced cardiac stress along with its mechanism of action which may open a new way for the management of cardiomyopathy.

Hyperglycemia is known to cause cardiac stress, which eventually leads to cardiomyopathy through increased activity of matrix metalloproteinases (MMPs) and extracellular matrix (ECM) remodeling [10]. MMPs are a family of secreted and membrane-bound zinc and calcium-dependent endopeptidases, which include collagenases, gelatinases, stromelysins, matrilysins, and a few peptidases [11–13]. The variation in the expression of MMPs and endogenous tissue inhibitors of matrix metalloproteinases (TIMPs), especially TIMP-1 and TIMP-2, may lead to the pathophysiology of various diseases including cardiovascular diseases, cancer, diabetes, and neurodegenerative disorders [14]. TIMPs act as inhibitors for active MMPs by binding to the Zn^{2+} in its catalytic domain [14, 15]. Their production is regulated by a variety of mediators including cytokines, chemokines, hormones, and growth factors [16]. The inflammatory cytokines and growth factors released at tissue damage sites lead to the enhancement of the expression of MMP-9 and among which $TNF-\alpha$ is found to be a potent stimulator of MMP-9 transcription and atherosclerosis [17].

The central role of MMPs in ECM remodeling, therefore, makes them a potential drug target in diabetic cardiomyopathy [18, 19]. One of the critical MMPs known to be activated in diabetes is MMP-9, the largest and the most complex member which otherwise remains latent in healthy hearts. During diabetic cardiomyopathies, gelatinase-B also called MMP-9 activated via Ras/Raf/MEK/ERK signaling cascade causes extensive degradation of ECM and decreases matrix turnover, which is associated with several cardiac abnormalities and heart failure [20]. Although there has been a big thrust towards the development of synthetic MMP inhibitors, their safe implementation and testing in successful clinical trials is still a challenge [21].

Overwhelming evidence from epidemiological, *in vivo*, *in vitro*, and clinical studies indicates that plant-based functional foods not only provide basic nutrition but also have the potential to suppress diseases and ensure good health and longevity. Therefore, efforts to identify new plant-based MMP inhibitors, with less toxicity and more specificity, are required [22]. To date, specific studies revealed the inhibition of MMPs by several natural products such as dietary gallic acid, epigallocatechins, anthocyanins, curcumin, and caffeic acid in various pathological conditions [23, 24].

Syzygium cumini has been extensively studied for its nutrient composition and found to be enriched with polyphenols and could serve as a source of a potential MMP inhibitor that can be effective in HG-induced cardiac stress [6, 25]. Our previous studies found that *S. cumini* MSE significantly suppressed the HG-induced stress in H9C2 cardiomyocytes by reducing mitochondrial membrane potential, reactive oxygen species (ROS) overproduction, and collagen levels, suggesting its potential as a functional food and supplementary diet to diabetic patients for suppression of cardiac stress [26]. In the present study, we have examined the role of MSE as well as the purified component of seed extract on MMP-9 expression and activity in HG-stressed cardiomyocytes. Our current study also proposes *S. cumini* to be a potent MMP inhibitor and a therapeutic agent in diabetes-induced cardiac complications.

2. Materials and Methods

A schematic representation of the methodology used in the present study is illustrated in Fig. S1.

2.1. Chemicals. All chemicals were purchased from Sigma Aldrich (St. Louis, MO, USA). All the antibodies were purchased from Santa Cruz Biotechnology Inc. (Dallas, TX, USA).

2.2. Seed Collection. *S. cumini* seeds were procured from a local vendor in the month of July-August and were authenticated by Dr. Anshu Rani, an eminent botanist, Department of Botany, Govt. P.G. College, Abu Road, Rajasthan, India. Further, the seeds were washed, ground, and dried.

2.3. Preparation of Methanol Extract of *S. cumini* Seeds. The methanol extract of *S. cumini* seeds (MSE) was prepared by using the Soxhlet solvent extraction method. Seed powder (20 g) was mixed with 200 ml methanol. The temperature was set at its boiling point ($64.7^{\circ}C$), and 12–14 cycles were run for complete extraction. After solvent evaporation in a rotary evaporator, the dried powder was reconstituted at the concentration of 1 mg/ml in molecular-grade water.

2.4. Cell Culture. The rat heart-derived H9C2 cardiomyoblast cells were obtained from the National Centre for Cell Science (NCCS), Pune, India (originally from ATCC, USA). H9C2 cells were cultured with Dulbecco's modified Eagle's medium (DMEM) supplemented with penicillin (100 unit/ml), streptomycin (100 μ g/ml), glucose (5.5 mM), L-glutamine (2 mmol/l), sodium bicarbonate (3.7 g/l), 10% fetal bovine serum (FBS), insulin (50 mg/ml), transferrin (27.5 mg/ml), selenium (0.025 mg/ml), and amphotericin B (5 μ g/ml) in a humidified CO_2 incubator (New Brunswick Scientific, NJ, USA) with 5% CO_2 at $37^{\circ}C$ [27].

2.5. Treatment of Cells with Glucose, *S. cumini* MSE, and Gallic Acid (GAL). H9C2 cells were induced with optimized doses of glucose and *S. cumini* MSE as standardized in our previous studies [28]. The gallic acid was used as a purified equivalent in all the experiments. Our study included six groups: (a) control (untreated) cells, (b) cells induced with

4.5 mg/ml glucose (HG), (c) high-glucose-induced cells treated with *S. cumini* MSE (9 μ g/ml) (HG+MSE), (d) MSE-treated cells (MSE), (e) high-glucose-induced cells treated with gallic acid (3.4 μ g/ml) (HG+GAL), and (f) gallic acid-treated cells (GAL).

2.6. Cell Viability Assay. Cell viability was determined by a 3-(4,5-dimethyl-thiazol-2-yl)-2,5-diphenyl tetrazolium bromide (MTT) assay (Ferrari, Fornasiero & Isetta, 1990). Approximately 8×10^3 H9C2 cells were seeded in 96-well plates. The H9C2 cells were treated as described above and incubated for 48 h at 37°C in a humidified incubator containing 5% CO₂. After completion of incubation, 10 μ l MTT (5 mg/ml) was added, and cells were further incubated for 3 h. The culture supernatant was then discarded, and formazan crystals were dissolved in 100 μ l DMSO. Absorbance was measured through an ELISA plate reader (ThermoFisher Scientific Inc., Waltham, MA, USA) at 570 nm. Cell viability was defined in relation to control cells as the ratio of absorbance of the treated sample to absorbance of the control sample.

2.7. Haematoxylin-Eosin (H&E) Staining. The H&E staining was performed for the determination of morphology of cells. H9C2 cells were seeded in six-well plates as per the experimental sets described earlier and incubated for 48 h. Subsequently, cells were washed with cold phosphate-buffered saline (PBS) and fixed with 100% chilled (-20°C) methanol. Haematoxylin (0.5% alcoholic solution) was added and incubated for 30 min at 25°C. After washing twice with PBS at room temperature, cells were counterstained with 5% eosin, washed, and mounted. The cells were observed under a light microscope, and images were captured at 40x magnification. The stained cells were eluted with 0.1 N NaOH, and the absorbance of samples was measured at 560 nm.

2.8. Extraction of Total Cell Protein. After completion of 48 h of incubation, cells were harvested and washed with cold PBS. The cell pellet was lysed in precooled 1x RIPA buffer (50 mM Tris-HCl (pH 7.5), 150 mM NaCl, 500 mM Na₂EDTA, 1 mM EGTA, 1% NP-40, 1% sodium deoxycholate, 2.5 mM sodium pyrophosphate, and protease inhibitor cocktail (104 mM AEBSF, 80 μ M aprotinin, 4 mM bestatin, 1.4 mM E-64, 2 mM leupeptin, and 1.5 mM pepstatin A) on ice for 1 h. The cell lysate was centrifuged at 13000 \times g for 15 min at 4°C in a refrigerated centrifuge. The concentration of total cell proteins in supernatant was estimated by a Bradford assay.

2.9. Gel Diffusion Assay. A solution containing 1.5% agarose, digestion buffer (50 mM Tris-Cl (pH 7.4), 150 mM NaCl, 5 mM CaCl₂, and 0.02% Brij-45), and 1 mg/ml gelatin was poured on a gel plate and allowed to solidify. An equal amount of protein (30 μ g/ml) from various experimental sets were loaded into wells punched in the solidified agarose gel and incubated overnight at 37°C. Zones of gelatin digestion were detected by staining the agarose gel in a solution containing 0.25% Coomassie Brilliant Blue R-250. The enzymatic activity was estimated as a function of the diameter of the digested zone compared to standard trypsin.

2.10. Zymographic Analysis of MMP-9 Production. The equal amount of protein (30 μ g/ml) from different experimental sets was mixed with 2x sample buffer (0.005% Bromophenol Blue, 20% glycerol, 4% SDS, 100 mM Tris-Cl (pH 6.8)) in equal proportion and subjected to electrophoresis in 10% polyacrylamide gel containing gelatin (1 mg/ml). After washing with 2.5% Triton X-100, the gels were incubated in digestion buffer, stained with 0.25% Coomassie Brilliant Blue R-250, and further destained to visualize gelatinolytic activities in zymogram which was observed as transparent bands against the background of Coomassie Blue-stained gelatin containing gel. The quantitation was done using NIH ImageJ software.

2.11. Cell In Situ Zymography. H9C2 cells were cultured on coverslips and were fixed with chilled (-20°C) methanol and implanted in the uniformly spread mixture of 0.5% agarose containing 0.1% fluorescein-conjugated gelatin on the glass slides. The cells were incubated at 37°C for 1 h in developing buffer (50 mM Tris-Cl (pH 7.4), 150 mM NaCl, 5 mM CaCl₂, 0.02% Brij-45) and visualized under a fluorescent microscope (Olympus Corporation, TYO, Japan). Images were captured at 40x magnification.

2.12. Immunocytochemistry. H9C2 cells were grown on coverslips under different experimental conditions and fixed with methanol. After washing the cells with PBS, blocking was done for 1 h at room temperature (25°C) using 3% BSA prepared in PBS followed by incubation with primary antibodies (against MMP-9, NF- κ B, GAPDH, and Lamin A/C) for 1 h at 37°C. Subsequently, cells were stained with FITC-conjugated secondary anti-goat antibody under similar conditions. Nuclei were counterstained with 4',6-diamidino-2-phenylindole (DAPI) as described previously [29] and observed under a fluorescent microscope (Olympus Corporation, TYO, Japan). Images were captured using a Progress capture camera fitted to the microscope. Overlay images were obtained by NIH ImageJ software.

2.13. RT-PCR. After completion of incubation, total RNA was extracted using a TRIzol reagent (Invitrogen Carlsbad, CA, USA) as per the manufacturer's manual. Reverse transcription of all sets with 0.1 μ g total RNA was performed using a RevertAid H Minus First Strand cDNA Synthesis Kit (ThermoFisher Scientific Inc., Waltham, MA, USA) as per instructions provided. The cDNA samples were diluted to 20 ng/ μ l. The thermal cycling conditions were composed of an initial denaturation step at 95°C for 5 min followed by 30 cycles at 95°C for 30 s each, the respective annealing temperature for 30 s and 72°C for 30 s, and a final extension of 10 min at 72°C. Amplified products were resolved on 2% agarose gels and visualized by ethidium bromide staining using GelDoc (BioRad Laboratories, CA, USA). The primer sequences for specific genes and their respective annealing temperatures were as follows: MMP-9: 5'-CACCGCTCACC TTCACCCG-3' (F), 5'-TGCCGAGTTGCCCCAGTTA-3' (R), 66°C; TNF- α : 5'-AGAAAGTCAGCCTCCTCTCC-3' (F), 5'-ACTCCAAAGTAGACCTGCCC-3' (R), 56°C; IL-6: 5'-CCTACCCCAACTTCCAATGCTC-3' (F), 5'-TTGGAT

GGTCTTGGTCCTTAGCC-3' (R), 58.5°C; and β -Actin: 5'-CATCGTACTCCTGCTTGCTG-3' (F), 5'-CCTCTATGC CAACACAGTGC-3' (R), 57.5°C. To further validate the semiquantitative results, qRT-PCR was carried out using SYBR Green PCR master mix of the PikoReal™ Real-Time PCR System (ThermoFisher Scientific Inc. Waltham, MA, USA). Upon completion, fold changes in gene expression were calculated by a delta delta Ct ($\Delta\Delta$ Ct) method. The fold change in gene expression was normalized to an internal β -actin control gene.

2.14. HPLC Analysis. Methanol extract of *S. cumini* seeds and 10 standards, namely, ellagic acid, gallic acid, p-coumaric acid, quercetin, protocatechuic acid, sinapic acid, caffeic acid, kaempferol, ferulic acid, and p-hydroxybenzoic acid (Sigma-Aldrich, St. Louis, MO, USA), was subjected to HPLC analysis by using Shimadzu LC instrument equipped with Hypersil C-18 column and PDA detector (Shimadzu Corporation, Kyoto, Japan). Mobile phase containing methanol/acetonitrile (98/2 v/v) was used to perform HPLC analysis [30–32]. The flow rate was set at 0.5 ml/min, and the absorbance used for this study was 254 nm. 100 μ l MSE, taken from 150 ml stock solution obtained from 10 g *S. cumini* seed powder, was diluted with 900 μ l HPLC-grade methanol and filtered through 0.2 μ filter (Millipore, MA, USA). From the diluted stock, 20 μ l was used for HPLC analysis. For HPLC analysis of the standards, 1 mg/ml stocks were prepared in methanol, and 20 μ l of each standard was subjected to HPLC analysis. The concentration of each component of the extract was calculated by using the area of different standards individually. The results are represented as the mean \pm SD, and each experiment is performed in triplicate.

2.15. Molecular Docking. AutoDock Vina was used for docking studies [33]. The X-ray crystallographic structure of MMP-9 (Pdb Id 4H82) was selected from the protein structure database (protein data bank RCSB PDB). The ligand molecular structure of ellagic acid, gallic acid, p-coumaric acid, quercetin, protocatechuic acid, sinapic acid, caffeic acid, kaempferol, ferulic acid, and p-hydroxybenzoic acid was designed and 3D optimized using ACD/ChemSketch 12.0. A grid box of 20 \times 20 \times 20 points was generated around the active site coordinates of MMP-9 protein. The binding free energies of the ligand-protein interactions were also calculated using the best-predicted conformations in the bounded state and compared with binding free energies of MMP-9-doxycycline interactions [34–39].

2.16. Statistical Analysis. The data are expressed as means \pm SD. Statistical analysis was performed using SPSS 16 software. Statistical comparisons were made with one-way ANOVA with Tukey's test. All the results were considered significant with a *p* value \leq 0.05. Each experiment was conducted in triplicates and repeated thrice.

3. Results

3.1. *S. cumini* Prevents Glucose-Induced Cardiac Stress. To evaluate the protective effect of *S. cumini* on glucose-

induced cardiac stress, H9C2 cardiomyocytes were treated with high glucose (4.5 mg/ml, 25 mM) alone or high glucose concomitantly with *S. cumini* MSE. Gallic acid which is a known cardioprotective agent under diabetes conditions was used as a positive control. Morphological assessment by H&E staining showed that although high-glucose treatment results in about 1.5-fold increase in cell size, treatment with MSE prevented the increase in cell size as effective as gallic acid treatment (Figure 1). Furthermore, neither MSE nor gallic acid resulted in any cytotoxic or morphological alterations indicating that either treatment does not exert any harmful effects on cardiac cells themselves but are protective under glucose-induced stress conditions.

3.2. *S. cumini* Prevents Glucose-Induced Gelatinase Activity in H9C2 Cardiomyocytes. Cardiac remodeling involving molecular changes that manifest as increased cell size under disease conditions is known to be regulated by ECM remodeling matrix metalloproteinases (MMPs 2 & 9), popularly known as gelatinases. We, therefore, studied whether the protective effect of *S. cumini* MSE is regulated by these gelatinases. We first studied the ability of lysates from H9C2 cardiomyocytes to digest gelatin as a substrate in a gel-diffusion assay evaluated by the area of the digestion zone (Figure 2(a)). We found that treatment with high glucose resulted in an enhanced gelatinase activity (equivalent to 102 U trypsin) compared to untreated controls (equivalent to 45 U trypsin) which was prevented upon concomitant treatment with *S. cumini* MSE (equivalent to 55 U trypsin). Likewise, gallic acid was also protective against glucose-induced gelatinase activity (equivalent to 58 U trypsin), and gallic acid or MSE treatment alone did not result in any significant change in gelatinase activity (equivalent to 49 U and 50 U trypsin, respectively) compared to controls. We then performed gelatin zymography using protein lysates under similar experimental conditions to evaluate the MMP activity (Figure 2(b)). We found similar results as obtained above where high-glucose treatment resulted in enhanced MMP activity which was prevented by concomitant treatment with *S. cumini* MSE or gallic acid. In order to further confirm the protective effects of *S. cumini* MSE on glucose-induced MMP activity, we then performed cell *in situ* zymography to map the in-position cell matrix metalloproteinase activity using FITC-conjugated gelatin (Figure 2(c)). We found that cells treated with high glucose alone were much more efficient in digesting FITC-gelatin resulting in enhanced fluorescence intensity compared to controls indicating an increased MMP activity. Intriguingly, treatment with either *S. cumini* MSE or gallic acid under high-glucose conditions resulted in only a weak fluorescence signal indicating a reduced MMP activity, and either treatment was protective. Akin to the results obtained above, MSE or gallic acid treatment alone did not have any significant effect on MMP activity compared to the control. Overall, these results suggested that *S. cumini* MSE exerts an inhibitory effect on glucose-induced MMP activity in cardiomyocytes which was as competent as gallic acid, a previously known cardioprotective agent as well as a phytochemical of *S. cumini*.

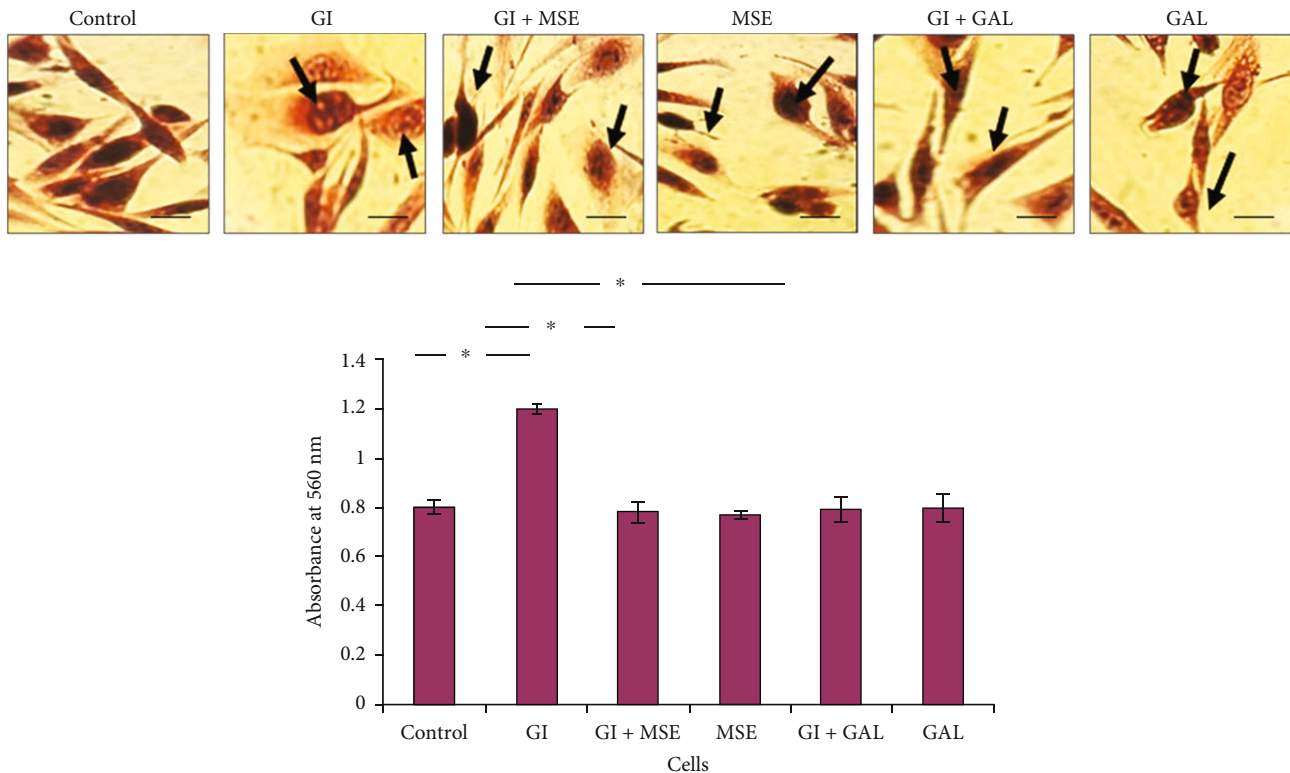


FIGURE 1: Morphological analysis in H9C2 cells by haematoxylin-eosin (H&E) staining. Light-field micrographs (40x magnifications) showing an increase in cell size in high-glucose- (HG-) induced H9C2 cells, and *S. cumini* methanol seed extract (MSE) treatment prevented such increase as indicated by arrows. Gallic acid treatment also showed decreased cell size near the control. Quantitation of cell size was represented by histogram (* $p \leq 0.05$). Scale bar: 20 μ .

3.3. *S. cumini* Prevents Glucose-Induced Gelatinase-B Expression in H9C2 Cardiomyocytes. Although a generalized MMP activation in cardiomyopathies has been witnessed, a specific induction of gelatinase-B has been reported in diabetic cardiomyopathy. We therefore selected gelatinase-B as a potential therapeutic target for further assessment. Semi-quantitative RT-PCR as well as qRT-PCR analysis showed that high-glucose treatment results in an elevated mRNA expression of gelatinase-B compared to the control (Figure 3(a)). Furthermore, treatment with *S. cumini* MSE under high-glucose conditions significantly prevented the increase in gelatinase-B mRNA expression. Intriguingly, this inhibitory effect of *S. cumini* MSE on gelatinase-B mRNA expression was stronger as compared to that of gallic acid. Immunohistochemistry analysis of H9C2 cardiomyocytes treated under similar conditions showed that *S. cumini* MSE treatment under high-glucose conditions prevented the increase in gelatinase-B protein expression (Figure 3(b)). Taken together, these results suggested that *S. cumini* MSE suppresses the gelatinase-B protein as well as mRNA expression in high-glucose-treated H9C2 cardiomyocytes.

3.4. *S. cumini* Prevents Glucose-Induced NF- κ B Nuclear Translocation and Cardiac Inflammation. MMP expression has been shown to be regulated by redox-sensitive transcription factor NF- κ B. Importantly, we observed that *S. cumini* treatment altered not only gelatinase-B protein expression but also its mRNA expression. This indicated that the protec-

tive effect of *S. cumini* on gelatinase-B could be regulated at the transcriptional level. NF- κ B transcriptional activity is dependent upon its translocation to the nucleus. Therefore, we studied the nuclear localization of NF- κ B protein using antibodies of p65 (RelA) subunit of NF- κ B protein by immunoblotting (Figure 4). We observed that upon high-glucose treatment, NF- κ B translocated more from the cytoplasm to the nucleus compared to controls indicating its activation. However, treatment of *S. cumini* along with high glucose shows a reduced localization of NF- κ B in the nucleus compared to the cytoplasm and was similar to that observed in controls. Similarly, gallic acid treatment under high glucose conditions also showed its predominant localization in the cytoplasm indicating its reduced activation. These results suggested that *S. cumini* MSE treatment inhibits NF- κ B nuclear translocation further controlling their gelatinase-B expression.

An increase in NF- κ B nuclear translocation would enhance not only gelatinase-B expression but other proinflammatory cytokines such as TNF- α and IL-6. We, therefore, evaluated the mRNA expression of these cytokines (Figures 5(a) and 5(b)). We found that high-glucose treatment exacerbated the expression of TNF- α and IL-6, respectively, and *S. cumini* MSE treatment was able to prevent it. Gallic acid treatment also decreased the expression of TNF- α and IL-6 similar to *S. cumini* MSE. On the one hand, these results suggested that *S. cumini* MSE is able to prevent glucose-induced cardiac inflammation; on the other hand,

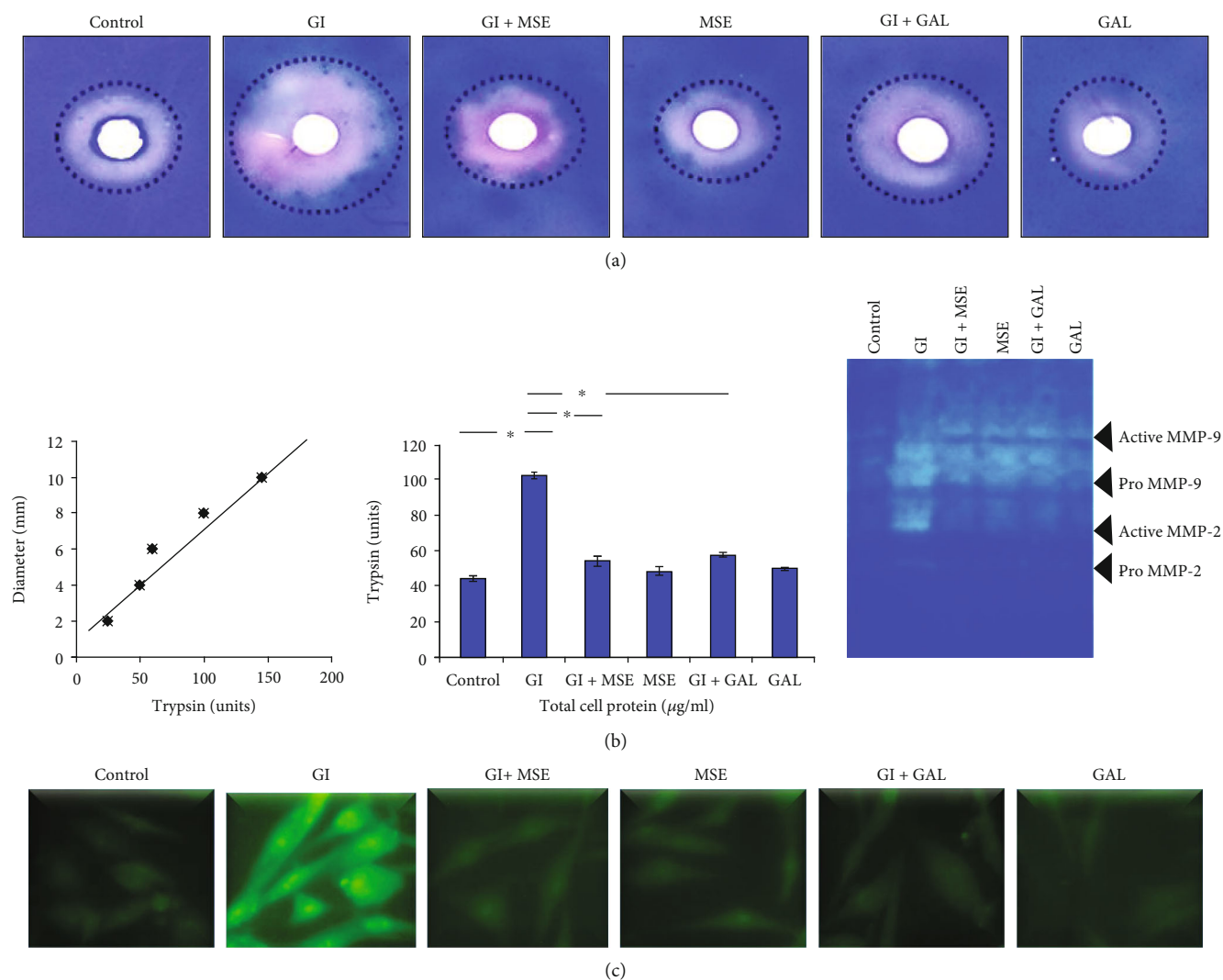


FIGURE 2: Effect of *S. cumini* methanol seed extract (MSE) on gelatinolytic activity. (a) Gel-diffusion assay: gelatinolytic activity was measured by digested zones of gelatin around the wells. Standard curve of trypsin was plotted (enzyme units), and enzyme activity for the samples was calculated from the standard graph of trypsin and represented as histogram. The width of the digested zone is proportional to the extent of substrate cleavage and can be used to quantitate protease activity. After giving treatment, we compared our results with trypsin digested zones and found the gelatinase activity in trypsin units. (b) Gelatin zymography: to depict the MSE effect on matrix metalloproteinase (MMP) enzyme activity. Lane 1: control; Lane 2: glucose induced (GI); Lane 3: glucose induced+*S. cumini* methanol seed extract (GI+MSE) treated; Lane 4: MSE-treated alone (MSE); Lane 5: glucose induced+gallic acid treated (GI+GAL); Lane 6: gallic acid alone (GAL) ($*p \leq 0.05$). (c) Cell *in situ* zymography: fluorescence micrographs showing the increase in gelatinolytic activity in HG-induced cells whereas *S. cumini* methanol seed extract (MSE) and gallic acid (GAL) treatment of HG-glucose stressed cells reverses the activity near the control. Images captured at 40x magnification ($*p \leq 0.05$). Scale bar 20 μm .

it corroborated a reduced activity of NF- κ B. However, additional evidence would be required to assert a direct correlation between NF- κ B activity and cytokine expression.

3.5. *S. cumini* Phenolic Compounds Block Gelatinase-B Substrate Binding. We have previously shown potent antioxidative potential of *S. cumini* extracts indicating that *S. cumini* is rich in phenolic compounds. To evaluate this, we performed reverse-phase HPLC of *S. cumini* MSE which showed that indeed *S. cumini* MSE is enriched with a concoction of polyphenols, viz., corilagin, doxycycline, ellagic acid, ferulic acid, epigallocatechin gallate, gallic acid, kaempferol, quercetin, and sinapic acid (Figure 6). The structures, reten-

tion time, and quantity of these polyphenols are shown in Table S1. The presence of these polyphenols was validated using standard polyphenols in HPLC (Fig. S2). The protective effects of these polyphenols have been shown to be implicated in several diseases.

Our results showed that *S. cumini* MSE has a protective function under high-glucose conditions by inhibiting NF- κ B translocation and gelatinase-B expression as well as activity, but whether it had a direct influence on gelatinase-B activity remains unresolved. We therefore evaluated if *S. cumini* polyphenols have a tendency to bind to MMP-9. *In silico* molecular docking studies showed that these polyphenols have a binding tendency to MMP-9 with variable

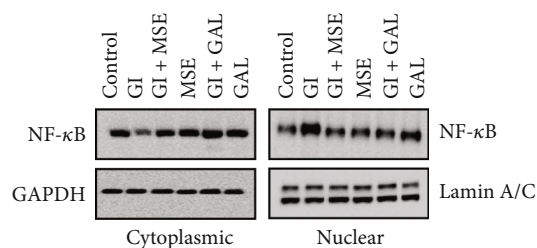


FIGURE 3: Expression analysis of gelatinase-B. (a) RT-PCR studies: Lane 1: control; Lane 2: glucose induced (GI); Lane 3: glucose induced+*S. cumini* methanol seed extract (GI+MSE) treated; Lane 4: MSE-treated alone (MSE); Lane 5: glucose induced+gallic acid treated (GI+GAL); Lane 6: gallic acid alone (GAL) ($*p \leq 0.05$). Expression levels of MMP-9 were obtained by qRT-PCR and normalized against β -actin. Fold changes were shown as histogram ($*p \leq 0.05$). (b) Immunocytochemistry for gelatinase-B: photomicrographs showing expression of MMP-9 in different experimental groups at 20x magnification. Scale bar 10 μm .

binding energies (Figures 7(a)–7(c)). Of these, quercetin had the maximum binding energy followed by kaempferol, ferulic acid, and caffeic acid. Interestingly, gallic acid showed the least binding energy explaining a better efficacy of *S. cumini* MSE than gallic acid in some of the results obtained above. Intriguingly, all the polyphenols were docked on the Zn^{2+} metal-binding site (consensus sequence HEBGHxLGLxHS), on three histidine residues (His226, His230, and His236) which belong to the substrate-binding site of MMP-9. These results show that despite the fact that *S. cumini* MSE regulates gelatinase-B expression via NF- κ B activity, the polyphenols within the MSE are capable of binding directly to gelatinase-B and could therefore have a direct effect on gelatinase-B activity.

4. Discussion

Diabetes and its long-term complications are a serious threat worldwide despite the availability of significant therapeutic options. Epidemiological and pathophysiological studies indicate that diabetes mellitus (DM) patients have increased risks of cardiovascular diseases. Even a slight increase in the hemoglobin A1c (HbA1c) level may lead to 20–30% upsurge in CVDs [40]. ECM dysfunction and alteration in MMP activity lead to the degradation of various structural proteins and several CVDs. MMP inhibitors have been shown to be effective in mediating efficient cardioprotection. However, due to the poor bioavailability, high toxicity, and failure of synthetic MMP inhibitors in clinical trials, attention has shifted to plant-derived MMP inhibitors [41].

The polyphenolic content-enriched functional food could have shown a promising approach towards the treatment of such diseases. Such natural product-derived drugs would have limited toxicity and side effects with better therapeutic indices [42]. The role of *S. cumini* seeds on HG-induced cardiac stress is not known so far; therefore, in the present study, methanol extract of *S. cumini* seeds was used to examine its effect on HG-induced cardiomyocytes. The effect was also examined with a purified form of a known constituent of *S. cumini* seed extract, gallic acid, a well-

known cardioprotectant in diabetes-induced myocardial dysfunction and also an antioxidant [43]. We found *S. cumini* MSE to be enriched with polyphenols and had the potential to suppress HG-induced gelatinase-B activity in H9C2 cells which was comparatively better than that of gallic acid. The following major findings have emerged from this study: (i) *S. cumini* MSE phytoconstituents are cardioprotective against HG-induced changes in H9C2 cell morphology, (ii) *S. cumini* MSE polyphenols significantly suppress MMP-9 expression and activity in HG-induced H9C2 cells, and (iii) *S. cumini* MSE inhibits HG-induced nuclear localization of NF- κ B and overexpression of TNF- α and IL-6, (iv) HPLC identified that *S. cumini* polyphenols show competitive inhibition with Zn^{2+} ions for the metal-binding domain of gelatinase-B in molecular docking study. *S. cumini* polyphenols bind more efficiently than the currently available FDA-approved synthetic MMP inhibitor, doxycycline, indicating the potential use of *S. cumini* polyphenols as safe MMP inhibitors since *S. cumini* MSE alone did not cause any significant change in cellular viability and morphology.

The H9C2 cell line is an efficient in vitro model for studying cardiac stress as it emulates the responses similar to those observed in primary cardiomyocytes [44]. The concentration of high glucose used in this study reflects in vitro hyperglycemic diabetic stress [45].

Adult cardiac myocytes are terminally differentiated cell types which do not proliferate but execute various physiological functions. Under various stress conditions, cardiomyocytes enlarge and undergo hypertrophy, a compensatory cellular response of the heart to the imposed hemodynamic burden for an increased cardiac output [46]. The increase in cell size is a major hallmark of cardiac cell hypertrophy, and the agonists such as norepinephrine, isoproterenol, and glucose induce hypertrophy of cardiomyocytes, which cause reexpression of some fetal genes, for instance, atrial natriuretic factor (ANF), brain natriuretic peptide (BNP), and β -myosin heavy chain (β -MHC) [47].

We observed similar significant enlargement of cardiomyocytes upon exposure to HG, which was reversed by *S. cumini* MSE treatment suggesting potential cardioprotective effect of *S. cumini* against HG-induced stress. Enhanced activity of MMPs by high glucose may contribute to matrix reorganization, whereas marked reduction in MMP activity by MSE treatment showed its ability to reverse HG-induced changes in cardiomyocytes. *In situ* zymography, a relatively superior method that helps to map the activity within the cell, showed increased activity of MMPs that was prevented by *S. cumini* MSE. These data strongly support that MSE possesses strong MMP-inhibiting activity.

Gelatinase-A (MMP-2) is constitutively expressed in the heart while gelatinase-B is an inducible protease, and we conducted our further study with gelatinase-B due to its inducible response to various stimuli [48]. Indeed, elevated levels of gelatinase-B have been proposed as a serological cardiac stress marker as its expression increases markedly in diabetic cardiomyopathy [49]. Interestingly, we observed a mild induction of gelatinase-B expression on treatment with MSE extract alone. Since the MSE extract is a crude preparation, it may contain several other phytochemicals which may

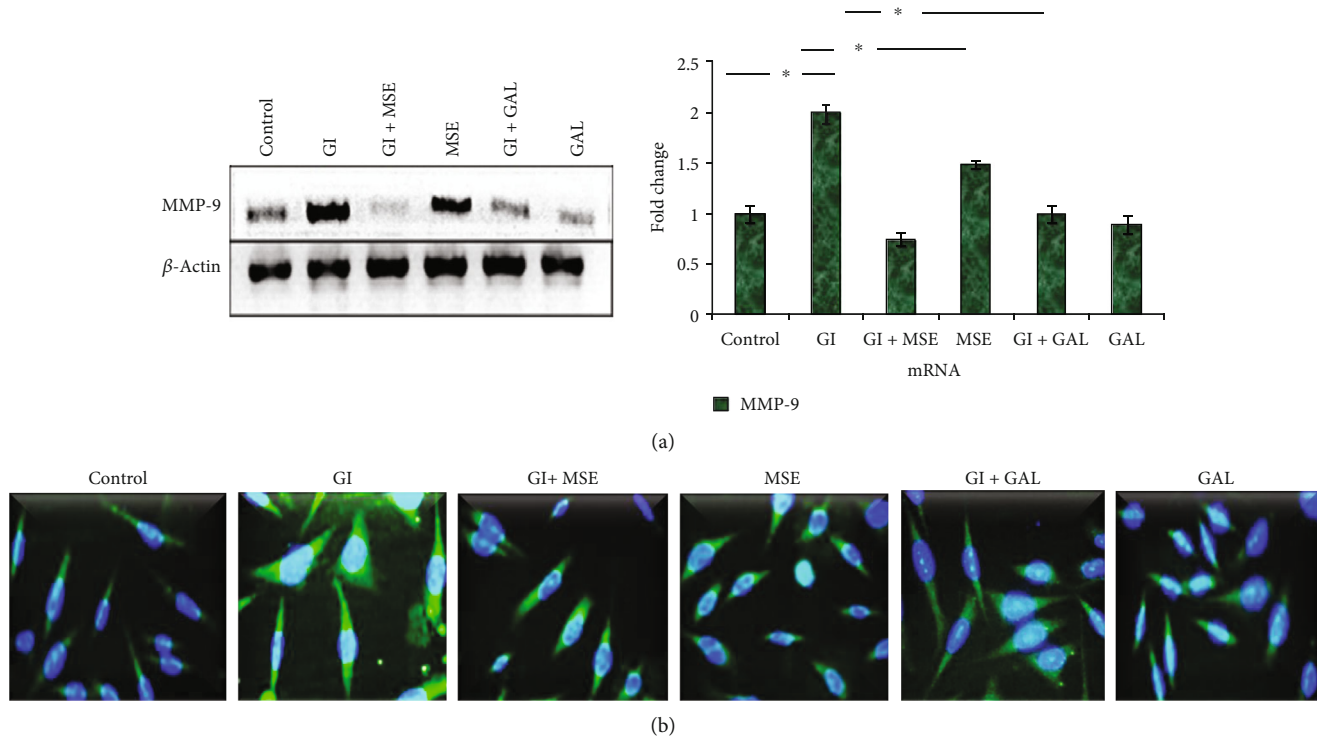


FIGURE 4: Nuclear factor- κ B (NF- κ B) localization in H9C2 cells. Western blotting to observe localization of NF- κ B from cytoplasm to nucleus using p65 antibody: nuclear localization of NF- κ B (green fluorescence in nuclei) in high-glucose- (HG-) induced cells. DAPI staining showed nuclear morphology. GAPDH and Lamin A/C were used as controls for cytoplasmic and nuclear extracts, respectively.

be responsible for this induction at baseline. Furthermore, the extract is protective under glucose-induced stress and behaves differently compared to baseline indicating its efficacy in disease conditions. Additionally, an increase in gelatinase-B expression may not be sufficient to create a functional effect, and we do not observe any effect of MSE extract on gelatinase-B activity at baseline.

To investigate the effect of *S. cumini* MSE on HG-induced gelatinase-B expression, we examined the activation and translocation of transcription factor NF- κ B. In fact, gelatinase-B promoter is highly conserved and contains an NF- κ B-binding site, and NF- κ B is known to upregulate the production of MMP-9 when induced by various proinflammatory cytokines [50]. The present study shows that HG induced the localization of NF- κ B from the cytoplasm to the nucleus indicating activation of gelatinase-B transcription. *S. cumini* MSE treatment regulated this alteration in nuclear localization of NF- κ B leading to decreased expression of gelatinase-B in HG-stimulated cardiomyocytes. Additionally, MSE also downregulated the expression of inflammatory markers such as TNF- α and IL-6 which were known to be critical in cardiomyopathy [51].

Thus, our study demonstrates that *S. cumini* MSE can be used as a potential functional food to suppress the expression of proinflammatory cytokines and gelatinase-B in HG-induced stress in cardiomyocytes. Although a clear mechanism is not yet known, the presence of hydroxyl/carbonyl groups on the phenolic rings of a number of MMP inhibitors has been suggested to chelate active Zn^{2+} ions and inhibit MMP activity [52].

S. cumini extracts prepared from different plant parts such as pulp, seed, leaves, and kernel have differential distribution of chemical constituents, especially the polyphenols, which are reported to possess a range of pharmacological potential. To know the status of polyphenols in MSE, a quantitative analysis was performed by HPLC, which indicated the presence of many polyphenols in MSE. The major polyphenols found in MSE (in 100 g of seed powder) were p-coumaric acid (71.9 ± 0.05 mg), gallic acid (53.0 ± 0.06 mg), protocatechuic acid (40.6 ± 0.10 mg), quercetin (29.6 ± 0.05 mg), sinapic acid (30.8 ± 0.14 mg), caffeic acid (15.8 ± 0.03 mg), kaempferol (10.2 ± 0.09 mg), ellagic acid (5.8 ± 0.09 mg), ferulic acid (2.71 ± 0.02 mg), and p-hydroxybenzoic acid (0.52 ± 0.04 mg) (Table S1).

The polyphenolic compounds that were identified and quantified in our study have been shown to exhibit cardioprotective potential as identified by various research groups using *in vitro* and models. p-Coumaric acid attenuated apoptosis in isoproterenol-induced myocardial infarction by inhibiting oxidative stress [53]. Gallic acid, a known cardioprotectant, has been found to suppress the expression of cardiac troponin-T, a cardiac arrest marker enzyme, lipid peroxidation products, and antioxidative enzymes [54].

Quercetin was reported to prevent endothelial dysfunction and decrease blood pressure, oxidative stress, and end-organ damage in hypertensive animals [55]. Derivatives of benzoic acid have been reported to activate Nrf2 signaling in the heart leading to overexpression of antioxidant enzymes, thereby decreasing oxidative stress and associated problems such as endothelial dysfunction and atherosclerosis [56].

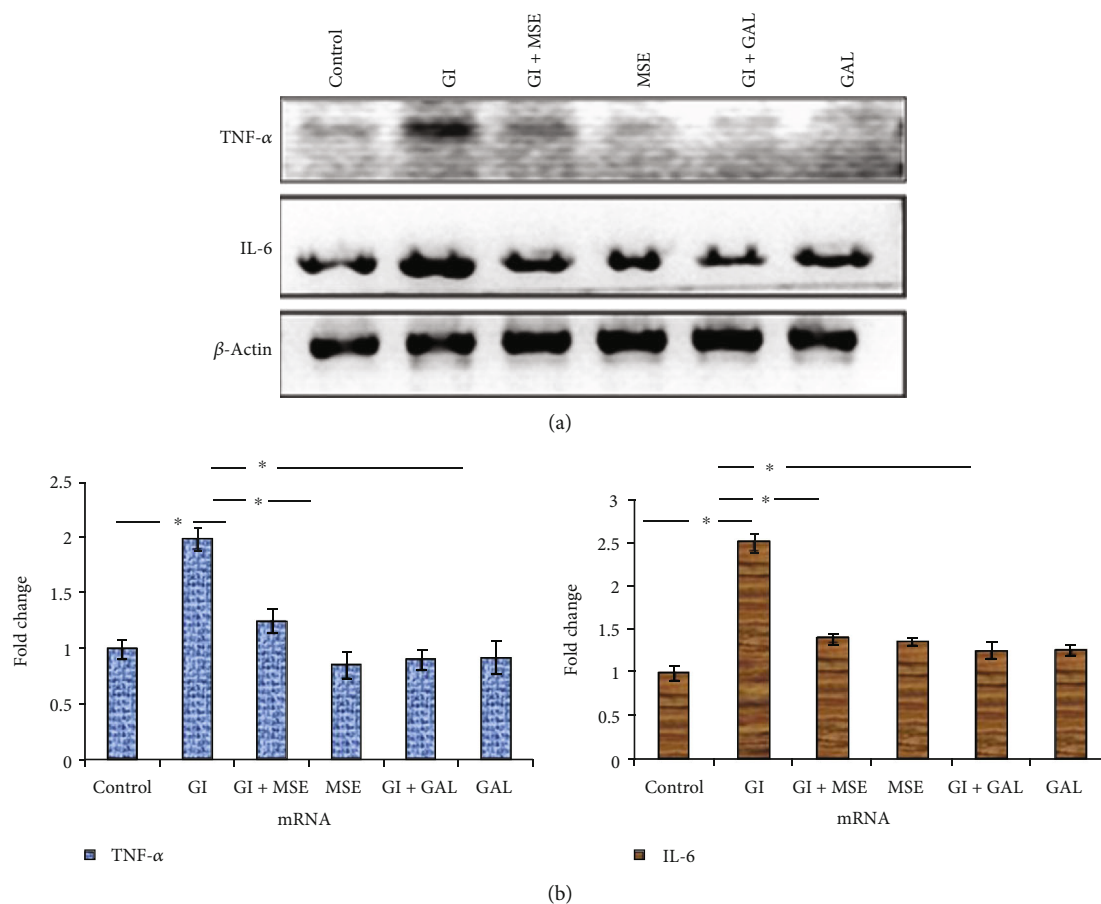


FIGURE 5: RT-PCR profiles of tumor necrosis factor- α (TNF- α) and interleukin-6 (IL-6) in different experimental groups. Lane 1: control; Lane 2: glucose induced (GI); Lane 3: glucose induced+*S. cumini* methanol seed extract (GI+MSE) treated; Lane 4: MSE-treated alone (MSE); Lane 5: glucose induced+gallic acid treated (GI+GAL); Lane 6: gallic acid alone (GAL). (a) Semiquantitative PCR showed significant increase in expression for both the markers in the cells treated with high glucose (HG). *S. cumini* methanol seed extract (MSE) and gallic acid (GAL) treatment reduced it remarkably up to the control. (b) Results obtained by qRT-PCR (real-time PCR) were normalized against β -actin and represented by histogram (* $p \leq 0.05$).

Sinapic acid prevented ischemia/reperfusion, cardiac hypertension, and remodeling [57]. Caffeic acid derivatives exerted a protective effect during streptozotocin- and isoproterenol-induced cardiac stress [58]. Kaempferol has been reported to be cardioprotective by regulating the membrane-bound ATPases in streptozotocin-induced diabetic rats [59]. Ferulic acid is also found to suppress anticancer drug-induced cardiotoxicity [60]. Ellagic acid improved arrhythmic condition by upregulating endothelial nitric oxide synthase (eNOS) and alleviating oxidative stress [61]. These evidences strengthen and support our hypothesis that MSE, which is a mix of these polyphenolics, could be a potential cardioprotective agent in HG-induced stress.

The mechanism of MMP-mediated cardioprotection by these compounds is not yet known. To understand this further, the polyphenols identified in HPLC were used to study interaction with the MMP-9 active site. Our docking studies revealed good binding energies of HPLC-identified molecules with MMP-9. Such ligand-protein interaction was based upon the inhibitor/substrate binding site, suggesting that MMP-9 inhibition by *S. cumini* MSE was due to polyphenols present in MSE that act as competitive inhibi-

tors with the substrate. The results of the docking study also explained that there was a direct interaction between gelatinase-B and the polyphenolic components of *S. cumini* MSE, which hindered its activity by targeting critical histidine residues of the metal-binding domain, thereby preventing the binding of Zn^{2+} to the active site which in turn could inhibit MMP activity. The docking results suggested that *S. cumini* polyphenols especially quercetin, kaempferol, caffeic acid, and ferulic acid could be efficient MMP-9 inhibitors and thereby may be potential suppressors of HG-induced cardiac stress.

Structure-activity relationship (SAR) was established on the basis of results obtained in docking studies which revealed that the two structural elements, namely, chromone ring and hydroxyl groups in the aromatic ring in the polyphenols of MSE, were the governing factors for the activity. Chromone core-bearing polyphenols such as quercetin and kaempferol showed excellent binding affinity with MMP-9 as compared to doxycycline. It also appeared that along with chromone moiety, the number and position of hydroxyl groups also played a critical role in deciding the MMP inhibitory activity of polyphenols. Other MSE polyphenols also

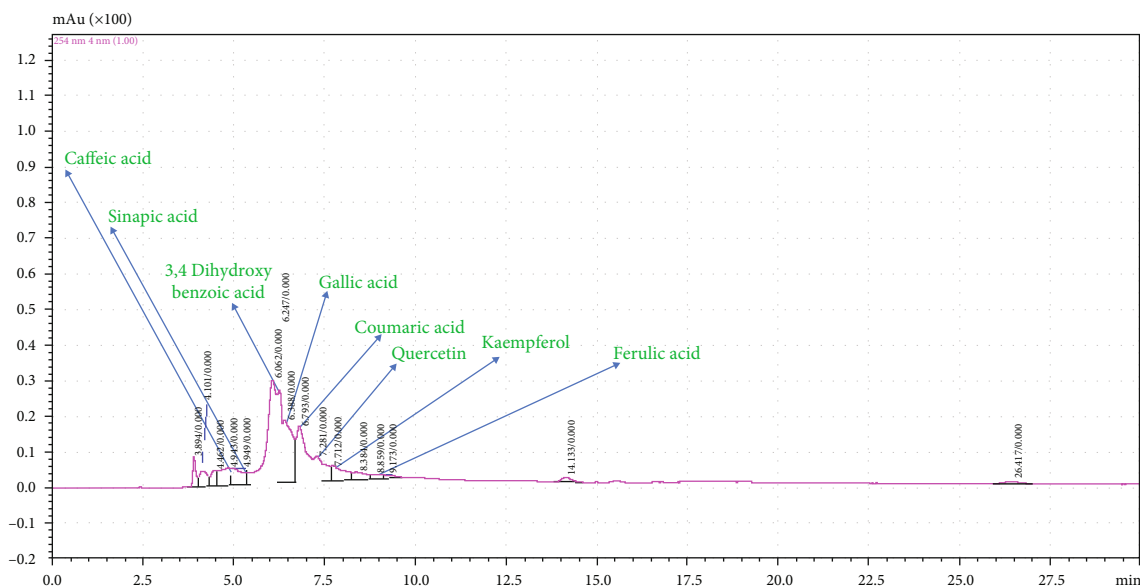


FIGURE 6: High-performance liquid chromatography (HPLC) analysis of *S. cumini* methanol seed extract (MSE). HPLC chromatogram to depict various peaks reflecting the presence of various polyphenols in MSE. Retention times 4.84, 4.94, 6.24, 6.39, 6.79, 7.28, 7.71, and 8.85 min. were detected for caffeic acid, sinapic acid, 3,4-dihydroxybenzoic acid, gallic acid, coumaric acid, quercetin, kaempferol, and ferulic acid, respectively.

displayed satisfactory binding affinity with MMP-9 possibly due to the presence of hydroxyl groups.

It was also observed that polyphenols having the hydroxyl group attached directly to the benzene ring had more binding affinity (*p*-hydroxybenzoic and protocatechuic acid) as compared to those having hydroxyl groups in the side chains (sinapic acid). The following order of affinity has been observed in docking analysis: quercetin > kaempferol > ferulic acid > caffeic acid/*p*-coumaric acid > *p*-hydroxybenzoic acid/protocatechuic acid > sinapic acid > gallic acid. Our docking studies, therefore, correlated very well with SAR wherein maximum binding affinity of quercetin with MMP-9 was observed due to the presence of chromonering and five hydroxyl groups responsible for its excellent affinity with MMP-9. Henceforth, the docking and SAR data suggested that *S. cumini* MSE polyphenols may act as potent MMP-9 inhibitors.

The greatest hurdle in using herbal supplements as potential drugs has been that researchers try to identify a single bioactive molecule to modify certain pathological parameters, whereas practically the crude extracts containing many bioactive components show better pharmacodynamic synergistic potency [62]. The crude extracts could be more helpful as they are derived from natural plant parts which are usually biocompatible with the human system and thus would have low toxicity and higher bioavailability [63]. Our results also supported the concept of collaborative interaction of phytochemical-enriched *S. cumini* extract that could act in synergy for effective cardioprotection under high-glucose stress.

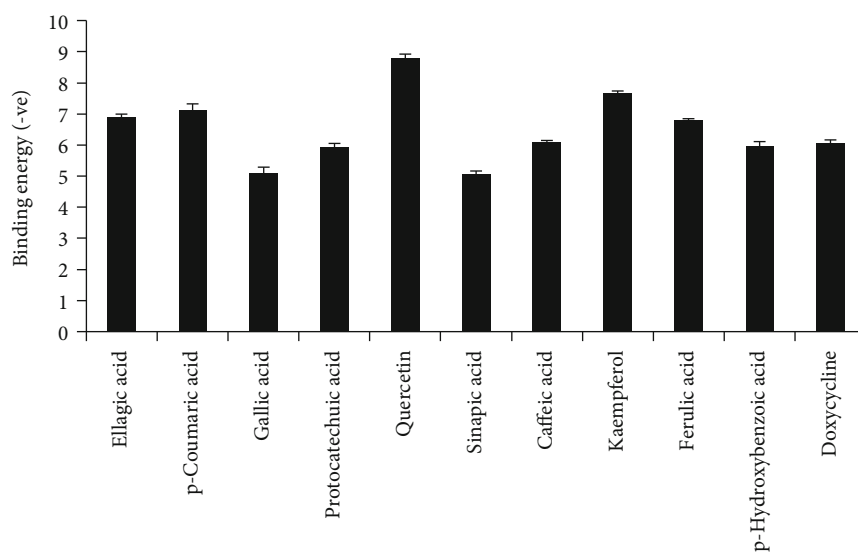
The polyphenol components of *S. cumini* MSE such as gallic acid alone are not used as dietary supplements as they inhibit the food intake as well as do not fulfill the criteria of effective oral dosing. Pharmacokinetic studies have shown that blood levels having 10^{-6} M concentration of gallic acid

restrict the appropriate functioning of the transport system [64]. Therefore, proposing the potential use of such a plant extract as *S. cumini* as a MMP inhibitor would be advantageous in terms of its cost, availability, and safety.

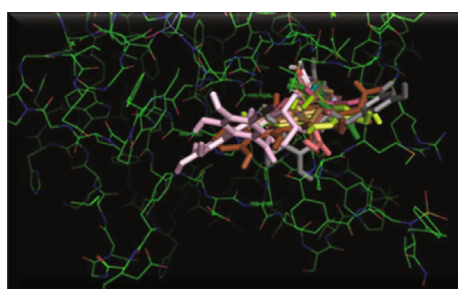
In this regard, use of *S. cumini* as a nutritional supplement or functional food for diabetics prove to be a potent natural suppresser for gelatinase-B-mediated stress in HG-induced condition. Based on the data of the present study, a model can be proposed to understand the effect of *S. cumini* as a MMP inhibitor and a cardiac stress reliever via targeting the molecules at multiple levels. The study has significant relevance for the society as most of the identified MMP inhibitors possess severe side effects like musculoskeletal syndrome (MSS). Doxycycline is the only FDA-approved MMP inhibitor in the market currently that is only for periodontal diseases.

Our results show the strong interaction of phytochemicals with gelatinase-B that may act in synergy for effective cardioprotection under hyperglycemic stress. In this regard, the usage of *S. cumini* as functional food proved to be a potent natural suppresser for gelatinase-B-mediated HG-induced stress. A significant relationship between ECM integrity in HG-induced stress and the content of phenolic components of MSE supported this perception. Taken together, the present results suggest the potential of *S. cumini* MSE as an herbal-based therapy for the treatment of HG-induced cardiac stress. Due to the overwhelming potentials of *S. cumini* polyphenols, further in-depth analysis of the extract and validation on appropriate animal models are required to understand the precise mechanism for designing specific therapies against ECM remodeling in diabetic cardiomyopathy.

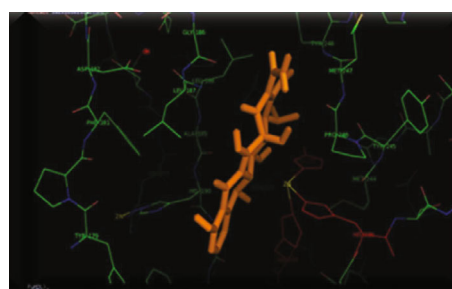
Myocardial remodeling could be categorized as either adaptive or pathological. Initial changes in the myocardium



(a)



(b)



(c)

FIGURE 7: (a) Matrix metalloproteinase-9 (MMP-9) and polyphenol binding energy interaction graph. The x-axis represented various MSE polyphenols/doxycycline, and the y-axis showed (-ve) binding energy. (b) Predicted binding mode of polyphenols and doxycycline to MMP-9 (gelatinase-B): docked structures of gallic acid (pink), p-hydroxybenzoic acid (dark green), ellagic acid (blue), kaempferol (gray), p-coumaric acid (orange), protocatechuic acid (yellow), sinapic acid (light green), caffeic acid (brown), ferulic acid (mustard), and quercetin (red) with MMP-9. (c) Docking pose of doxycycline with MMP-9.

may appear phenotypically similar in both cases, but the physiological effects of each are drastically different. Adaptive myocardial remodeling occurs due to high stress on the vascular walls or increased workload. It helps to counter the stress and restore normal ventricular function. Observations in the myocardium of high functioning athletes show changes in Left Ventricular (LV) geometry allowing improved compliance, enhanced filling through LV dilation, and better stroke volume [65]. On the other hand, in pathological remodeling, the LV chamber dilation leads to diminished compliance and significantly lower forward stroke volume [66]. MMP-2 has a crucial role in the progression of cardiac remodeling in response to pressure overload. An increase in MMP-2 activity can lead to fibrosis in LV hypertrophy, which may be due to direct proteolysis of cardiac ECM components, as well as by generating a profibrotic response, which further results in adaptive remodeling [67]. MMP-9 is a critical marker of LV remodeling; a higher MMP-9 level indicates more extensive adaptive LV remodeling [68]. It is also observed that in the patients having LV hypertrophy and with a history of hypertension, plasma levels of MMP-2 were significantly enhanced as compared to control subjects [67]. However, MMP-9 acti-

vates various chemokines, such as CXCL5, CXCL6, and CXCL8, releases cell surface receptors (e.g., tumor necrosis factor- α receptor), and eventually contributes to pathological remodeling. It has several other inflammatory mediators such as activator protein-1, specificity protein-1, and NF- κ B sites that make it a possible target for myocardial remodeling in atherosclerosis and heart failure [69].

5. Conclusion

In conclusion, the present study on the one hand highlights the role of MMPs, especially gelatinase-B, in HG-induced cardiomyopathy in rat heart-derived H9C2 cardiomyoblast cells, and on the other hand, it elaborates the role of *S. cumini* MSE in suppressing HG-stimulated gelatinase-B expression and activity in cardiomyocytes. Further, strong binding energy of interaction of *S. cumini* polyphenols and gelatinase-B protein suggests close interaction of the polyphenols with gelatinase-B which could be responsible for its inhibition. Taken together, being a potent source of polyphenols with MMP inhibition potential, *S. cumini* may be useful as a functional food and dietary supplement in HG-induced

and gelatinase-B-mediated cardiac stress and cardiomyopathy. This study will certainly enhance the scientific opportunities in deriving the novel inhibitors from functional foods in developing countries.

Data Availability

Data will be available on request.

Disclosure

Shrey Kohli is presently in the Institute for Clinical Chemistry and Pathobiochemistry, Otto Von Guericke University (Medical Faculty), Universitätsklinikum, Haus 39 Leipziger Str 44, 39120 Magdeburg, Germany.

Conflicts of Interest

The authors declare that they have no conflicts of interest.

Authors' Contributions

Neha Atale and Chandra Bhushan Mishra contributed equally to this work.

Acknowledgments

We acknowledge Jaypee Institute of Information Technology, Deemed to be University, for providing infrastructural support. This research work was funded by the National Research Foundation (NRF) of Korea, supported by the Korean government (MSIP) (Grant Nos: 2019R1F1A1057386 and 2019H1D3A2A02102142).

Supplementary Materials

Supplementary 1. Fig. S1: schematics of the methodology adopted to study the protective effect of *S. cumini* methanol seed extract (MSE) on high-glucose- (HG-) induced cardiac stress.

Supplementary 2. Fig. S2: HPLC chromatogram: (A) gallic acid and p-coumaric acid, (B) quercetin and ellagic acid, (C) kaempferol and ferulic acid, (D) protocatechuic acid and sinapic acid, and (E) caffeic acid and p-hydroxybenzoic acid.

Supplementary 3. Table S1: HPLC analysis of methanol seed extract of *S. cumini*.

References

- [1] S. Sneha and D. Madhusweta, "Nutritive, therapeutic and processing aspects of Jamun, *Syzygium cumini* (L.) skeels- an overview," *Indian Journal of Natural Product Research*, vol. 5, pp. 295–307, 2014.
- [2] A. G. V. Costa, D. F. Garcia-Diaz, P. Jimenez, and P. I. Silva, "Bioactive compounds and health benefits of exotic tropical red-black berries," *Journal of Functional Foods*, vol. 5, no. 2, pp. 539–549, 2013.
- [3] S. G. Jaiswal, M. Patel, and S. N. Naik, "Physico-chemical properties of *Syzygium cumini* (L.) Skeels jam and comparative antioxidant study with other fruit jams," *Indian Journal of Natural Products and Resources*, vol. 6, pp. 9–15, 2015.
- [4] B. S. Shrikant, S. J. T. Nayan, M. P. Meghatai, and M. H. Parag, "Jamun (*Syzygium cumini* (L.)): a review of its food and medicinal uses," *Food and Nutrition Sciences*, vol. 3, pp. 1100–1117, 2012.
- [5] Y. C. Cheng, J. M. Sheen, W. L. Hu, and Y. C. Hung, "Polyphenols and oxidative stress in atherosclerosis-related ischemic heart disease and stroke," *Oxidative Stress & Cellular Longevity*, vol. 2017, pp. 1–16, 2017.
- [6] M. Ayyanar and P. Subash-Babu, "*Syzygium cumini* (L.) skeels: a review of its phytochemical constituents and traditional uses," *Asian Pacific Journal of Tropical Biomedicine*, vol. 2, no. 3, pp. 240–246, 2012.
- [7] A. C. Dametto, D. Agustoni, T. F. Moreira et al., "Chemical composition and *in vitro* chemoprevention assessment of *Eugenia jambolana* Lam. (Myrtaceae) fruits and leaves," *Journal of Functional Foods*, vol. 36, pp. 490–502, 2017.
- [8] A. Rawshani, A. Rawshani, S. Franzén et al., "Mortality and cardiovascular disease in type 1 and type 2 diabetes," *New England Journal of Medicine*, vol. 376, no. 15, pp. 1407–1418, 2017.
- [9] T. R. Einarson, A. Acs, C. Ludwig, and U. H. Panton, "Prevalence of cardiovascular disease in type 2 diabetes: a systematic literature review of scientific evidence from across the world in 2007–2017," *Cardiovascular Diabetology*, vol. 17, no. 1, pp. 83–102, 2018.
- [10] M. Valko, D. Leibfritz, J. Moncol, M. T. D. Cronin, M. Mazur, and J. Telser, "Free radicals and antioxidants in normal physiological functions and human disease," *International Journal of Biochemistry and Cell Biology*, vol. 39, no. 1, pp. 44–84, 2007.
- [11] M. K. Lindsey and T. K. Borg, "Understanding the role of the extracellular matrix in cardiovascular development and disease: where do we go from here?," *Journal of Molecular and Cellular Cardiology*, vol. 48, no. 3, pp. 431–432, 2010.
- [12] M. Bellafiore, G. Battaglia, A. Bianco, F. Farina, A. Palma, and A. Paoli, "The involvement of MMP-2 and MMP-9 in heart exercise-related angiogenesis," *Journal of Translational Medicine*, vol. 11, no. 1, pp. 283–290, 2013.
- [13] S. A. Peeters, L. Engelen, J. Buijs et al., "Plasma matrix metalloproteinases are associated with incident cardiovascular disease and all-cause mortality in patients with type 1 diabetes: a 12-year follow-up study," *Cardiovascular Diabetology*, vol. 16, no. 1, pp. 55–67, 2017.
- [14] K. Brew and H. Nagase, "The tissue inhibitors of metalloproteinases (TIMPs): an ancient family with structural and functional diversity," *Biochimica et Biophysica Acta*, vol. 1803, no. 1, pp. 55–71, 2010.
- [15] S. Naphade, A. Embusch, K. L. Madushani, K. L. Ring, and L. M. Ellerby, "Altered expression of matrix metalloproteinases and their endogenous inhibitors in a human isogenic stem cell model of Huntington's disease," *Frontiers in Neuroscience*, vol. 11, 2018.
- [16] C.-W. Lee, C.-C. Lin, W.-N. Lin et al., "TNF- α induces MMP-9 expression via activation of Src/EGFR, PDGFR/PI3K/Akt cascade and promotion of NF- κ B/p300 binding in human tracheal smooth muscle cells," *American Journal of Physiology Lung Cell and Molecular Physiology*, vol. 292, no. 3, pp. L799–L812, 2007.
- [17] A. Yabluchanskiy, Y. Ma, A. P. Iyer, M. E. Hall, and M. L. Lindsey, "Matrix metalloproteinase-9: many shades of

- function in cardiovascular disease,” *Physiology*, vol. 28, no. 6, pp. 391–403, 2013.
- [18] B. Fingleton, “Matrix metalloproteinases as valid clinical target,” *Current Pharmaceutical Design*, vol. 13, no. 3, pp. 333–346, 2007.
- [19] Y. Y. Li, C. F. McTiernan, and A. M. Feldman, “Interplay of matrix metalloproteinases, tissue inhibitors of metalloproteinases and their regulators in cardiac matrix remodeling,” *Cardiovascular Research*, vol. 46, no. 2, pp. 214–224, 2000.
- [20] P. K. Mishra, V. Chavali, N. Metreveli, and S. C. Tyagi, “Ablation of MMP9 induces survival and differentiation of cardiac stem cells into cardiomyocytes in the heart of diabetics: a role of extracellular matrix,” *Canadian Journal of Physiology and Pharmacology*, vol. 90, no. 3, pp. 353–360, 2012.
- [21] V. Mohan, D. Talmi-Frank, V. Arkadash, N. Papo, and I. Sagi, “Matrix metalloproteinase protein inhibitors: highlighting a new beginning for metalloproteinases in medicine,” *Dovepress*, vol. 2016, pp. 31–47, 2016.
- [22] J. Hever and R. J. Cronise, “Plant-based nutrition for healthcare professionals: implementing diet as a primary modality in the prevention and treatment of chronic disease,” *Journal of Geriatric Cardiology*, vol. 14, no. 5, pp. 355–368, 2017.
- [23] L. Crasci, M. R. Lauro, G. Puglisi, and A. Panico, “Natural antioxidant polyphenols on inflammation management: anti-glycation activity vs metalloproteinases inhibition,” *Critical Reviews in Food Science & Nutrition*, vol. 58, pp. 893–904, 2017.
- [24] N. Wang, Z.-Y. Wang, S.-L. Mo et al., “Ellagic acid, a phenolic compound, exerts anti-angiogenesis effects via VEGFR-2 signaling pathway in breast cancer,” *Breast Cancer Research Treatment*, vol. 134, no. 3, pp. 943–955, 2012.
- [25] K. Amutha and S. Aishwarya, “Evaluation of antibacterial and antidiabetic activity and phytochemical analysis of *Syzygium cumini* seeds,” *Research Journal of Pharmacology and Pharmacodynamics*, vol. 2, no. 5, pp. 348–350, 2010.
- [26] N. Atale, S. Malhotra, G. Nirmala, R. T. Narendhirakannan, S. Mohanty, and V. Rani, “Synthesis and characterization of *Syzygium cumini* nanoparticles for its protective potential in high glucose induced cardiac stress: a green approach,” *Applied Biochemistry and Biotechnology*, vol. 181, no. 3, pp. 1140–1154, 2017.
- [27] P. Sreejit, S. Kumar, and R. S. Verma, “An improved protocol for primary culture of cardiomyocyte from neonatal mice,” *In vitro Cell Developmental Biology Animal*, vol. 44, no. 3–4, pp. 45–50, 2008.
- [28] N. Atale, M. Chakraborty, S. Mohanty et al., “Cardioprotective role of *Syzygium cumini* against glucose-induced oxidative stress in H9C2 cardiac myocytes,” *Cardiovascular Toxicology*, vol. 13, no. 3, pp. 278–289, 2013.
- [29] N. Atale, K. Gupta, and V. Rani, “Protective effect of *Syzygium cumini* against pesticide-induced cardiotoxicity,” *Environmental Science Pollution Research International*, vol. 21, no. 13, pp. 7956–7972, 2014.
- [30] C. B. Mishra, S. Kumari, A. Angeli, S. Bua, M. Tiwari, and C. T. Supuran, “Discovery of benzenesulfonamide derivatives as carbonic anhydrase inhibitors with effective anticonvulsant action: design, synthesis, and pharmacological evaluation,” *Journal of Medicinal Chemistry*, vol. 61, no. 7, pp. 3151–3165, 2018.
- [31] C. B. Mishra, S. Kumari, A. Angeli et al., “Discovery of potent anti-convulsant carbonic anhydrase inhibitors: design, synthesis, in vitro and in vivo appraisal,” *European Journal of Medicinal Chemistry*, vol. 156, pp. 430–443, 2018.
- [32] C. B. Mishra, S. Kumari, A. Angeli et al., “Discovery of benzenesulfonamides with potent human carbonic anhydrase inhibitory and effective anticonvulsant action: design, synthesis and pharmacological assessment,” *Journal of Medicinal Chemistry*, vol. 60, no. 6, pp. 2456–2469, 2017.
- [33] O. Trott and A. J. Olson, “AutoDock Vina: improving the speed and accuracy of docking with a new scoring function, efficient optimization, and multithreading,” *Journal of Computational Chemistry*, vol. 31, no. 2, pp. 455–461, 2009.
- [34] N. Kumari, C. B. Mishra, A. Prakash, N. Kumar, R. Mongre, and P. M. Luthra, “8-(Furan-2-yl)-3-phenethylthiazolo[5,4-e][1,2,4]triazolo[1,5-c]pyrimidine-2(3H)-thione as novel, selective and potent adenosine A_{2A} receptor antagonist,” *Neuroscience Letters*, vol. 558, pp. 203–207, 2014.
- [35] C. B. Mishra, D. Sharma, A. Prakash, N. Kumari, N. Kumar, and P. M. Luthra, “Design and synthesis of (4E)-4-(4-substitutedbenzylideneamino)-3-substituted-2,3-dihydro-2-thioxothiazole-5-carbonitrile as novel A_{2A} receptor antagonists,” *Bioorganic & Medicinal Chemistry*, vol. 21, no. 19, pp. 6077–6083, 2013.
- [36] S. K. Barodia, C. B. Mishra, A. Prakash, J. B. S. Kumar, N. Kumari, and P. M. Luthra, “Novel 8-(furan-2-yl)-3-benzylthiazolo [5,4-e][1,2,4] triazolo [1,5-c] pyrimidine-2(3H)-thione as selective adenosine A_{2A} receptor antagonist,” *Neuroscience Letters*, vol. 488, no. 1, pp. 1–5, 2011.
- [37] C. B. Mishra, S. K. Barodia, A. Prakash, and P. M. Luthra, “Novel 8-(furan-2-yl)-3-substituted thiazolo [5,4-_e][1,2,4] triazolo[1,5-_c] pyrimidine-2(3-_H)-thione derivatives as potential adenosine A_{2A} receptor antagonists,” *Bioorganic & Medicinal Chemistry*, vol. 18, no. 7, pp. 2491–2500, 2010.
- [38] C. B. Mishra, P. Pandey, R. D. Sharma et al., “Identifying the natural phenol catechin as a multitargeted agent against SARS-CoV-2 for the plausible therapy of COVID-19: an integrated computational approach,” *Briefings in Bioinformatics*, vol. bbaa378, 2020.
- [39] P. M. Luthra, A. Prakash, S. K. Barodia, R. Kumari, C. B. Mishra, and J. B. S. Kumar, “_In silico_ study of naphtha [1, 2-d] thiazol-2-amine with adenosine A_{2A} receptor and its role in antagonism of haloperidol- induced motor impairments in mice,” *Neuroscience Letters*, vol. 463, no. 3, pp. 215–218, 2009.
- [40] K. T. Khaw, N. Wareham, S. Bingham, R. Luben, A. Welch, and N. Day, “Association of hemoglobin A1c with cardiovascular disease and mortality in adults: the European prospective investigation into cancer in Norfolk,” *Annals of Internal Medicine*, vol. 141, no. 6, pp. 413–420, 2004.
- [41] R. E. Vandenbroucke and C. Libert, “Is there new hope for therapeutic matrix metalloproteinase inhibition?,” *Nature Reviews Drug Discovery*, vol. 13, no. 12, pp. 904–927, 2014.
- [42] Y. Wang, L. Zhao, C. Wang et al., “Protective effect of quercetin and chlorogenic acid, two polyphenols widely present in edible plant varieties, on visible light-induced retinal degeneration in vivo,” *Journal of Functional Foods*, vol. 33, pp. 103–111, 2017.
- [43] S. P. Snehal and K. G. Ramesh, “Cardioprotective effects of gallic acid in diabetes-induced myocardial dysfunction in rats,” *Pharmacognosy Research*, vol. 3, pp. 239–245, 2011.
- [44] S. J. Watkins, G. M. Borthwick, and H. M. Arthur, “The H9C2 cell line and primary neonatal cardiomyocyte cells show similar hypertrophic responses in vitro,” *In vitro Cell Developmental Biology Animal*, vol. 47, no. 2, pp. 125–131, 2011.

- [45] F. Deng, S. Wang, L. Zhang et al., "Propofol through upregulating caveolin-3 attenuates post-hypoxic mitochondrial damage and cell death in H9C2 cardiomyocytes during hyperglycemia," *Cellular Physiology and Biochemistry*, vol. 44, no. 1, pp. 279–292, 2018.
- [46] S. Kohli, S. Ahuja, and V. Rani, "Transcription factors in heart: promising therapeutic targets in cardiac hypertrophy," *Current Cardiology Reviews*, vol. 7, no. 4, pp. 262–271, 2011.
- [47] S. Ahuja, S. Kohli, S. Krishnan, D. Dogra, D. Sharma, and V. Rani, "Curcumin: a potential therapeutic polyphenol, prevents noradrenaline-induced hypertrophy in rat cardiac myocytes," *Journal of Pharmacy and Pharmacology*, vol. 63, no. 12, pp. 1604–1612, 2011.
- [48] J. M. Parente and M. M. Castro, "Matrix metalloproteinase in the cardiovascular remodeling of hypertension: current insights and therapeutic potential," *Metalloproteinases In Medicine*, vol. Volume 5, pp. 1–11, 2018.
- [49] G. Li, W. Xing, M. Zhang et al., "Antifibrotic cardioprotection of berberine via downregulating myocardial IGF-1 receptor-regulated MMP-2/MMP-9 expression in diabetic rats," *American Journal of Physiology Heart & Circulatory Physiology*, vol. 315, no. 4, pp. H802–H813, 2018.
- [50] S. O. Sullivan, C. Medina, M. Ledwidge, M. W. Radomski, and J. F. Gilmer, "Nitric oxide-matrix metalloproteinase-9 interactions: biological and pharmacological significance: NO and MMP-9 interactions," *Biochimica et Biophysica Acta (BBA) - Molecular Cell Research*, vol. 1843, no. 3, pp. 603–617, 2014.
- [51] N. A. Turner and K. E. Porter, "Regulation of myocardial matrix metalloproteinase expression and activity by cardiac fibroblasts," *IUBMB Life*, vol. 64, no. 2, pp. 143–150, 2012.
- [52] F. Mannello, "Natural bio-drugs as matrix metalloproteinase inhibitors: new perspectives on the horizon?," *Recent Patents on Anti Cancer Drug Discovery*, vol. 1, no. 1, pp. 91–103, 2006.
- [53] P. S. M. Prince and A. J. Roy, "p-Coumaric acid attenuates apoptosis in isoproterenol-induced myocardial infarcted rats by inhibiting oxidative stress," *International Journal of Cardiology*, vol. 168, no. 4, pp. 3259–3266, 2013.
- [54] D. H. Priscilla and P. S. Prince, "Cardioprotective effect of gallic acid on cardiac troponin-T, cardiac marker enzymes, lipid peroxidation products and antioxidants in experimentally induced myocardial infarction in Wistar rats," *Chemico-Biological Interaction*, vol. 179, no. 2-3, pp. 118–124, 2009.
- [55] R. L. Castillo, E. A. Herrera, A. G. Candia et al., "Quercetin prevents diastolic dysfunction induced by a high-cholesterol diet: role of oxidative stress and bioenergetics in hyperglycemic rats," *Oxidative Medicine & Cellular Longevity*, vol. 2018, pp. 1–14, 2018.
- [56] B. H. Juurlink, H. J. Azouz, A. M. Aldalati, B. M. ATinawi, and P. Ganguly, "Hydroxybenzoic acid isomers and the cardiovascular system," *Nutrition*, vol. 13, no. 1, pp. 63–72, 2014.
- [57] T. Silambarasan, J. Manivannan, M. KrishnaPriya, N. Suganya, S. Chatterje, and B. Raja, "Sinapic acid prevents hypertension and cardiovascular remodeling in pharmacological model of nitric oxide inhibited rats," *PLoS One*, vol. 9, no. 12, article e115682, 2014.
- [58] Y.-J. Ho, A.-S. Lee, W.-P. Chen et al., "Caffeic acid phenethyl amide ameliorates ischemia/reperfusion injury and cardiac dysfunction in streptozotocin-induced diabetic rats," *Cardiovascular Diabetology*, vol. 13, no. 1, pp. 98–110, 2014.
- [59] M. Zhou, H. Ren, J. Han, W. Wang, Q. Zheng, and D. Wang, "Protective effects of kaempferol against myocardial ischemia/reperfusion injury in isolated rat heart via antioxidant activity and inhibition of glycogen synthase kinase-3," *Oxidative Medicine and Cellular Longevity*, vol. 2015, 8 pages, 2015.
- [60] J. B. Lian, Z. J. Wu, Q. J. Fang, J. Yu, and R. L. He, "Sodium ferulate protects against daunorubicin-induced cardiotoxicity in juvenile rats," *Zhongguo Ying Yong Sheng Li Xue Za Zhi*, vol. 31, no. 1, pp. 54–58, 2015.
- [61] T. Berkban, P. Boonprom, S. Bunbupha et al., "Ellagic acid prevents l-NAME-induced hypertension via restoration of eNOS and p47phox expression in rats," *Nutrients*, vol. 7, no. 7, pp. 5265–5280, 2015.
- [62] P. Rasoanaivo, C. W. Wright, M. L. Willcox, and B. Gilbert, "Whole plant extracts versus single compounds for the treatment of malaria: synergy and positive interactions," *Malaria Journal*, vol. 10, pp. 4–16, 2011.
- [63] L. Li, J. Xu, Y. Mu et al., "Chemical characterization and anti-hyperglycaemic effects of polyphenol enriched longan (*Dimocarpus longan* Lour.) pericarp extracts," *Journal of Functional Foods*, vol. 13, pp. 314–322, 2015.
- [64] A. T. Roberts, C. K. Martin, Z. Liu et al., "The safety and efficacy of a dietary herbal supplement and gallic acid for weight loss," *Journal of Medicinal Food*, vol. 10, no. 1, pp. 184–188, 2007.
- [65] K. T. Weber, P. Anversa, P. W. Armstrong et al., "Remodeling and reparation of the cardiovascular system," *Journal of the American College of Cardiology*, vol. 20, no. 1, pp. 3–16, 1992.
- [66] A. Pelliccia, F. M. Di Paolo, and B. J. Maron, "The athlete's heart: remodeling, electrocardiogram and preparticipation screening," *Cardiology in Review*, vol. 10, no. 2, pp. 85–90, 2002.
- [67] J. N. Cohn, R. Ferrari, and N. Sharpe, "Cardiac remodeling—concepts and clinical implications: a consensus paper from an international forum on cardiac remodeling," *Journal of the American College of Cardiology*, vol. 35, no. 3, pp. 569–582, 2000.
- [68] K. Y. DeLeon-Pennell and C. A. Meschiari, "Matrix metalloproteinases in myocardial infarction and heart failure," *Progress in Molecular Biology and Translational Science*, vol. 147, pp. 75–100, 2017.
- [69] H. Matsusaka, T. Ide, S. Matsushima et al., "Targeted deletion of matrix metalloproteinase 2 ameliorates myocardial remodeling in mice with chronic pressure overload," *Hypertension*, vol. 47, no. 4, pp. 711–717, 2006.

Review Article

New Approaches to Identify Sepsis Biomarkers: The Importance of Model and Sample Source for Mass Spectrometry

Angélique Blangy-Letheule,¹ Antoine Persello,^{1,2} Bertrand Rozec ,¹ Michel De Waard ,^{1,3} and Benjamin Lauzier ¹

¹Université de Nantes, CHU Nantes, CNRS, INSERM, l'institut du thorax, F-44000 Nantes, France

²InFlectis BioScience, Nantes, France

³Labex ICST, Valbonne, France

Correspondence should be addressed to Benjamin Lauzier; benjamin.lauzier@univ-nantes.fr

Received 13 October 2020; Revised 17 November 2020; Accepted 27 November 2020; Published 24 December 2020

Academic Editor: Luc Demaison

Copyright © 2020 Angélique Blangy-Letheule et al. This is an open access article distributed under the Creative Commons Attribution License, which permits unrestricted use, distribution, and reproduction in any medium, provided the original work is properly cited.

Septic shock is a systemic inflammatory response syndrome associated with circulatory failure leading to organ failure with a 40% mortality rate. Early diagnosis and prognosis of septic shock are necessary for specific and timely treatment. However, no predictive biomarker is available. In recent years, improvements in proteomics-based mass spectrometry have improved the detection of such biomarkers. This approach can be performed on different samples such as tissue or biological fluids. Working directly from human samples is complicated owing to interindividual variability. Indeed, patients are admitted at different stages of disease development and with signs of varying severity from one patient to another. All of these elements interfere with the identification of early, sensitive, and specific septic shock biomarkers. For these reasons, animal models of sepsis, although imperfect, are used to control the kinetics of the development of the pathology and to standardise experimentation, facilitating the identification of potential biomarkers. These elements underline the importance of the choice of animal model used and the sample to be studied during preclinical studies. The aim of this review is to discuss the relevance of different approaches to enable the identification of biomarkers that could indirectly be relevant to the clinical setting.

1. Introduction

Sepsis and septic shock are common causes for admission to intensive care units. Sepsis is defined as organ dysfunction resulting from a deregulated host response to infection [1]. In 2017, this pathology affected 48.9 million people worldwide, resulting in the deaths of 11 million patients [2]. Over the last 50 years, studies have demonstrated that myocardial dysfunction is a common finding in septic patients and approximately 50% of septic patients present signs of myocardial decompensation with variable development kinetics depending on the patient resulting in excess mortality of more than 60% [3]. Oxygen delivery is impaired in the tissues of sepsis patients with organ dysfunction. Septic shock is the most severe manifestation of sepsis. It is characterized by persistent hypotension, associated with metabolic dysfunction and significant tissue suffering. A 10% increase in mortality

is associated with septic shock for each additional hour of delay between the diagnosis and the implementation of an adequate treatment in hospital settings [4]. Since 2017, the World Health Organization (WHO) has made sepsis one of the world's top priorities and has adopted resolutions to improve the prevention, diagnosis, and management of this disease [5]. Septic shock is a complex and multifactorial pathology presenting a great heterogeneity of clinical manifestations. This therefore explains the differences in the kinetics of organ dysfunction and complicates its early diagnosis and appropriate management. Timely management could save 80% of patients with sepsis [6]. The use of early biomarkers and therapeutic targets that are sensitive and specific to the evolution of the pathology would facilitate rapid diagnosis and therefore early management of patients, limiting organ dysfunctions, particularly cardiac dysfunction, and optimizing patient chances of survival. Over the last few

years, numerous studies have proposed new biomarkers (Table 1). It should be noted that it is easier to standardise experimentation and control the kinetics of the evolution of the pathology in animal studies. It is then possible to, respectively, limit both the phenotypic heterogeneity between individuals and identify early versus late biomarkers. Over the past 20 years, a large number of biomarkers and therapeutic targets related to sepsis have been proposed [7]. However, the inherent heterogeneity of the pathology and the absence of similar reference bases in the different studies have made it difficult to confirm the quality and accuracy of these biomarkers for the diagnosis of sepsis [8]. For research teams working on sepsis, it is therefore important to implement improved investigation methods to generate better results and more reliable biomarkers. In recent years, omics technologies have gained momentum and increasing significance with improved splitting techniques and instrument performance. Analytical approaches have made it possible to identify proteins of low abundance in complex samples thereby improving the identification of new biomarkers. Proteomics based on mass spectrometry (MS) enable the use of different samples such as biological tissues or fluids based on patient cohorts or animal models in order to identify biomarkers and/or therapeutic targets. In the context of septic shock, the ideal biomarker should possess the following qualities: (i) be measurable during the early phase of the pathology, (ii) be easy to detect, (iii) be inexpensive, and (iv) be sufficiently sensitive and specific. The choice of the model and the relevance of the biological samples analysed by proteomics are essential for the identification of clinically usable biomarkers. This review seeks to discuss the quality and properties of different models that will enable the potential identification of clinically relevant biomarkers.

2. Mass Spectrometry for the Identification of Sepsis Biomarkers

MS is a very powerful and sensitive analytical method that identifies and quantifies molecules by measuring their mass. MS can provide information on several identified molecules at a time using a targeted approach or hundreds or even thousands of compounds via a nontargeted approach. Nontargeted MS approaches are typically used in the discovery phases to compare samples from two or more different populations. Once a compound that is present at a differential amount between these populations has been identified, a targeted approach can be used at a later stage to characterise the suspected biomarker(s) in a focused manner (Figure 1). Herein, only nontargeted mass spectrometry will be described since it provides identification of a larger set of biomarkers.

In recent years, improvements in selective depletion techniques, splitting techniques, mass spectrometry instrumentation, and analytical approaches have improved proteome analysis. This has led to a better understanding of molecular processes involved in many disease states and to the identification of new biomarkers. An example of the search for diagnostic markers by proteomic analysis is the detection in

TABLE 1: Nonexhaustive table of potential biomarkers recently studied.

	Biomarkers	References
Inflammation	S100A8	[9]
	High-mobility group box 1	[10]
	C-reactive protein	[11]
	Presepsin	[12]
Acute phase response	Haptoglobin	[13]
	Serum amyloid A	[14]
	Pentraxin-3	[7]
Lipid metabolism	Serum paraoxonase	[15]
	Apolipoprotein A-V	[16]
Oxidative stress	Glutathione peroxidase 3	[17]
	Histidine-rich glycoprotein	[18]

cerebrospinal fluid of the protein 14-3-3 σ as a marker of the Creutzfeldt-Jakob disease [19].

2.1. MS-Based Proteomics. The study of proteins gained increased maturity in the 1990s with the advent of MS. Over the last ten years, this technique has become an almost indispensable approach for research of diagnostic and prognostic biomarkers as well as for monitoring the development of pathologies. Proteomic studies can be carried out on different samples such as tissues or various biological fluids such as urine or blood. Indeed, they have already been used to identify a panel of metabolites for the stratification of patients suspected of developing sepsis [11]. However, the biological samples selected for identification of biomarkers should be considered carefully. The pathophysiology of sepsis and associated clinical constraints such as accessibility to biological tissue could limit the identification of biomarkers. It is therefore necessary to select the type of sample to be studied during preclinical work to enable identification of biomarkers that are relevant to the clinical setting.

2.1.1. The Search for Biomarkers in Organs. In sepsis, the inflammatory response can lead to damage and failure of organs such as the lungs, heart, or kidneys which are associated with excess mortality. The underlying mechanisms are not well understood, and without adapted diagnostic or prognostic biomarkers, the pathology will evolve toward septic shock and potentially death. In order to search for such biomarkers, several studies have focused on the proteome of organs that were damaged during sepsis itself by performing and studying biopsies. For example, a study on the temporal profile of renal proteome changes induced by sepsis highlighted that ceruloplasmin (CR) and haptoglobin (Hp) are upregulated 90 minutes after the onset of sepsis [20]. Similarly, a cardiac tissue proteome study reported that the oligomerization of pentraxin-3 (PTX-3) increased in patients who did not survive sepsis [21]. The octameric PTX-3 level in patients with sepsis could therefore be predictive of an unfavourable clinical state. In all of these studies, MS, performed on tissue, made it possible to identify proteins that

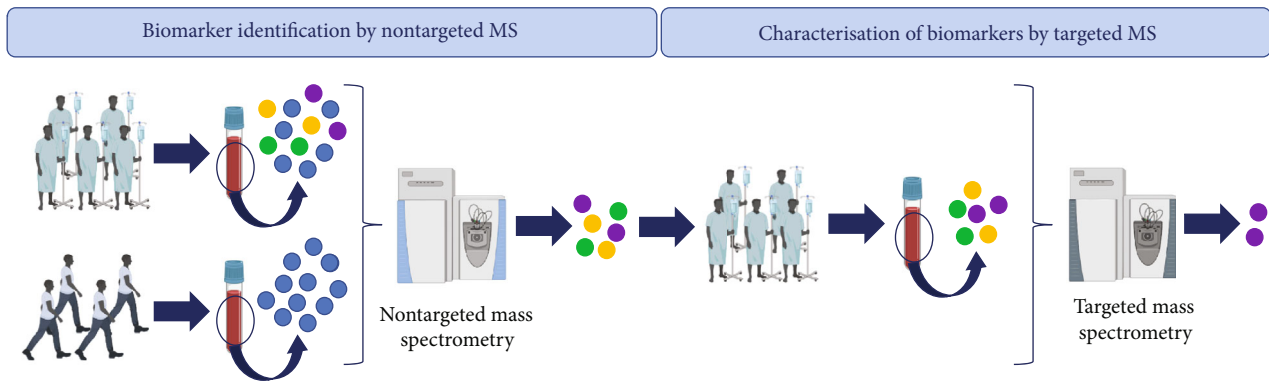


FIGURE 1: Process implemented in the search for MS-based biomarkers of septic shock. Potential biomarkers are first analysed by nontargeted MS and then characterised by targeted MS.

are deregulated during sepsis. These proteins could serve as biomarkers or therapeutic targets specific to a tissue/organ during sepsis. However, potential biomarkers identified by MS must be clinically usable to assist in medical decision-making. Indeed, the study of a tissue requires a biopsy, an invasive procedure, therefore limiting its use for routine biomarker research in clinics (Table 2). As a result, research has shifted toward the study of biological fluids that are more easily accessible in a clinical setting, and in particular, routinely used in clinics for other pathologies [22].

2.1.2. The Search for Biomarkers in Exosomes. Exosomes are membrane vesicles found in many biological fluids (such as blood or urine) that transmit signals between cells [23]. In the urine, the number of exosomes and extracellular vesicles increases continuously between 6 and 48 hours after induction of sepsis, suggesting that they could be potentially involved in this pathology [24]. It has been shown that exosomes play a role in sepsis through the interaction of various compounds released by the septic condition on membrane receptors. Proteomic analyses of exosomes in patient plasma samples could be an effective approach for the identification of protein biomarkers to be used for the diagnosis of sepsis. A study of exosomes in plasma from patients with sepsis identified 238 proteins [25]. Among these proteins, a negative correlation between serine palmitoyltransferase 3 (SPTLC 3) and the progression profile of the pathology was demonstrated, suggesting that SPTLC 3 could play a role in the development of sepsis [23]. SPTLC 3 enables the synthesis of ceramide from palmitate and serine. Studies have shown that sepsis leads to an increase in ceramide levels which play a role in sepsis-induced cardiac dysfunction [25]. Thus, the increase in SPTLC 3 could predict cardiac dysfunction in patients with sepsis. However, it should be noted that the preparation of exosomes is a cumbersome process. The search for biomarkers from exosomes is therefore not the best strategy in the case of sepsis since diagnosis cannot be made rapidly enough. Rapid diagnosis is a key criterion in this pathology to limit the mortality associated with the disease (Table 2).

Most studies to detect biomarkers have focused on the proteome which is defined as set of proteins in a cell compartment, cell, or tissue. More recently, much work has

focused on proteins in plasma, serum, or urine. It would therefore be more appropriate in this case to use the term “secretome” which is defined as the set of proteins secreted or liberated by a cell, tissue, or organism at a given time and under given conditions, which would explain their presence in biological fluids [26].

2.2. “Secretomics.” Secretome is a dynamic and complex entity that varies according to cell type or organism, functional state, and time. Indeed, depending on the stimuli they receive, the proteins released by a given cell may vary. For example, during an infection, the high-mobility group box 1 (HMGB1), which belongs to the alarmin family, is released into the extracellular space and participates in the pathogenesis of sepsis [10]. Thus, any alteration in the release of a given protein and the abundance of such a protein in a given environment could reflect a pathological state [27]. Although the term secretome was first mentioned in 2000 in a study by Tjalsma et al. on the proteins secreted by the bacterium *Bacillus subtilis*, the concept of circulating factors in plasma/serum is older [28]. Parillo et al. showed 35 years ago that the transfer of serum from patients in septic shock to rat healthy cardiomyocytes induces a decrease in both the extent and velocity of shortening during contraction. This work demonstrated the existence of circulating blood factors favouring myocardial depression during septic shock in humans [29]. More recently, Mastronardi et al. studied this concept and reported that intravenous administration of “microparticles” present in the plasma of patients in septic shock at an early stage leads to increased expression of proinflammatory proteins such as nuclear factor- κ B (NF- κ B) in the heart and lungs [30]. In the same year, a study by van Hees et al. demonstrated that the transfer of plasma from patients in septic shock to skeletal muscle tissue leads to a loss of myosin from skeletal myocytes. The factors that contribute to such muscle weakness are released during sepsis. Proinflammatory cytokines such as IL-6, TNF- α , interferon- γ , or interleukin-1 β (IL-1 β) are known to be involved in muscle degeneration pathologies [31]. In this study, they showed that the plasma level of IL-6 correlates with the severity of myosin loss. However, it was also found that the addition of IL-6 alone to control plasma is not associated with muscle atrophy [31]. Hence, these results suggest that additional

TABLE 2: Summary of the advantages and disadvantages, in the context of sepsis, for proteomic analyses of each sample source described.

Samples	 Tissues/organs	 Biological fluids			Exosomes
	Kidney/heart	Plasma	Serum	Urine	
Advantages	(i) Study of the desired organ.	(i) Poorly invasive (ii) Inexpensive analyses	(i) Poorly invasive (ii) Inexpensive analyses	(i) Noninvasive	(i) Poorly invasive (ii) Provides information on the state of the cells
Disadvantages	(i) Not clinically applicable (ii) Biopsies difficult to obtain (iii) Highly invasive	(i) Wide range of concentrations	(i) Time of analysis (ii) Wide range of concentrations (iii) Loss of proteins associated with coagulation	(i) Poorly reproducible in clinics	(i) Time of analysis

circulating factors in addition to IL-6, not currently identified, are also involved in the transmission and/or amplification of the pathological phenotype according to mechanisms that remain to be defined. The study of proteins that constitute the secretome could lead to a better understanding of the mechanisms underlying septic shock in addition to facilitating the identification of a number of biomarkers or a combination of them (coming as a signature) in the early phase of this pathology. However, analysis of the secretome is rendered difficult by the dynamic range of protein expression which is a major technical difficulty in proteomic studies. For example, plasma contains a wide dynamic range of more than ten orders of magnitude. As a result, 90% of the proteins contained in the plasma consist of only 10 well-identified proteins such as albumin, immunoglobulin, or transferrin [11]. This wide dynamic range of concentrations makes it particularly difficult to analyse proteins of low abundance by MS, thereby hindering the identification of new biomarker candidates. To avoid this, strategies for selective depletion of abundant proteins have been developed to facilitate analyses of the secretome and identify new biomarkers from biological fluids.

2.2.1. Selective Depletion Techniques. Various approaches for processing proteomic samples have been developed in recent years to reduce the complexity of biological samples, including selective depletion. During proteomic analyses, these techniques enable detection of the signal of low abundance proteins in a complex protein sample by reducing the dynamic concentration range of the proteins. Two approaches are particularly used: immunodepletion and ProteoMiner™. The immunodepletion technique is simply based on a pulldown thanks to the interaction between an antibody and a protein in the sample. The choice of antibody or antibodies is based on knowledge of the proteins studied [32]. The immunodepletion process can easily be performed on plasma or serum samples. However, immunodepletion can cause protein-protein interactions, resulting in depletion of nontargeted proteins [33]. In addition, the high cost of sample preparation prevents this method from being routinely used in clinical settings. Contrary to immunodepletion, ProteoMiner™ does not use antibodies. It is based on the interac-

tion of a high combination of 6-amino acid peptide sequences, called hexapeptides, with the proteins from the sample. These sequences are randomly generated so that all of the proteins in the sample will be able to interact with one or more hexapeptides. Since the binding capacity of hexapeptides is limited, a significant fraction of the highly abundant proteins is eliminated during the wash phase. The proteins bound to the hexapeptides will then be recovered during the elution phase for MS analyses [34]. This technique therefore appears to be particularly appropriate for nontargeted analysis. The biggest inconvenience of using ProteoMiner™ is most probably that the probability of catching small molecular weight proteins or peptides is much lower than larger molecular weight proteins, implying that it has a cut-off efficacy for lower molecular weight proteins (approximately 2 kDa). Hence, the technique is not as good for analysing the relative abundance of cytokines despite their being relevant targets in septic shock.

2.2.2. Detection of Biomarkers in Urine. Since biopsies are not appropriate for the detection of early biomarkers in clinical investigations for sepsis, several studies have turned to urine analyses. The collection of urine samples is noninvasive, unlike blood samples.

The search for early biomarkers in human urine samples has identified 39 deregulated proteins in urine from septic patients. Among these proteins, levels of β -2-microglobulin (B2M) and α -1-antitrypsin (SERPINA1) are increased during sepsis-induced acute kidney injuries (AKI) while levels of α fibrinogen (FGA) chains are decreased. The combination of these markers could therefore predict the onset of AKI [35]. In a recent study, 123 deregulated proteins were detected in urine samples from rats in sepsis or sepsis patients. Among these targets, the acidic nucleic protein deglycase DJ-1 (PARK7) and cadherin 16 (CDH16) were found in samples from both models. This study also showed that the diagnostic sensitivities and specificities of PARK7 and CDH16 were greater than that of neutrophil gelatinase-associated lipocalin (NGAL), which is currently used to diagnose AKI [24]. Thus, these two proteins could potentially be considered as early biomarkers of sepsis-induced AKI. Study of the urinary proteome provides identification of potential

biomarkers or therapeutic targets of sepsis. However, patients with sepsis have low diuresis, making it difficult to study urinary biomarkers in the clinic (Table 2). Moreover, a large portion of the deregulated proteins could result from kidney damage, suggesting that they could represent late biomarkers instead of early ones. Therefore, the use of blood samples appears to be more appropriate to look for biomarkers allowing for rapid diagnosis and patient follow-up.

2.2.3. Detection of Biomarkers in Blood Samples. Whole blood consists of plasma, cells, erythrocytes, and platelets. Cells contained in the blood are eliminated to obtain plasma and serum which makes their analyses simpler. As a result, MS studies are mainly performed on plasma or serum samples. Therefore, this review will not address the search for biomarkers in whole blood.

(1) Serum. Unlike plasma, serum is devoid of blood cells or fibrinogen. This biological fluid is rich in proteins, easily accessible, and capable of providing dynamic information on the circulatory system and the evolution of the disease. Proteomic analyses of patient sera revealed a combination of ten proteins that are deregulated during sepsis, including antithrombin III (AT-III), clusterin (CLUS), and serum amyloid A-1 (SAA-1) [14]. The latter is increased in the sepsis patient group, indicating a response to inflammation and tissue damage [14]. Similarly, Hayashi et al., who studied the patient proteome over time, showed a significant decrease in haemoglobin beta 1 and 2 chains in the group of patients who did not survive sepsis [36]. These molecules could be markers of sepsis severity. Both studies identified the biomarkers of sepsis in serum. However, there are no common biomarkers between these studies. This can in part be explained by the fact that Hayashi et al. incorporated the concept of kinetics of pathology development into their study which forces one to study the evolution of the secretome and not its state at a given time. Serum samples contain little or no coagulation-associated proteins, but sepsis is also accompanied by coagulation abnormalities [37]. Thus, plasma would make it possible to study proteins involved in the coagulation cascade which would appear to be relevant for biomarker research and potential therapeutic strategy. This makes plasma a more appropriate source for the detection of nontargeted biomarkers or therapeutic targets (Table 2).

(2) Plasma. Proteomic analyses of plasma have been widely used to identify sepsis biomarkers. Conducted over the past 10 years, a number of them have examined plasma proteomic changes in animal models or in patients with sepsis. In 2019, a study on the plasma proteome of a mouse model of sepsis caused by five different pathogens sought to understand the molecular connections that lead to the progression of the pathology. The analysis of the different plasma samples identified a network of 84 proteins. According to bibliographic data, these proteins have already been described as being involved in human sepsis. In addition, the authors showed that these proteins could be separated into functional networks including those involved in immune suppression, vascular homeostasis, coagulation, or the complement cascade

[38]. More recently, a study conducted on plasma from patients with sepsis showed an increase in acetylated truncated S100A8 and S100A9 as well as monooxidized S100A8 in nonsurviving patients with septic shock [9]. The increase in monooxidized S100A8 protein can be explained by the increased production of ROS by neutrophils and monocytes in sepsis or septic shock. This ROS production contributes to organ damage, and the protein S100A8 could also reflect an organic dysfunction. These proteins, which are in the family of alarmins, appear to be potential markers that could improve the management of patients at risk of dying of septic shock.

A major limitation to the use of plasma and serum for biomarker research is that it is not known to what extent different affected tissues alter the composition of plasma during a disease state [39]. Based on the elements developed in this paragraph, it appears that despite the limitations mentioned above, plasma is the most relevant biological sample for the identification of early sepsis biomarkers.

To conclude, mass spectrometry can analyse different types of biological samples to identify candidate sepsis biomarkers. Given the complexity of this pathology and the great heterogeneity between patients, it would seem more appropriate to analyse plasma for a protein combination whose level changes during sepsis. Such a combination would improve the sensitivity and specificity of these potential biomarkers.

The obvious disadvantage of working with human samples is that the kinetics of the pathology's evolution are not controlled and that blood sampling occurs at various stages of disease progression. Indeed, some patients will present a reduced early phase and will very quickly develop complications such as organ dysfunction associated with the pathology. Others will develop such complications later or not at all. This heterogeneity interferes with the identification of "ideal" biomarkers—in other words early, sensitive, and specific to the pathology. Therefore, many studies have focused on animal models as a first step.

3. Animal Models

Animal models of sepsis have been developed to reproduce the haemodynamic and molecular changes that occur in human sepsis. By studying the evolution of the pathology, these models enable us to understand the underlying mechanisms and thus identify potential biomarkers or therapeutic targets. They have the advantage of being better controlled from the viewpoint of kinetics and interindividual variability. However, the results obtained with the animal model are not always transposable to humans. These elements underline the importance of the choice of the animal model as a rationale for the identification of new biomarkers and in the search for molecules to improve the management of sepsis. The different models of sepsis clearly remain a compromise between standardisation and clinical relevance.

3.1. Nonsurgical Models

TABLE 3: Summary of advantages and disadvantages of animal sepsis models.

	Model	Advantages	Disadvantages
Nonsurgical 	Exogenous molecules	(i) Normalisation of the injected dose and route of administration (ii) Reproduces myocardial alterations	(i) Different cytokinetics (ii) Does not reflect the complexity of human pathophysiological responses
	Bacteria	(i) Normalisation of bacteria dose (ii) Production of different infectious sites	(i) Brutal injection of bacteria (ii) Poorly reproduces the response caused by sepsis
	Caecal slurry	(i) Simple to achieve (ii) Standardisation of the injected dose and route of administration (iii) Reproducible (iv) Similar response to human sepsis	(i) Lack of hindsight on this model (ii) Model exceedingly difficult to implement
	Implantation	(i) Controllable and reproducible model (ii) Progressive systemic diffusion (iii) Limited death incidence	(i) One bacterial strain used (ii) Complicated model to set up
Surgical 	CLP	(i) Improved clinical relevance (ii) Severity variable according to needle diameter, number of punctures and length of ligated caecum	(i) Develops acute sepsis or intra-abdominal abscess (ii) Not controllable (iii) Dependent on experimenter (iv) Not very reproducible (v) Long to set up
	CASP	(i) Adjustable sepsis severity according to the diameter of the stent	(i) Continuous bacterial release (ii) Dependent on experimenter (iii) Long to set up
	CLI	(i) Polymicrobial model of sepsis (ii) Progressive systemic diffusion	(i) High death incidence (ii) Dependent on experimenter (iii) Poorly reproducible (iv) Long to set up

Adapted from the work of Murando et al. [50]. CLP: caecal ligation and puncture; CLI: caecal ligation and incision; CASP: colon ascendant stent peritonitis.

(1) *Injection of Exogenous Molecules.* In these models, bacterial products or endotoxins, injected intravenously (iv) or intraperitoneally (ip), replace the bacteria. They are simple to use, robust, and reproducible models. The most used molecules are lipopolysaccharides (LPS), deoxyribonucleic acid (DNA), ribonucleic acid (RNA), or synthetic oligodeoxynucleotides containing unmethylated CpG units (ODN-CpG). These patterns can be standardised by normalising the injected doses. Endotoxin-treated animals therefore present a clinical picture that is similar to sepsis with systemic arterial hypotension; impaired myocardial contractility; and increased circulating levels of lactate, tumour necrosis factor (TNF), and interleukin-6 (IL-6) [40–42]. However, the kinetics of sepsis development observed in endotoxemic shock do not mimic those observed in the patient. Indeed, it has been shown that after endotoxin injection, a strong and rapid increase in several proinflammatory cytokines was observed in mouse models in contrast to the smaller and progressive increase in sepsis patients [43]. Finally, endotoxemic models are characterized by the injection of LPS from a single bacterial strain with no initial infectious focus. LPS are mainly recognized at the extracellular stage by Toll-like receptors (TLRs) and by TLR4. The activation of these receptors will stimulate the pathways associated with inflammation, notably through the activation of the nuclear factor- κ B (NF- κ B) which regulates the transcription of numerous cytokines [44]. However, septic shock is, in most cases, caused by a

polymicrobial infection that activates multiple signalling pathways. Although exogenous injection models are the most widely used according to the literature, they do not completely reproduce the characteristics of sepsis in humans (Table 3).

(2) *Injection of Bacteria.* To reduce the limitations of the models described above, models for injecting live and dead bacteria have been developed. Bacteria can be administered by intravenous, intraperitoneal, intramuscular, or intratracheal injection. The use of whole bacteria exposes the organism to numerous bacterial components that can activate different receptors in the host and contributes to the complexity of these models. These models, which are simple to set up, make it possible to generate different infectious sites. These models can be used to reproduce pneumosepsis, urosepsis, or peritonitis [45, 46]. The caecal slurry peritonitis model, used in the study of paediatric sepsis in particular, consists in injecting the caecal contents of other animals, including humans, to induce polymicrobial sepsis in the animals studied [47]. The model's advantage is that bacterial injection can be standardised by normalising the titre administered and the site and time of administration. Animals that received the bacteria presented alterations in myocardial contractility and haemodynamic and physiological changes that are associated with sepsis in humans [48]. However, these models involve the administration of high doses of

bacteria to overcome host defences which effectively eliminates low doses of bacteria. These high doses will not interact with the host as in regular infection and for instance will not colonise the peritoneal cavity. Hence, this approach is not identical and will not accurately reproduce the host response which is often due to the rapid lysis of bacteria by the complement system [49]. In addition, the clinical relevance of these exogenous models could be affected by the bacterial load, the virulence of the strain of bacteria used, or the site of infection (Table 2).

3.2. Surgical Models. Surgical models are much more complex to set up, yet they create a more representative infectious site that better simulates a pathophysiological systemic immune response such as peritonitis.

(1) Implantation Model. Described in 1970, the implantation of a fibrin clot containing a standardised number of bacteria in the peritoneal cavity allows for the progressive release of the bacteria into the bloodstream (Table 3). Studies have shown that this model generates myocardial depression and a cytokine response similar to those observed in humans [51]. However, the use of a single organism in the fibrin clot is subject to the same criticisms as the injection of bacterial cultures with respect to clinical relevance (Table 3). In addition, this model requires major surgery to implant a fibrin clot in the peritoneal cavity with variable host response. The peritonitis model is therefore the currently preferred model.

(2) Model of Peritonitis. The peritonitis model has been widely used over the past 30 years to study the pathogenesis and therapeutic targets of sepsis [52]. This model involves the induction of intestinal lesions that cause microbial flora leakage into the normally sterile peritoneal cavity. For this purpose, caecal ligation and puncture (CLP), caecal ligation and incision (CLI), or colon ascendant stent peritonitis (CASP) can be performed [52, 53]. In all three models, the caecum, which contains a wide variety of bacteria, is perforated by one or more needle punctures (CLP), incision (CLI), or the introduction of a stent into the ascending colon distal to the ileocaecal valve (CASP). In the CLP and CLI models, the haemodynamic, metabolic, immunological, and apoptotic responses, characteristic of organ dysfunction, are more similar to those of human sepsis, which supports the validity of this model [53, 54]. The study of plasma biomarkers also indicates that CLP is clinically relevant [55]. In this model, the severity of sepsis can be modulated by the proportion of ligated caecum, their size, and the number of punctures. However, this aspect also represents a weakness of these models because the procedure is experimenter-dependent, resulting in a lack of reproducibility within and between different research groups. Furthermore, CLI is associated with remarkably high mortality. To more accurately reproduce a case of peritonitis following intestinal perforation in humans, the CASP model has been developed [50, 56]. This model is generated by the insertion of a stent,

which limits blood flow without stopping it. The CASP model limits necrosis and the associated responses and generates diffuse peritonitis with a continuous bacterial translocation from the bowel to the peritoneal cavity. It leads to organ dysfunction as in the CLP and CLI models or septic patients. With this model, the severity of sepsis is adjustable according to the diameter of the stent and mortality is also associated with stent size [57]. The main limitation of these surgical models is that they are very poorly reproducible, so although they better represent the pathology, their use remains complex and limited (Table 2). In addition, the microbiota varies from one model to another and may interfere with the identification of candidate biomarkers. All of these data tend to place the CPL model as the most adequate model to model sepsis.

3.3. Limits Associated with the Animal Model. The sepsis models described above have been used with the animal models. To date, the mouse model remains the most widely used because it is less expensive and has a wider range of reagents available for biochemical studies compared with other species. Laboratory animals are chosen to have similar gene heritage, age, weight, and nutritional status, which does not reflect the heterogeneity among humans. Secondly, the mouse model does not have the same immune system as humans, resulting in a different form of resistance to infection than humans (Table 4). Pigs or sheep, which are more susceptible to infection, could therefore be more relevant [50]. No attempt has been made to introduce best practices, management guidelines, and standardisation in sepsis research, creating confusion with conflicting data resulting from variations in the definition of sepsis or the duration of study [58]. The animal models set up and the samples analysed as well as the time taken to collect these samples vary from one study to another. The lack of standardisation of preclinical data makes it difficult to use the results to identify potential biomarkers or therapeutic targets [59].

In this context, one could suggest withdrawing preclinical animal models. Nevertheless, it is recognized that, for instance, many of the pathways of acute inflammation have been elucidated by the rodent CLP model, considered as a pertinent polymicrobial model [60]. In addition, by refining the animal model of sepsis—i.e., by “humanising” animal diet and microbiome, by studying animals of various ages and both sexes in the presence or absence of underlying chronic comorbidities, and incorporating the basic treatment (fluids, antibiotics)—it could be possible to evaluate models of sepsis and septic shock pathological conditions closer to those of human cases with more relevance such as septic cardiomyopathy [61]. Finally, the “online” translational comparison with biological samples harvested from patients in septic shock will make it possible to confirm or overrule the relevance of a therapeutic target.

4. Conclusion/Discussion

The use of “secretomics”/proteomics based on MS has led to the identification of many promising biomarkers for the early diagnosis of sepsis and the prevention of organ

TABLE 4: Summary of the major differences between humans and the most used animal models of septic shock.

	Human	Mouse	Rat
			
Heart rhythm 	70 bpm	500-700 bpm	250-400 bpm
Respiratory rhythm 	12-20/min	100-200/min	70-110/min
Surface ratio of small intestine/colon 	18	400	400
Endotoxin	High sensitivity	High resistance	High resistance
Main protein in acute phase	CRP	SAP	SAP
Immune system	Neutrophils	Lymphocytes	Lymphocytes
Largest fraction of blood cells			
Complement system	High plasma activity	Poor plasma activity	Poor plasma activity

Adapted from the work of Cavaillon et al. [62]. Bpm: beats per minute; CRP: C-reactive protein; SAP: serum amyloid protein.

dysfunction, particularly cardiac dysfunction. However, the validity and clinical utility of many of these biomarkers have not been tested. In clinical practice, these biomarkers must be validated to human cases of sepsis. They should then be routinely usable, in other words, they must be rapidly quantifiable and relatively cheap. Anyway, MS analyses from biological fluids appear to be more transferable to the clinical setting. Since January 2015, 1,495 studies have focused on the use of biomarkers for the diagnosis of sepsis [7]. The lack of early and specific biomarkers of sepsis and septic shock could be partly related to the fact that there are several limitations in proteomic studies that hinder the identification of clinically usable biomarkers. Indeed, although studies use proteomics to identify new biomarkers, they differ in the experimental protocol used. All of these differences result in proteomic signatures that vary from one study to another. The lack of standardisation of preclinical data makes it difficult to use the results to identify clinically relevant biomarkers. It is therefore crucial that research teams standardise their experience to provide better comparisons of results from one laboratory to another, increasing the quantity of data and limiting the heterogeneity that results from the pathology.

Data Availability

The data supporting this review are from previously reported studies and datasets, which have been cited.

Conflicts of Interest

Authors declare that no conflicts of interest exist.

Authors' Contributions

A. Blangy-Letheule drafted the review. A. Persello reviewed the article for intellectual content. B. Rozec, M. De Waard, and B. Lauzier reviewed the article for intellectual content and gave final approval of the version or any revised version to be submitted. Bertrand Rozec, Michel De Waard, and Benjamin Lauzier codirected this work.

Acknowledgments

This work was supported by the Agence Nationale de la Recherche through a grant to the laboratory of excellence "Ion Channels, Science, and Therapeutics" (Grant No. ANR-11-LABX-0015). We also thank the financial support of Inserm and the "Région Pays de la Loire" with a "New Team" grant to M. De Waard. This work was also directly supported by "Agence Nationale de la Recherche" (20-ASTC-0032-01-HEROISME) (Paris, France).

References

- [1] M. Singer, C. S. Deutschman, C. W. Seymour et al., "The Third International Consensus Definitions for Sepsis and Septic Shock (Sepsis-3)," *JAMA*, vol. 315, no. 8, pp. 801–810, 2016.
- [2] K. E. Rudd, S. C. Johnson, K. M. Agesa et al., "Global, regional, and national sepsis incidence and mortality, 1990–2017: analysis for the Global Burden of Disease Study," *The Lancet*, vol. 395, no. 10219, pp. 200–211, 2020.
- [3] M. Ferron, J. Cadiet, A. Persello et al., "O-GlcNAc stimulation: a new metabolic approach to treat septic shock," *Scientific Reports*, vol. 9, no. 1, p. 18751, 2019.
- [4] A. Trzeciak, A. P. Pietropaoli, and M. Kim, "Biomarkers and associated immune mechanisms for early detection and

- therapeutic management of sepsis,” *Immune Network*, vol. 20, no. 3, 2020.
- [5] K. Reinhart, R. Daniels, N. Kissoon, F. R. Machado, R. D. Schachter, and S. Finfer, “Recognizing Sepsis as a Global Health Priority — A WHO Resolution,” *New England Journal of Medicine*, vol. 377, no. 5, pp. 414–417, 2017.
- [6] E. Harberts, T. Liang, S. H. Yoon et al., “Toll-like receptor 4-independent effects of lipopolysaccharide identified using longitudinal serum proteomics,” *Journal of Proteome Research*, vol. 19, no. 3, pp. 1258–1266, 2020.
- [7] A. Teggert, H. Datta, and Z. Ali, “Biomarkers for point-of-care diagnosis of sepsis,” *Micromachines*, vol. 11, no. 3, p. 286, 2020.
- [8] C. A. Siloși, I. Siloși, V. Pădureanu et al., “Sepsis and identification of reliable biomarkers for postoperative period prognosis,” *Romanian Journal of Morphology and Embryology*, vol. 58, 2018.
- [9] C. Dubois, D. Payen, S. Simon et al., “Top-down and bottom-up proteomics of circulating S100A8/S100A9 in plasma of septic shock patients,” *Journal of Proteome Research*, vol. 19, no. 2, pp. 914–925, 2020.
- [10] M. Deng, M. J. Scott, J. Fan, and T. R. Billiar, “Location is the key to function: HMGB1 in sepsis and trauma-induced inflammation,” *Journal of Leukocyte Biology*, vol. 106, no. 1, pp. 161–169, 2019.
- [11] K. R. Ludwig and A. B. Hummon, “Mass spectrometry for the discovery of biomarkers of sepsis,” *Molecular BioSystems*, vol. 13, no. 4, pp. 648–664, 2017.
- [12] M. Y. Memar and H. B. Baghi, “Presepsin: a promising biomarker for the detection of bacterial infections,” *Biomedicine & Pharmacotherapy*, vol. 111, pp. 649–656, 2019.
- [13] M. G. Snipsøyr, H. Wiggers, M. Ludvigsen et al., “Towards identification of novel putative biomarkers for infective endocarditis by serum proteomic analysis,” *International Journal of Infectious Diseases*, vol. 96, pp. 73–81, 2020.
- [14] S. Garcia-Obregon, M. Azkargorta, I. Seijas et al., “Identification of a panel of serum protein markers in early stage of sepsis and its validation in a cohort of patients,” *Journal of Microbiology, Immunology and Infection*, vol. 51, no. 4, pp. 465–472, 2018.
- [15] I. Bednarz-Misa, M. Mierzchala-Pasierb, P. Lesnik et al., “Cardiovascular insufficiency, abdominal sepsis, and patients’ age are associated with decreased paroxonase-1 (PON1) activity in critically ill patients with multiple organ dysfunction syndrome (MODS),” *Disease Markers*, vol. 2019, Article ID 1314623, 12 pages, 2019.
- [16] C. Wang, Y. Cui, H. Miao et al., “Apolipoprotein A-V is a novel diagnostic and prognostic predictor in pediatric patients with sepsis: a prospective pilot study in PICU,” *Mediators of Inflammation*, vol. 2020, 9 pages, 2020.
- [17] W.-J. Lee, Y.-L. Chen, Y.-W. Chu, and D.-S. Chien, “Comparison of glutathione peroxidase-3 protein expression and enzyme bioactivity in normal subjects and patients with sepsis,” *Clinica Chimica Acta*, vol. 489, pp. 177–182, 2019.
- [18] H. Wake, Y. Takahashi, Y. Yoshii et al., “Histidine-rich glycoprotein possesses antioxidant activity through self-oxidation and inhibition of hydroxyl radical production via chelating divalent metal ions in Fenton’s reaction,” *Free Radical Research*, vol. 54, pp. 1–13, 2020.
- [19] M. Foote and Y. Zhou, “14-3-3 proteins in neurological disorders,” *International Journal of Biochemistry and Molecular Biology*, vol. 3, no. 2, pp. 152–164, 2012.
- [20] B. Róka, P. Tod, T. Kaucsár et al., “The acute phase response is a prominent renal proteome change in sepsis in mice,” *International Journal of Molecular Sciences*, vol. 21, no. 1, p. 200, 2020.
- [21] F. Cuello, M. Shankar-Hari, U. Mayr et al., “Redox state of pentraxin 3 as a novel biomarker for resolution of inflammation and survival in sepsis,” *Molecular & Cellular Proteomics*, vol. 13, no. 10, pp. 2545–2557, 2014.
- [22] Q. S. Wells, D. K. Gupta, J. G. Smith et al., “Accelerating biomarker discovery through electronic health records, automated biobanking, and proteomics,” *Journal of the American College of Cardiology*, vol. 73, no. 17, pp. 2195–2205, 2019.
- [23] Y. Xu, X. Ku, C. Wu, C. Cai, J. Tang, and W. Yan, “Exosomal proteome analysis of human plasma to monitor sepsis progression,” *Biochemical and Biophysical Research Communications*, vol. 499, no. 4, pp. 856–861, 2018.
- [24] Y. Li, J. Long, J. Chen et al., “Analysis of spatiotemporal urine protein dynamics to identify new biomarkers for sepsis-induced acute kidney injury,” *Frontiers in Physiology*, vol. 11, 2020.
- [25] H.-Y. Chung, A. Kollmeier, A. Schrepper et al., “Adjustment of dysregulated ceramide metabolism in a murine model of sepsis-induced cardiac dysfunction,” *International Journal of Molecular Sciences*, vol. 18, no. 4, p. 839, 2017.
- [26] O. K. Kwon, W. Lee, S. J. Kim et al., “In-depth proteomics approach of secretome to identify novel biomarker for sepsis in LPS-stimulated endothelial cells,” *Electrophoresis*, vol. 36, no. 23, pp. 2851–2858, 2015.
- [27] F. Vizoso, N. Eiro, S. Cid, J. Schneider, and R. Perez-Fernandez, “Mesenchymal stem cell secretome: toward cell-free therapeutic strategies in regenerative medicine,” *International Journal of Molecular Sciences*, vol. 18, no. 9, p. 1852, 2017.
- [28] H. Tjalsma, A. Bolhuis, J. D. H. Jongbloed, S. Bron, and J. M. van Dijk, “Signal peptide-dependent protein transport in *Bacillus subtilis*: a genome-based survey of the secretome,” *Microbiology and Molecular Biology Reviews*, vol. 64, no. 3, pp. 515–547, 2000.
- [29] J. E. Parrillo, C. Burch, J. H. Shelhamer, M. M. Parker, C. Natanson, and W. Schuette, “A circulating myocardial depressant substance in humans with septic shock. Septic shock patients with a reduced ejection fraction have a circulating factor that depresses in vitro myocardial cell performance,” *Journal of Clinical Investigation*, vol. 76, no. 4, pp. 1539–1553, 1985.
- [30] M. L. Mastrorandi, H. A. Mostefai, F. Mezzani, M. C. Martínez, P. Asfar, and R. Andriantsitohaina, “Circulating microparticles from septic shock patients exert differential tissue expression of enzymes related to inflammation and oxidative stress,” *Critical Care Medicine*, vol. 39, no. 7, pp. 1739–1748, 2011.
- [31] H. W. H. van Hees, W.-J. M. Schellekens, M. Linkels et al., “Plasma from septic shock patients induces loss of muscle protein,” *Critical Care*, vol. 15, no. 5, p. R233, 2011.
- [32] S. Xu, J. Jiang, Y. Zhang et al., “Discovery of potential plasma protein biomarkers for acute myocardial infarction via proteomics,” *Journal of Thoracic Disease*, vol. 11, no. 9, pp. 3962–3972, 2019.
- [33] J. Hajduk, J. Matysiak, and Z. J. Kokot, “Challenges in biomarker discovery with MALDI-TOF MS,” *Clinica Chimica Acta*, vol. 458, pp. 84–98, 2016.
- [34] S. Li, Y. He, Z. Lin et al., “Digging more missing proteins using an enrichment approach with ProteoMiner,” *Journal of Proteome Research*, vol. 16, no. 12, pp. 4330–4339, 2017.

- [35] E. Carrick, J. Vanmassenhove, G. Glorieux et al., “Development of a MALDI MS-based platform for early detection of acute kidney injury,” *PROTEOMICS - Clinical Applications*, vol. 10, no. 7, pp. 732–742, 2016.
- [36] N. Hayashi, S. Yamaguchi, F. Rodenburg et al., “Multiple biomarkers of sepsis identified by novel time-lapse proteomics of patient serum,” *PLoS One*, vol. 14, no. 9, 2019.
- [37] M. Levi and T. van der Poll, “Coagulation and sepsis,” *Thrombosis Research*, vol. 149, pp. 38–44, 2017.
- [38] G. Pimienta, D. M. Heithoff, A. Rosa-Campos et al., “Plasma proteome signature of sepsis: a functionally connected protein network,” *Proteomics*, vol. 19, no. 5, article e1800389, 2019.
- [39] E. Malmström, O. Kilsgård, S. Hauri et al., “Large-scale inference of protein tissue origin in gram-positive sepsis plasma using quantitative targeted proteomics,” *Nature Communications*, vol. 7, no. 1, 2016.
- [40] M. P. Fink, “Animal models of sepsis,” *Virulence*, vol. 5, no. 1, pp. 143–153, 2013.
- [41] D. Roul, B. Rozec, M. Ferron et al., “B1-adrenergic cardiac contractility is increased during early endotoxemic shock: involvement of cyclooxygenases,” *Life Sciences*, vol. 236, article 116865, 2019.
- [42] J. E. Slotta, C. Scheuer, M. D. Menger, and B. Vollmar, “Immunostimulatory CpG-oligodeoxynucleotides (CpG-ODN) induce early hepatic injury, but provide a late window for protection against endotoxin-mediated liver damage,” *Journal of Hepatology*, vol. 44, no. 3, pp. 576–585, 2006.
- [43] D. G. Remick and P. A. Ward, “Evaluation of endotoxin models for the study of sepsis,” *Shock*, vol. 24, Supplement 1, pp. 7–11, 2005.
- [44] H.-J. Kim, H.-I. Joe, Z. Zhang et al., “Anti-inflammatory effect of *Acalypha australis* L. via suppression of NF- κ B signaling in LPS-stimulated RAW 264.7 macrophages and LPS-induced septic mice,” *Molecular Immunology*, vol. 119, pp. 123–131, 2020.
- [45] S. Knapp, M. J. Schultz, and T. van der Poll, “Pneumonia models and innate immunity to respiratory bacterial pathogens,” *Shock*, vol. 24, Supplement 1, pp. 12–18, 2005.
- [46] H. Wu, Z. Wang, S. Zhu et al., “Uroseptic shock can be reversed by early intervention based on leukocyte count 2 h post-operation: animal model and multicenter clinical cohort study,” *Inflammation*, vol. 41, no. 5, pp. 1835–1841, 2018.
- [47] M. E. Starr, A. M. Steele, M. Saito, B. J. Hacker, B. M. Evers, and H. Saito, “A new cecal slurry preparation protocol with improved long-term reproducibility for animal models of sepsis,” *PLoS One*, vol. 9, no. 12, article e115705, 2014.
- [48] M. J. Lee, K. Kim, Y. H. Jo, J. H. Lee, and J. E. Hwang, “Dose-dependent mortality and organ injury in a cecal slurry peritonitis model,” *Journal of Surgical Research*, vol. 206, no. 2, pp. 427–434, 2016.
- [49] J. A. Buras, B. Holzmann, and M. Sitkovsky, “Animal models of sepsis: setting the stage,” *Nature Reviews Drug Discovery*, vol. 4, no. 10, pp. 854–865, 2005.
- [50] F. Murando, A. Peloso, and L. Cobianchi, “Experimental abdominal sepsis: sticking to an awkward but still useful translational model,” *Mediators of Inflammation*, vol. 2019, Article ID 8971036, 8 pages, 2019.
- [51] C. Natanson, M. P. Fink, H. K. Ballantyne, T. J. MacVittie, and J. J. Conklin, “Gram-negative bacteremia produces both severe systolic and diastolic cardiac dysfunction in a canine model that simulates human septic shock,” *Journal of Clinical Investigation*, vol. 78, no. 1, pp. 259–270, 1986.
- [52] S. M. K. Kingsley and B. V. Bhat, “Differential paradigms in animal models of sepsis,” *Current Infectious Disease Reports*, vol. 18, no. 9, 2016.
- [53] P. Scheiermann, S. Hoegl, M. Revermann et al., “Cecal ligation and incision: an acute onset model of severe sepsis in rats,” *Journal of Surgical Research*, vol. 151, no. 1, pp. 132–137, 2009.
- [54] S. K. Mishra and S. Choudhury, “Experimental protocol for cecal ligation and puncture model of polymicrobial sepsis and assessment of vascular functions in mice,” in *Traumatic and Ischemic Injury: Methods and Protocols*, B. Tharakan, Ed., pp. 161–187, Springer, New York, NY, USA, 2018.
- [55] J.-L. Li, G. Li, X.-Z. Jing et al., “Assessment of clinical sepsis-associated biomarkers in a septic mouse model,” *The Journal of International Medical Research*, vol. 46, no. 6, pp. 2410–2422, 2018.
- [56] A. J. Lewis, C. W. Seymour, and M. R. Rosengart, “Current murine models of sepsis,” *Surgical Infections*, vol. 17, no. 4, pp. 385–393, 2016.
- [57] S. Maier, T. Traeger, M. Entleutner et al., “Cecal ligation and puncture versus colon ascendens stent peritonitis: two distinct animal models for polymicrobial sepsis,” *Shock*, vol. 21, no. 6, pp. 505–512, 2004.
- [58] D. G. Remick, A. Ayala, I. H. Chaudry et al., “Premise for standardized sepsis models,” *Shock*, vol. 51, no. 1, pp. 4–9, 2019.
- [59] M. F. Osuchowski, A. Ayala, S. Bahrami et al., “Minimum Quality Threshold in Pre-Clinical Sepsis Studies (MQTiPSS): an international expert consensus initiative for improvement of animal modeling in sepsis,” *Shock*, vol. 50, no. 4, pp. 377–380, 2018.
- [60] J. C. Alverdy, R. Keskey, and R. Thewissen, “Can the cecal ligation and puncture model be repurposed to better inform therapy in human sepsis?,” *Infection and Immunity*, vol. 88, no. 9, 2020.
- [61] A. Guillon, Translational Research Committee of the French Intensive Care Society (Société de Réanimation de Langue Française), S. Preau et al., “Preclinical septic shock research: why we need an animal ICU,” *Annals of Intensive Care*, vol. 9, no. 1, 2019.
- [62] J.-. M. Cavaillon, M. Singer, and T. Skirecki, “Sepsis therapies: learning from 30 years of failure of translational research to propose new leads,” *EMBO Molecular Medicine*, vol. 12, no. 4, article e10128, 2020.

Research Article

Uncovering the Molecular Mechanism of the Qiang-Xin 1 Formula on Sepsis-Induced Cardiac Dysfunction Based on Systems Pharmacology

Shasha He ^{1,2,3}, Jingxia Zhao ^{1,2,3}, Xiaolong Xu ^{1,2,3}, Xuran Cui ^{1,2,3}, Ning Wang^{1,2}, Xuyang Han ^{1,2}, Yuhong Guo ^{1,2,3} and Qingquan Liu ^{1,2,3}

¹Beijing Hospital of Traditional Chinese Medicine, Capital Medical University, Beijing, China

²Beijing Institute of Traditional Chinese Medicine, Beijing, China

³Beijing Key Laboratory of Basic Research with Traditional Chinese Medicine on Infectious Diseases, Beijing, China

Correspondence should be addressed to Yuhong Guo; 8snakes@163.com and Qingquan Liu; liuqingquan_2003@126.com

Received 30 April 2020; Revised 22 July 2020; Accepted 27 July 2020; Published 27 August 2020

Guest Editor: Luc Demaison

Copyright © 2020 Shasha He et al. This is an open access article distributed under the Creative Commons Attribution License, which permits unrestricted use, distribution, and reproduction in any medium, provided the original work is properly cited.

Cardiac dysfunction is a critical manifestation of sepsis-induced multiorgan failure and results in the high mortality of sepsis. Our previous study demonstrated that a traditional Chinese medicine formula, Qiang-Xin 1 (QX1), ameliorates cardiac tissue damage in septic mice; however, the underlying pharmacology mechanism remains to be elucidated. The present study was aimed at clarifying the protective mechanism of the QX1 formula on sepsis-induced cardiac dysfunction. The moderate sepsis model of mice was established by cecal ligation and puncture surgery. Treatment with the QX1 formula improved the 7-day survival outcome, attenuated cardiac dysfunction, and ameliorated the disruption of myocardial structure in septic mice. Subsequent systems pharmacology analysis found that 63 bioactive compounds and the related 79 candidate target proteins were screened from the QX1 formula. The network analysis showed that the QX1 active components quercetin, formononetin, kaempferol, taxifolin, cryptotanshinone, and tanshinone IIA had a good binding activity with screened targets. The integrating pathway analysis indicated the calcium, PI3K/AKT, MAPK, and Toll-like receptor signaling pathways may be involved in the protective effect of the QX1 formula on sepsis-induced cardiac dysfunction. Further, experimental validation showed that the QX1 formula inhibited the activity of calcium/calmodulin-dependent protein kinase II (CaMKII), MAPK (P38, ERK1/2, and JNK), and TLR4/NF- κ B signaling pathways but promoted the activation of the PI3K/AKT pathway. A cytokine array found that the QX1 formula attenuated sepsis-induced upregulated levels of serum IFN- γ , IL-1 β , IL-3, IL-6, IL-17, IL-4, IL-10, and TNF- α . Our data suggested that QX1 may represent a novel therapeutic strategy for sepsis by suppressing the activity of calcium, MAPK, and TLR4/NF- κ B pathways, but promoting the activation of AKT, thus controlling cytokine storm and regulating immune balance. The present study demonstrated the multicomponent, multitarget, and multipathway characteristics of the QX1 formula and provided a novel understanding of the QX1 formula in the clinical application on cardiac dysfunction-related diseases.

1. Introduction

Sepsis, defined as life-threatening organ dysfunction caused by a dysregulated host response to infection, affects more than 19 million people per year and is the main cause of death in intensive care units [1, 2]. Cardiac dysfunction is critical to sepsis-induced multiorgan failure. Cardiac dysfunction occurs in over 40% of sepsis patients, which is associated with high mortality and poor prognosis [3]. Despite

improvements in antibiotic therapies and critical care techniques, the management of cardiac dysfunction in patients with sepsis remains challenging since basic interventions for cardiac dysfunction or sepsis alone are contradictory in key areas, including fluid resuscitation [4]. The pathological mechanisms of cardiac dysfunction in sepsis are multifactorial, including inflammatory mediator disorder, mitochondrial dysfunction, apoptosis, and calcium regulation disorder [5, 6]. Therefore, developing a drug that can inhibit

these pathological changes would be of great clinical significance for the prevention of sepsis-induced cardiac dysfunction.

Traditional Chinese medicine (TCM) is an integral medicine system with clinical practice over thousands of years. Our previous study showed that the TCM prescription Qiang-Xin 1 (QX1) ameliorates cardiac tissue damage in mice suffering from sepsis partly by inhibiting endoplasmic reticulum- and mitochondria-related apoptosis [7]. However, a holistic understanding underlying mechanisms of the QX1 formula in improving sepsis-induced cardiac dysfunction still is needed in further study.

Systems pharmacology, an emerging systematic methodology combining pharmacology and systems biology, provides a holistic analysis approach to explore the molecular mechanism of TCM [8]. Systems pharmacology includes pharmacokinetics evaluation (absorption, distribution, metabolism, excretion, and toxicity [ADME/T] characteristics of herbs), target protein prediction, and network analysis. At present, systems pharmacology has been widely used to reveal the potential mechanism of TCM formulas in the treatment of cancer, inflammatory bowel disease, and cardiovascular disease [9–11].

The present study was aimed at investigating the molecular mechanism of the QX1 formula in the treatment of sepsis-induced cardiac dysfunction. First, the effect of the QX1 formula on survival rate and cardiac dysfunction was assessed in septic mice. Then, the material basis and potential interaction mechanism of the QX1 formula were analyzed by systems pharmacology. Finally, we further verified the mechanism of the QX1 formula on the main signaling pathways integrated by systemic pharmacology in septic mice. The workflow of the current study was shown in Figure 1.

2. Materials and Methods

2.1. Animals and Ethics Statement. BALB/c mice (male, 18–22 g, 8 weeks old) provided by Beijing HFK Bioscience Co., Ltd. (Beijing, China) were housed under a pathogen-free environment with free access to food and water. All procedures performed on the animals were conducted in accordance with the National Institutes of Health Guidelines on Laboratory Research and approved by the Animal Care and Use Committee of the Beijing Institute of Traditional Chinese Medicine (permit number: 2018040206).

2.2. Preparation of the QX1 Formula. The QX1 formula is composed of five herbs: *Astragalus membranaceus* (Fisch.) (HQ), *Polygonum orientale* L. (SHHZ), *Poria cocos* (Schw.) Wolf (FL), *Salvia miltiorrhiza* Bge. (DS), and *Schisandra chinensis* (Turcz.) Baill. (WWZ). All herbs were obtained from the Chinese Pharmacy of Beijing Hospital of Traditional Chinese Medicine and were mixed in the proportion of 3:3:2:2:1, with a total weight of 110 g. After soaking for 1 h, the QX1 decoction was prepared by water extraction twice. The extract was then filtered and condensed to 110 ml, with a concentration equal to 1 g herb/ml.

2.3. Cecal Ligation and Puncture- (CLP-) Induced Sepsis. A mouse model with moderate sepsis was established by cecal

ligation and puncture (CLP) surgery according to the protocol described previously [12]. Briefly, mice were anesthetized with 1% pentobarbital sodium, and a 1–2 cm longitudinal skin midline incision was made to expose the internal organs. The cecum was exposed and ligated in the mid position, which comprised 50% of the cecum, and punctured through and through with a 21-gauge needle. Then, a small amount of feces was extruded from the puncture holes to make sure patency. The cecum was transferred to the abdominal cavity, and the peritoneum and skin were closed by applying sutures. After surgery, mice were injected with sterile saline solution (0.9%, 24 ml/kg of body weight) for fluid resuscitation. In the sham group, the procedure was carried out in the same way as the CLP described above, except without ligation and puncture of the cecum.

2.4. Treatment Protocol of the QX1 Formula. After a 7-day acclimation period, 90 mice were randomly assigned to five groups: (1) sham group (sham, $n = 10$), wherein mice received a sham operation without drug treatment; (2) CLP group (CLP, $n = 20$), wherein mice received a CLP operation without QX1 decoction treatment; (3) low-dose QX1 decoction group (QX1 Low, $n = 20$), wherein mice received a CLP operation with 5 g/kg QX1 decoction treatment; (4) high-dose QX1 decoction group (QX1 High, $n = 20$), wherein mice received a CLP operation with 10 g/kg QX1 decoction treatment; and (5) trimetazidine group (TMZ, $n = 20$), wherein mice received a CLP operation with 20 mg/kg TMZ treatment. The mice in QX1 Low, QX1 High, and TMZ groups were orally administered intragastrically with different concentrations of QX1 decoction at 6 and 18 h after the CLP operation, respectively, whereas mice in the sham and CLP groups were administered with the same volume of water. In a survival test, another 20 mice from each group were used to assess survival rates during seven days.

2.5. Sample Collection. At 24 h after the CLP operation, mice were anesthetized with 1% pentobarbital sodium and blood samples were collected. Serum was separated for quantitative analysis of cytokines. The heart tissues were harvested and divided into three parts: one was stored in 10% buffered formalin phosphate for histological analysis, one was fixed in 4% glutaraldehyde for ultrastructure analysis, and the other was stored at -80°C for Western blot analysis.

2.6. Hematoxylin and Eosin (H&E) Staining. The heart samples were immersed in 10% neutral buffered formaldehyde at room temperature for 48 h, and the fixed samples were then embedded in liquid paraffin and sectioned into $5\ \mu\text{m}$ thickness. The sections were stained with hematoxylin and eosin, and the cardiac morphological changes were observed under a light microscope (Zeiss GmbH, Jena, Germany).

2.7. Transmission Electron Microscopy (TEM). The cardiac tissue samples were fixed with 4% glutaraldehyde overnight, postfixed in cold 1% osmium tetroxide, and then washed with cacodylate buffer three times. Subsequently, cardiac tissue was dehydrated in a series of graded acetone and embedded in an epoxy resin. Ultrathin sections were stained with saturated uranyl acetate in 50% ethanol and lead citrate and

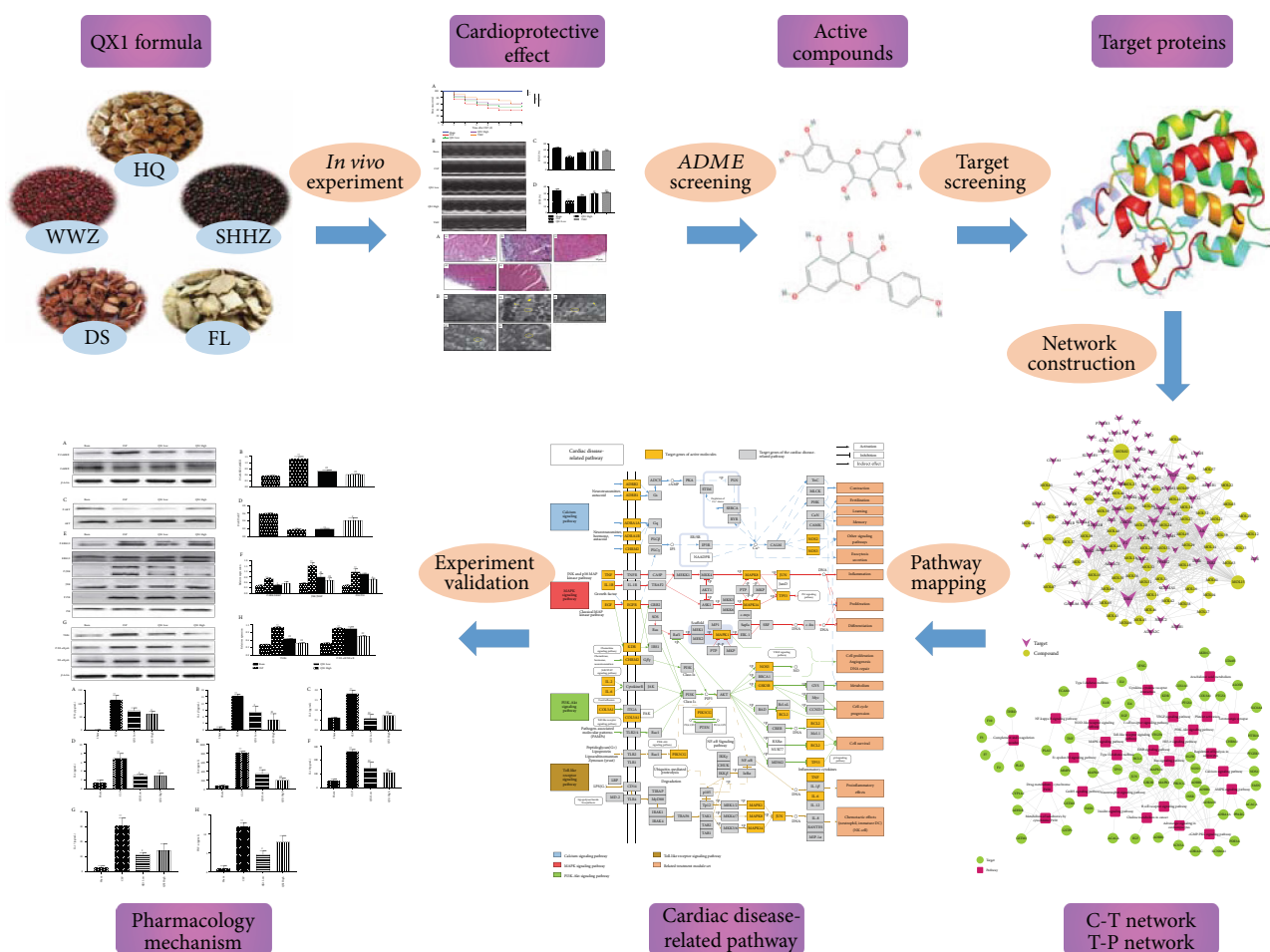


FIGURE 1: Workflow of the current study.

observed under an HT7700 transmission electron microscope (Hitachi, Tokyo, Japan).

2.8. Echocardiography Analysis. At 24h after CLP or sham surgery, echocardiography was performed using the Vevo 770 ultrasound system (Visual Sonics Inc., Toronto, Canada) to assess the cardiac function. Briefly, mice were anesthetized with isoflurane at a concentration of 4% (induction) or 1.5% (maintenance) in 100% oxygen. The left ventricular (LV) M-mode tracing was gained from the transthoracic parasternal short-axis view. Through these images, the left ventricular internal dimensions at diastole/systole (LVIDd/LVIDs) and the left ventricular volume at diastole/systole (LVVd/LVV_s) were measured and used to determine the left ventricular ejection fraction (LVEF) and left ventricular fractional shortening (LVFS). Each parameter was recorded in least three consecutive cardiac cycles.

2.9. Database Construction. The chemical ingredients of all herbs in the QX1 formula were data-mined from the Traditional Chinese Medicine Systems Pharmacology Database (TCMSP, <http://lsp.nwu.edu.cn/tcmspsearch.php>) and a large number of related literature mining, including PubMed and China National Knowledge Infrastructure (CNKI) databases. Finally, we obtained 513 chemical ingredients and

their physicochemical properties from QX1: 87 compounds of HQ, 130 compounds of WWZ, 202 compounds of DS, 34 compounds of FL, and 60 compounds of SHHZ.

2.10. Active Compound Screening

2.10.1. Oral Bioavailability (OB). OB is one of the most important pharmacokinetic parameters in ADME (absorption, distribution, metabolism, and excretion) characteristics, which indicates the efficiency of active drug delivery to the systemic circulation. In the present study, the OBioavail.1.1 model was used to estimate OB values [13]. And compounds from QX1 satisfy $OB \geq 28\%$ as a candidate active molecule for subsequent step screening.

2.10.2. Druglikeness (DL). DL is used to assess the similarity of physical properties of compounds with known drugs. According to previous reports, the drug-like active molecules were picked out from QX1 based on molecular descriptors and the Tanimoto coefficient [14]. In this study, a compound with $DL \geq 0.18$ was selected as the active compound of herbs for further study.

2.10.3. Drug Half-Life. Half-life refers to the time it takes for the concentration of a drug to be degraded to half in the body and is considered to be an essential pharmaceutical property,

which is mainly used as a time measure for defining the efficacy of a compound. The $HL \geq 4$ was adopted as the criterion to screen the candidate active compound of QX1 in this study.

2.10.4. Caco-2 Cell Permeability. The human intestinal cell line Caco-2 is commonly used as an effective in vitro model to study the passive diffusion of drugs through the intestinal epithelium. We used the transport rate of drug molecules in Caco-2 cell monolayers as an evaluation of intestinal absorption. Those chemical ingredients with Caco-2 cell permeability ≥ -0.4 were filtered out as candidate active compounds.

2.11. Target Prediction. To identify the target molecules of the candidate active compounds is a key step to reveal the mechanism of QX1. Currently, the weighted ensemble similarity (WES) model was applied to predict the potential targets of QX1 compound [15]. Then, a similarity based on chemical fingerprinting is used to obtain potential targets (<http://sea.bkslab.org/search/>). Finally, the targets from different sources were named uniformly in the UniProt database (<http://www.uniprot.org>) and then submitted to the Pharmacogenomics Knowledgebase (PharmGKB, <https://www.pharmgkb.org/>), Therapeutic Targets Database (TTD, <http://database.idrb.cqu.edu.cn/TTD/>), and Comparative Toxicogenomics Database (CTD, <http://ctdbase.org/>) to remove redundant and erroneous targets, so as to ensure the accuracy of the target database.

2.12. Network Construction. Traditional Chinese medicine (TCM) is a whole system with multicomponent and multitarget characteristics. There is a complicated relationship between effective active compounds, active targets, and pathways. Therefore, the network visualization analysis software Cytoscape was used to draw the compound-target (C-T) network and target-pathway (T-P) network.

In order to investigate the molecular mechanism of the QX1 formula against cardiac injury, an integrated “cardiac disease-related pathway” was established. Firstly, the active targets were mapped to the KEGG database (<http://www.kegg.jp/>). Then, according to the latest pathological information of a cardiac disease-related pathway, an integrated compound-target pathway diagram was constructed by combining C-T network and T-P network analyses.

2.13. Target-Tissue Location. To understand QX1 formula therapy for cardiac disease at the organ level, first, GO analysis showed the most obvious targets among the screened compound targets, and then, their distribution in tissues and organs was analyzed. The tissue distribution of the targets was identified based on microarray analysis of different tissue types in the BioGPS database (<http://biogps.org>).

2.14. Ultraperformance Liquid Chromatography Coupled with Orbitrap Q Exactive Mass Spectrometry (UPLC-MS). Plasma samples were collected at 0, 15, 30, 60, and 120 min after oral administration with 10 g/kg QX1 decoction. The reference standards of quercetin, formononetin, kaempferol, taxifolin, cryptotanshinone, and tanshinone IIA were pur-

chased from the National Institutes for Food and Drug Control (Beijing, China). The plasma samples and standard solutions were analyzed using ultraperformance liquid chromatography coupled with Orbitrap Q Exactive mass spectrometry (Thermo Scientific, San Jose, USA). Briefly, acetonitrile (A) and 0.1% formic acid aqueous solution (B) were selected as the mobile phases. The gradient mobile phase was as follows: 0% A from 0 to 1 min, 0% to 95% A from 1 to 10 min, 95% to 98% A from 10 to 14.5 min, 98% to 0% A from 14.5 to 14.6 min, and 0% A from 14.6 to 16 min. The column temperature was 45°C, and the flow rate was 0.3 ml/min. An HSS T3 chromatographic column (100 × 2.1 mm, 1.8 μm, Waters, USA) was adopted. The system was equipped with an ESI source, and the detection conditions were under positive ion modes. The heater temperature was 320°C and the capillary temperature was 300°C, and the capillary voltage was 3.5 kV. Quercetin, formononetin, kaempferol, taxifolin, cryptotanshinone, and tanshinone IIA were identified as the main bioactive compounds using reference standards. The UPLC-MS analysis was performed using Xcalibur 2.2 software (Thermo Scientific, San Jose, USA).

2.15. Western Blot Analysis. Western blot procedures were performed as previously described [16]. The primary antibodies were rabbit anti-calcium/calmodulin-dependent protein kinase II (CaMKII) (1:1000, ab52476, Abcam, Cambridge, United Kingdom), rabbit anti-phospho-(P-) CaMKII (1:1000, ab5683, Abcam), rabbit anti-AKT (1:1000, #4685, Cell Signaling Technology, Danvers, MA, USA), rabbit anti-P-AKT (1:1000, #4060, Cell Signaling Technology), rabbit anti-P-ERK1/2 (1:1000, #4370, Cell Signaling Technology), rabbit anti-ERK1/2 (1:1000, #4695, Cell Signaling Technology), rabbit anti-P-p38 (1:1000, #9215, Cell Signaling Technology), rabbit anti-p38 (1:1000, #9212, Cell Signaling Technology), rabbit anti-P-SAPK/JNK (1:1000, #4668, Cell Signaling Technology), rabbit anti-SAPK/JNK (1:1000, #9258, Cell Signaling Technology), rabbit anti-TLR4 (1:1000, #14358, Cell Signaling Technology), rabbit anti-NF-κB p65 (1:1000, #8242, Cell Signaling Technology), rabbit anti-P-NF-κB p65 (1:1000, #3033, Cell Signaling Technology), and rabbit anti-β-actin (1:2000, #4970, Cell Signaling Technology). Horseradish peroxidase (HRP-) conjugated goat anti-rabbit IgG (1:5000, A8275, Sigma-Aldrich) was used as a secondary antibody.

2.16. Mouse Cytokine Array. Serum samples were harvested from each group at 24 h after CLP surgery. For each sample, 60 μl serum was used to determine the concentration of 20 cytokines including granulocyte-macrophage colony-stimulating factor (GM-CSF), interferon-gamma (IFN-γ), interleukin- (IL-) 1α, IL-1β, IL-2, IL-3, IL-4, IL-5, IL-6, IL-9, IL-10, IL-12, IL-13, IL-17, keratinocyte-derived chemokine (KC), monocyte chemoattractant protein-1 (MCP-1), macrophage colony-stimulating factor (M-CSF), regulated upon activation normal T expressed and secreted (RANTES), tumor necrosis factor-α (TNF-α), and vascular endothelial growth factor (VEGF) using Quantibody Mouse Cytokine Array 1 (RayBiotech, Inc., Norcross, GA, USA) according

to the manufacturer's instruction. The data were analyzed with RayBiotech cytokine antibody array software [17].

2.17. Statistical Analysis. Data were presented as means \pm standard deviation (SD). Statistical analysis was performed using the GraphPad Prism 7 program (GraphPad, La Jolla, USA). One-way analysis of variance (ANOVA) was performed to compare the statistical differences of data among three or more groups. A P value of <0.05 was considered statistically significant.

3. Results

3.1. QX1 Formula Improved the Survival Outcome and Attenuated Cardiac Dysfunction in Septic Mice. We initially investigated whether administration of the QX1 formula conferred a survival advantage to septic mice (Figure 2(a)). The survival rate of CLP mice was approximately 55% within 3 days and 40% within 7 days. The Kaplan-Meier survival analysis showed that mice in the QX1 Low group exhibited an increased 7-day survival rate to 50% compared to the CLP mice. Both the high dose of the QX1 formula and TMZ treatment significantly improved the 7-day survival rate to 60% as compared with that of CLP mice ($P < 0.05$ and $P < 0.05$, respectively). Then, we performed echocardiography analysis to assess the effect of the QX1 formula on cardiac function in septic mice (Figure 2(b)). Echocardiography analysis found that mice that underwent CLP surgery had significantly reduced LVEF and LVFS compared with sham mice, while low or high dose of the QX1 formula significantly increased LVEF and LVFS ($P < 0.05$ and $P < 0.01$, respectively, Figures 2(c) and 2(d)). The LVEF and LVFS of mice in the TMZ group also significantly increased compared to those of mice in the CLP group ($P < 0.05$ and $P < 0.05$, respectively).

3.2. QX1 Formula Ameliorated the Disruption of Cardiac Structure in Septic Mice. H&E staining was used to observe the effect of QX1 formula treatment on the pathological changes of cardiac tissue in septic mice (Figure 3(a)). The sham group showed normal histological features. In the CLP group, the cardiac structure was damaged, accompanied by a loose arrangement of myogenic fibers and inflammatory cell infiltration. Treatment with low or high dose of the QX1 formula or TMZ alleviated the loosening of cardiomyocytes and inflammatory cell infiltration. Further, the changes of cardiac structure were observed using TEM (Figure 3(b)). In the sham group, the myofibrils were organized orderly, the Z-line of the sarcomere was clear and straight, and the mitochondrial structure was completely arranged between the myofibrils. Compared with the sham group, in the CLP group, myofibril arrangement was loose and tortuous, with local dissolution and cavitation, the Z-line of the sarcomere was broken or blurred, the color of mitochondria became darker, and the arrangement was loose and swollen. In the QX1 Low group, myofibril arrangement was loose, the Z-line of the sarcomere was clear, and the mitochondria were swollen and proliferated. Compared with the CLP group,

the myofibrils, Z-line, and mitochondrial structure were significantly improved in the QX1 High and TMZ groups.

3.3. Active Compound Screening. In this study, we initially obtained 513 chemical ingredients and their physicochemical properties from the QX1 formula from the TCMSP database and based on a large number of literatures. Then, the ADME system was applied to screen the potential active compounds of QX1. Finally, we screened 63 compounds which reached the standard of $OB \geq 28\%$, $DL \geq 0.18$, $HL \geq 4$, and Caco-2 cell permeability ≥ -0.4 as candidate active molecules (Table 1). There were 9, 10, 5, 11, and 31 active compounds in HQ, WWZ, FL, SHHZ, and DS, respectively. Among the active ingredients, quercetin (MOL02) and kaempferol (MOL15) were both in HQ and SHHZ, and hederagenin (MOL07) was found in both HQ and FL. On the basis of structure analysis, the 63 active compounds mainly belonged to diterpenoids, flavonoids, and lignans.

3.4. Drug Targeting and Analysis. In order to clarify the mechanism of QX1 active substances in the treatment of cardiac-related diseases, we need to clarify the possible targets of active compounds. A total of 79 potential targets for the 63 bioactive compounds were achieved using the WES algorithms and assigning them to the CTD, TTD, and PharmGKB databases (Supplementary Table 1). The results showed that most active compounds can act on multiple targets, and one target can be also possibly associated with multiple active compounds. The active compound quercetin (MOL02) can act on 56 targets, while the estrogen receptor (ESR1) was the target of 57 compounds, accounting for 90% of the total active compound targets.

3.5. Compound-Target Network Analysis. The C-T network diagram was constructed based on 142 nodes (63 potential compounds and 79 potential targets) and 686 edges (Figure 4). The degree parameter of topological analysis showed that the average degrees of potential compounds and targets were 10.9 and 8.7, respectively, indicating that the active compounds and targets were closely related in the QX1 formula. Quercetin (MOL02) is the key component of the QX1 formula and displayed the highest number of target interactions (degree = 56), followed by kaempferol (MOL15, degree = 33), beta-sitosterol (MOL10, degree = 24), tanshinone IIA (MOL50, degree = 19), formononetin (MOL13, degree = 16), cryptotanshinone (MOL35, degree = 14), and taxifolin (MOL21, degree = 11). Among potential protein targets, the top 10 high-degree targets acted on multiple compounds, namely, ESR1 (degree = 57), PTGS2 (degree = 55), AR (degree = 52), NOS2 (degree = 46), ESR2 (degree = 43), GSK3 β (degree = 43), F2 (degree = 40), PPARG (degree = 35), PTGS1 (degree = 32), and MAPK14 (degree = 30) (Supplementary Table 2). These high-degree targets in the network may be the major mediators of the QX1 formula in the treatment of cardiac-related diseases.

3.6. Target-Protein Association Network Analysis. The T-P network consists of 60 targets and 30 pathways significantly enriched by these targets (Figure 5). Obviously, most of the target proteins (40/60) appeared in multiple pathways,

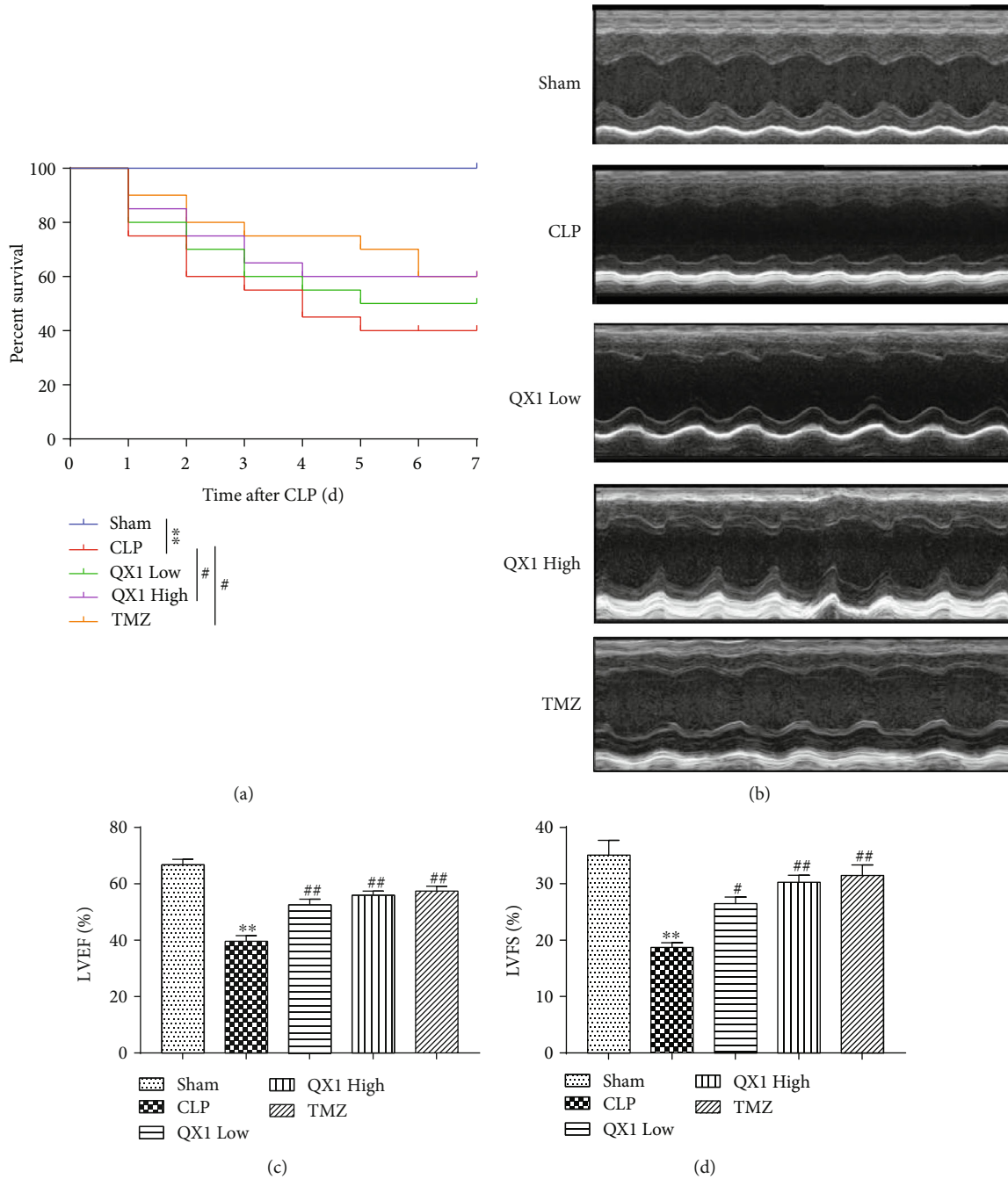
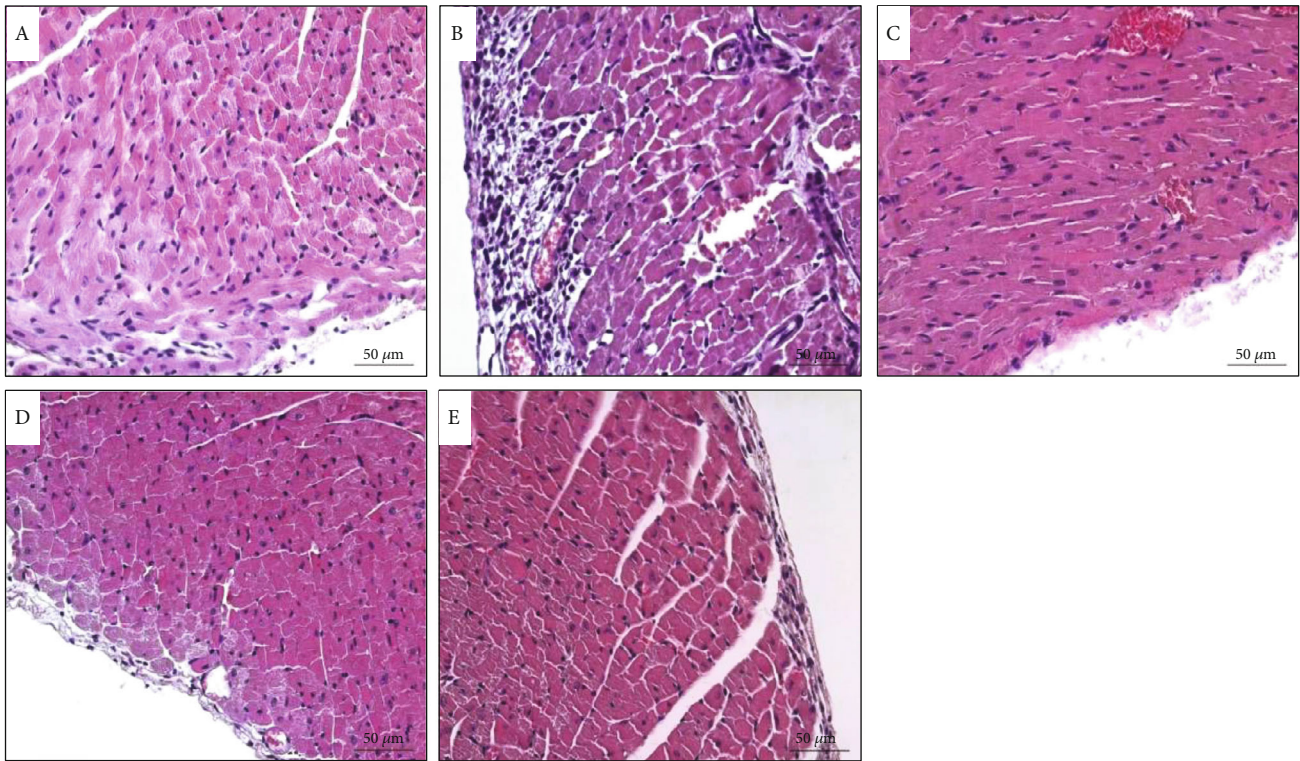


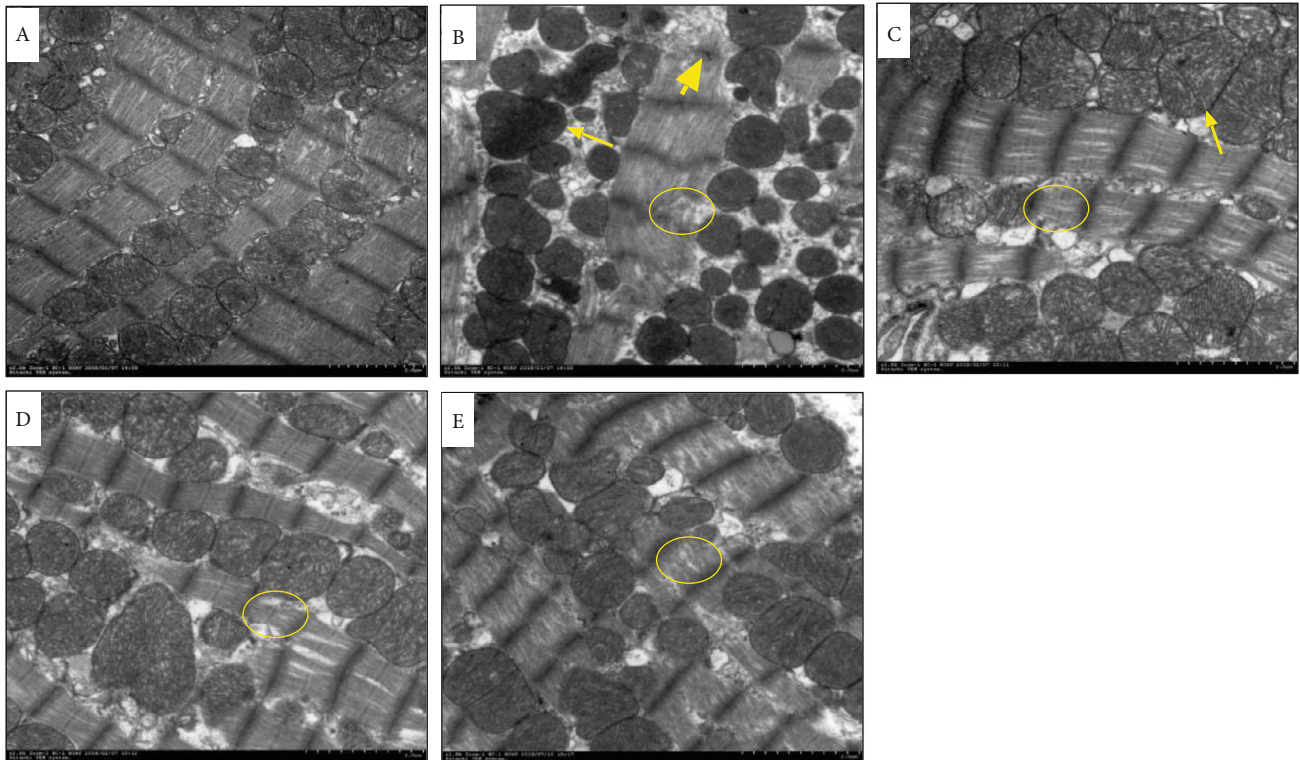
FIGURE 2: The QX1 formula improved the survival outcome and cardiac dysfunction in septic mice. Mice were orally administered with low (5 g/kg) or high (10 g/kg) dose of the QX1 formula or TMZ (20 mg/kg) at 6 h and 18 h after CLP surgery, respectively. (a) Kaplan-Meier survival curves. Twenty mice of each group were used to analyze the 7-day mortality. (b) Representative M-mode echocardiograms after CLP surgery. (c) Left ventricle ejection fraction (EF) and (d) fractional shortening (FS) were calculated. Data were presented as means \pm SD, and differences between means were compared using one-way ANOVA with Tukey's multiple comparison test. ** $P < 0.01$ compared to the sham group; # $P < 0.05$, ## $P < 0.01$ compared to the CLP group.

indicating that the target proteins of the QX1 formula interacted with each other in different pathways and carried out signal transmission for cardiac diseases. Meanwhile, many pathways (11/30) were also regulated by multiple target proteins (≥ 8), which might be the key mechanism of the QX1 formula in the treatment of cardiac-related

diseases. As shown in Supplementary Table 3, the crucial target-protein associated pathways included the PI3K/AKT signaling pathway (degree = 16), HIF-1 signaling pathway (degree = 11), calcium signaling pathway (degree = 10), MAPK signaling pathway (degree = 9), cytokine-cytokine receptor interaction (degree = 9), adrenergic signaling in



(a)



(b)

FIGURE 3: The QX1 formula ameliorated the disruption of cardiac structure in septic mice. (a) Representative H&E staining images of the left ventricular myocardium (scale bar = 50 μm). (b) Representative images of transmission electron microscopy of the left ventricular myocardium (scale bar = 2 μm). (A) Sham group, (B) CLP group, (C) QX1 Low group, (D) QX1 High group, and (E) TMZ group. The short yellow arrow indicated that the Z-line of the sarcomere was broken and blurred. The yellow circles indicated that myofibrils were loosely arranged and partially dissolved. The long yellow arrows indicated that mitochondria were swollen.

TABLE 1: Active compounds and their corresponding ADME parameters in the QX1 formula.

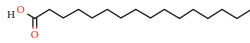
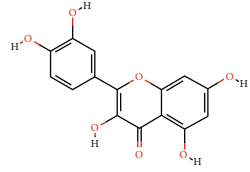
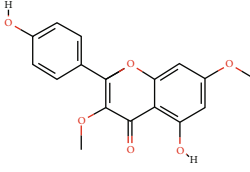
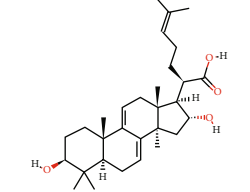
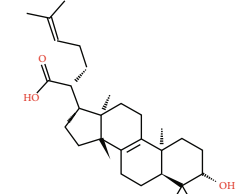
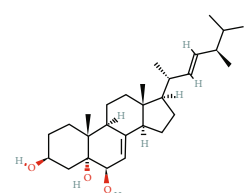
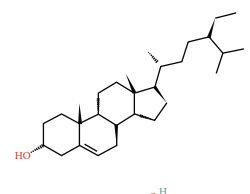
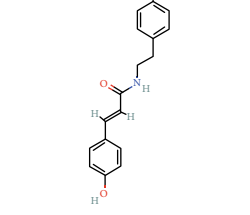
Molecular ID	Compounds	Herb	OB	Caco-2	DL	HL	Degree	Structure
MOL01	Palmitic acid	FL	19.30	1.09	0.10	0.00	10	
MOL02	Quercetin	HQ/SHHZ	46.43	0.05	0.28	14.40	56	
MOL03	Jaranol	HQ	50.83	0.61	0.29	15.50	10	
MOL04	(2R)-2-[(3S,5R,10S,13R,14R,16R,17R)-3,16-Dihydroxy-4,4,10,13,14-pentamethyl-2,3,5,6,12,15,16,17-octahydro-1H-cyclopenta[a]phenanthren-17-yl]-6-methylhept-5-enoic acid	FL	30.93	0.01	0.81	6.81	3	
MOL05	Trametenolic acid	FL	38.71	0.52	0.80	7.78	4	
MOL06	Cerevisterol	FL	37.96	0.28	0.77	5.31	4	
MOL07	Hederagenin	HQ/FL	36.91	1.32	0.75	5.35	15	
MOL08	n-Coumaroyltyramine	SHHZ	85.63	0.69	0.20	4.82	8	

TABLE 1: Continued.

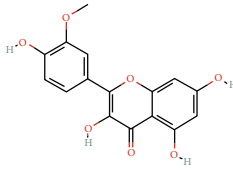
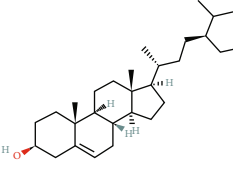
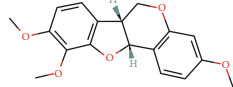
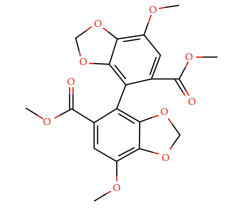
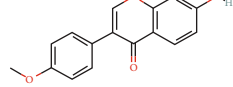
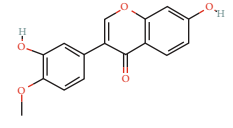
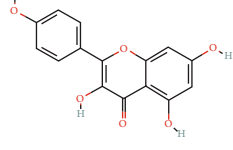
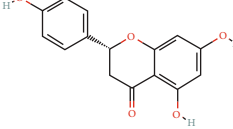
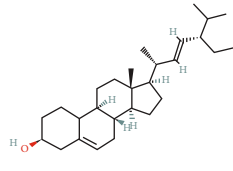
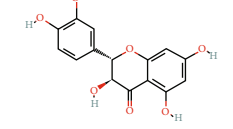
Molecular ID	Compounds	Herb	OB	Caco-2	DL	HL	Degree	Structure
MOL09	Isorhamnetin	HQ	49.60	0.31	0.31	14.34	15	
MOL10	Beta-sitosterol	SHHZ	36.91	1.32	0.75	5.36	24	
MOL11	3,9-Di-O-methylnissolin	HQ	53.74	1.18	0.48	9.00	17	
MOL12	Bifendate	HQ	31.10	0.15	0.67	17.96	9	
MOL13	Formononetin	HQ	69.67	0.78	0.21	17.04	16	
MOL14	Calycosin	HQ	47.75	0.52	0.24	17.10	11	
MOL15	Kaempferol	HQ/SHHZ	41.88	0.26	0.24	14.74	41	
MOL16	(2R)-5,7-Dihydroxy-2-(4-hydroxyphenyl)chroman-4-one	SHHZ	42.36	0.38	0.21	16.83	11	
MOL17	Poriferasterol	DS	43.83	1.44	0.76	5.34	4	
MOL18	(-)-Taxifolin	SHHZ	60.51	-0.24	0.27	14.37	10	

TABLE 1: Continued.

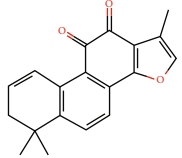
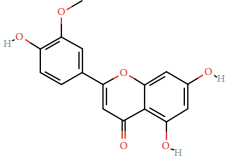
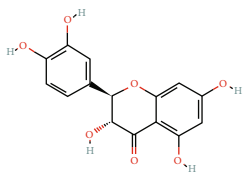
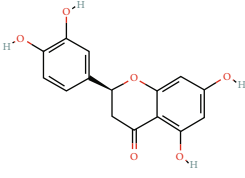
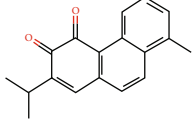
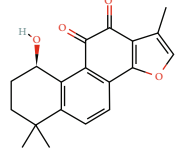
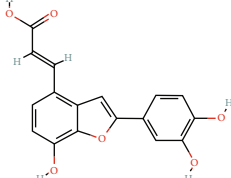
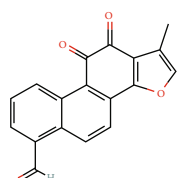
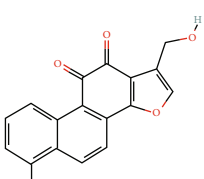
Molecular ID	Compounds	Herb	OB	Caco-2	DL	HL	Degree	Structure
MOL19	Dehydrotanshinone II A	DS	43.76	1.02	0.40	23.71	13	
MOL20	Chryseriol	SHHZ	35.85	0.39	0.27	16.31	10	
MOL21	Taxifolin	SHHZ	57.84	-0.23	0.27	14.41	11	
MOL22	Eriodictyol	SHHZ	71.79	0.17	0.24	15.81	12	
MOL23	2-Isopropyl-8-methylphenanthrene-3,4-dione	DS	40.86	1.23	0.23	14.89	19	
MOL24	3 α -HydroxytanshinoneIIa	DS	44.93	0.53	0.44	23.78	10	
MOL25	(E)-3-[2-(3,4-Dihydroxyphenyl)-7-hydroxybenzofuran-4-yl]acrylic acid	DS	48.24	0.18	0.31	8.87	6	
MOL26	Formyltanshinone	DS	73.44	0.54	0.42	24.12	10	
MOL27	Przewaquinone B	DS	62.24	0.39	0.41	24.94	10	

TABLE 1: Continued.

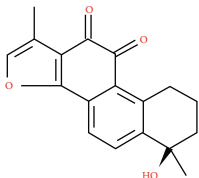
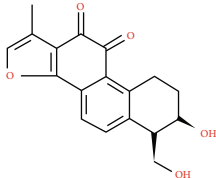
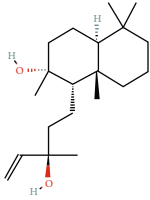
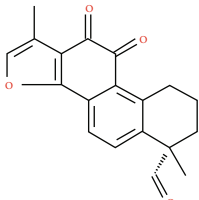
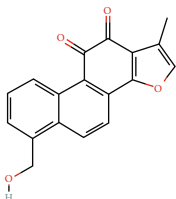
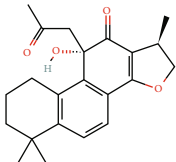
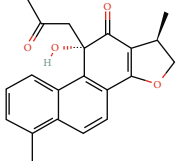
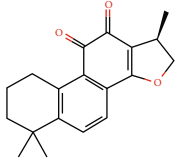
Molecular ID	Compounds	Herb	OB	Caco-2	DL	HL	Degree	Structure
MOL28	Przewaquinone C	DS	55.74	0.42	0.40	23.70	15	
MOL29	Przewaquinone F	DS	40.31	-0.09	0.46	22.45	8	
MOL30	Sclareol	DS	43.67	0.84	0.21	4.71	4	
MOL31	Tanshinaldehyde	DS	52.47	0.57	0.45	23.49	10	
MOL32	Tanshinol A	DS	21.31	0.36	0.41	0.00	10	
MOL33	Danshenol B	DS	57.95	0.53	0.56	4.28	7	
MOL34	Danshenol A	DS	56.97	0.33	0.52	5.15	15	
MOL35	Cryptotanshinone	DS	52.34	0.95	0.40	17.30	14	

TABLE 1: Continued.

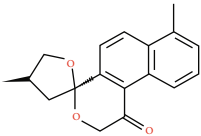
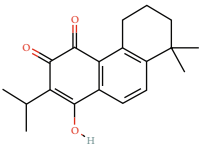
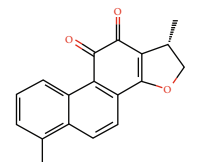
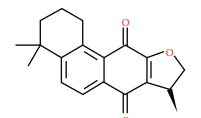
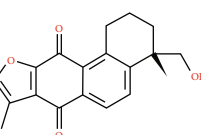
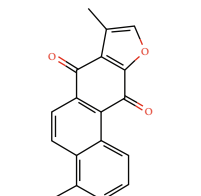
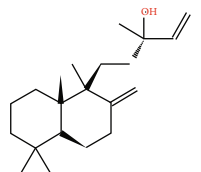
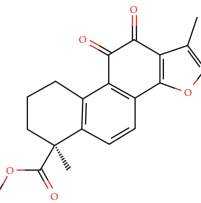
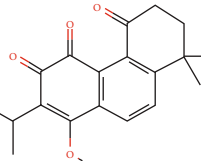
Molecular ID	Compounds	Herb	OB	Caco-2	DL	HL	Degree	Structure
MOL36	Danshenspiroketalactone	DS	50.43	0.88	0.31	15.19	16	
MOL37	Deoxyneocryptotanshinone	DS	49.40	0.85	0.29	27.17	14	
MOL38	Dihydrotanshinone I	DS	45.04	0.95	0.36	18.32	16	
MOL39	Isocryptotanshinone	DS	54.98	0.93	0.39	31.92	14	
MOL40	Isotanshinone II	DS	49.92	1.03	0.40	24.73	11	
MOL41	Isotanshinone I	DS	29.72	1.01	0.36	0.00	12	
MOL42	Manool	DS	45.04	1.28	0.20	5.81	2	
MOL43	Methyltanshinonate	DS	19.19	0.56	0.55	0.00	11	
MOL44	Miltionone I	DS	49.68	0.35	0.32	41.49	16	

TABLE 1: Continued.

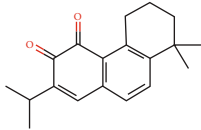
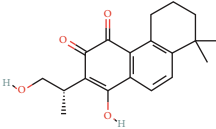
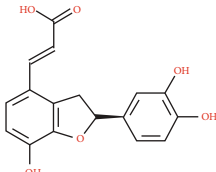
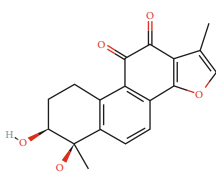
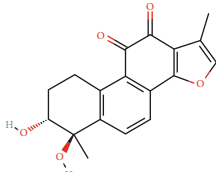
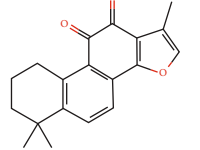
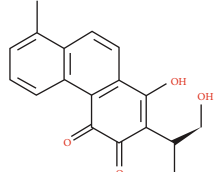
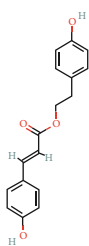
Molecular ID	Compounds	Herb	OB	Caco-2	DL	HL	Degree	Structure
MOL45	Miltirone	DS	38.76	1.23	0.25	14.82	15	
MOL46	Neocryptotanshinone	DS	52.49	0.35	0.32	14.46	12	
MOL47	Prolithospermic acid	DS	64.37	0.10	0.31	8.82	10	
MOL48	Tanshindiol B	DS	42.67	0.05	0.45	22.25	7	
MOL49	Przewaquinone E	DS	42.85	-0.04	0.45	22.44	7	
MOL50	Tanshinone Iia	DS	49.89	1.05	0.40	23.56	19	
MOL51	Tanshinone VI	DS	45.64	0.48	0.30	15.21	12	
MOL52	2-(4-Hydroxyphenyl)ethyl (E)-3-(4-hydroxyphenyl)prop-2-enoate	SHHZ	93.36	0.68	0.21	5.24	5	

TABLE 1: Continued.

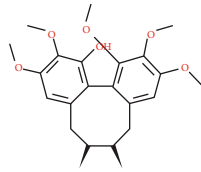
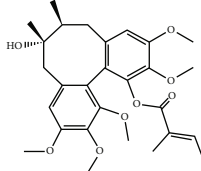
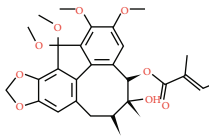
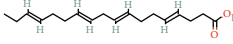
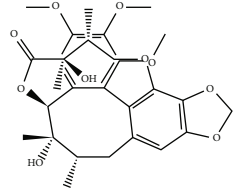
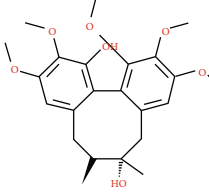
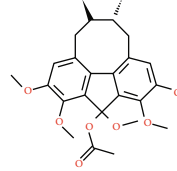
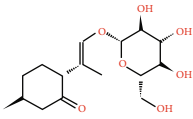
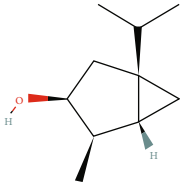
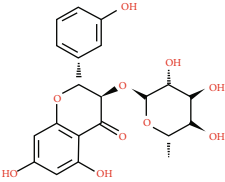
Molecular ID	Compounds	Herb	OB	Caco-2	DL	HL	Degree	Structure
MOL53	Schisanhenol	WWZ	22.98	1.88	0.06	0.00	8	
MOL54	4,7-Dimethyl-7-(4-methylpent-3-enyl)bicyclo[2.2.1]heptan-3-ol	WWZ	30.71	0.66	0.83	9.40	1	
MOL55	Angeloylgomisin H	WWZ	29.70	1.83	0.09	0.00	3	
MOL56	Schizandrer B	WWZ	25.37	0.10	0.04	0.00	2	
MOL57	Clupanodonic acid	WWZ	30.69	0.63	0.78	5.09	3	
MOL58	Gomisin D	WWZ	32.68	0.73	0.83	8.50	2	
MOL59	Gomisin H	WWZ	34.84	0.60	0.86	9.54	2	
MOL60	Schisanhenol acetate	WWZ	27.20	1.86	0.02	0.00	4	
MOL61	Schizonepetoside A	WWZ	48.80	1.39	0.03	11.35	4	

TABLE 1: Continued.

Molecular ID	Compounds	Herb	OB	Caco-2	DL	HL	Degree	Structure
MOL62	Thuja alcohol	WWZ	46.27	1.08	0.84	8.72	5	
MOL63	Kaempferol-3-O- α -L-rhamnoside	SHHZ	41.88	-1.29	0.69	16.15	1	

cardiomyocytes (degree = 9), Toll-like receptor signaling pathway (degree = 8), and T cell receptor signaling pathway (degree = 8).

3.7. Cardiac Disease-Related Pathway Analysis. Considering the complex mechanism of QX1 in the treatment of cardiac-related diseases, an integrated map of “cardiac disease-related pathways” was constructed by integrating the key pathways that were obtained from the KEGG database and combined with T-P network analysis (Figure 6). The cardiac disease-related pathways were comprised of four important pathways: calcium signaling pathway, MAPK signaling pathway, PI3K/AKT signaling pathway, and TLR signaling pathway. As shown in Figure 6, the cardiac disease-related pathways were involved in several biological functions, such as contraction, inflammation, proliferation, differentiation, cell survival, cell cycle, and chemotactic effects. The QX1 formula may play a therapeutic role in cardiac disease by regulating these biological functions.

3.8. Target-Tissue Location Analysis. Understanding the localization of protein targets on multiple organs at the system level is useful to clarify the therapeutic target of QX1 against cardiac functional diseases. A total of 79 targets were mapped on 84 normal tissues based on the BioGPS database. The tissue distribution network of the 79 targets was divided into heart, spleen, kidney, and brain tissue modules (Figure 7). Most targets acted on two or more tissues, which suggested that these tissues were closely correlated. Specifically, there were 62 targets that contained high mRNA expression in the heart, accounting for 78% of all the targets. Besides, 52 targets in the kidney, 47 targets in the brain, and 24 targets in the spleen were found, respectively. The results suggested that the target of the QX1 formula is closely linked to cardiac disease.

3.9. Identification of the Main Bioactive Compounds in Plasma. The six main bioactive compounds, including quercetin, formononetin, kaempferol, taxifolin, cryptotanshinone, and tanshinone IIA, were identified in plasma after oral administration of QX1 decoction by UPLC-MS. The

chromatograms of the six main bioactive compounds at 30 min after oral administration of QX1 decoction are shown in Figure 8. The retention times were approximately 6.29 min for taxifolin, 6.78 min for quercetin, 11.08 min for tanshinone IIA, 10.34 min for cryptotanshinone, 7.83 min for formononetin, and 7.32 min for kaempferol. The chromatograms of analytes in blank plasma and blank plasma spiked with the six main bioactive compounds are shown in Supplementary Figure 1A and B.

3.10. Effect of the QX1 Formula on the Activity of Cardiac Disease-Related Pathways. In order to evaluate the consequences of systematic pharmacological analysis, we examined the effect of the QX1 formula on key proteins in the integrated “cardiac disease-related pathways,” including calcium, MAPK, PI3K/AKT, and TLR4 signaling pathways using Western blot. CLP surgery significantly increased the expression of P-CaMKII protein in the cardiac tissue of mice compared with the sham group, while low or high dose of QX1 formula treatment inhibited this increase (Figures 9(a) and 9(b)). Compared with the sham group, expression of P-AKT protein was decreased in the CLP group (Figures 9(c) and 9(d)). Compared with the CLP group, expression of P-AKT protein was increased in the QX1 High group, but not in the QX1 Low group. Furthermore, we investigated the effect of the QX1 formula on the activity of three well-characterized subfamilies of MAPK pathways, ERK1/2, JNK, and p38 (Figures 9(e) and 9(f)). CLP surgery induced the activation of ERK1/2, JNK, and P38 compared with the sham group, whereas the CLP-induced activation of JNK was inhibited by low or high dose of QX1 formula treatment. Compared with the CLP group, decreased expression of P-ERK1/2 and P-P38 was observed in the QX1 Low group and QX1 High group, respectively. In addition, the activity of the TLR4 pathway was also examined. CLP treatment significantly increased the expression of TLR4, and this increase was inhibited by low or high dose of QX1 formula treatment (Figures 9(g) and 9(h)). Compared with the sham group, increased expression of P-NF- κ B p65 downstream of TLR4 was observed in the CLP group, whereas this increase was inhibited by high but not low dose of QX1 formula treatment.

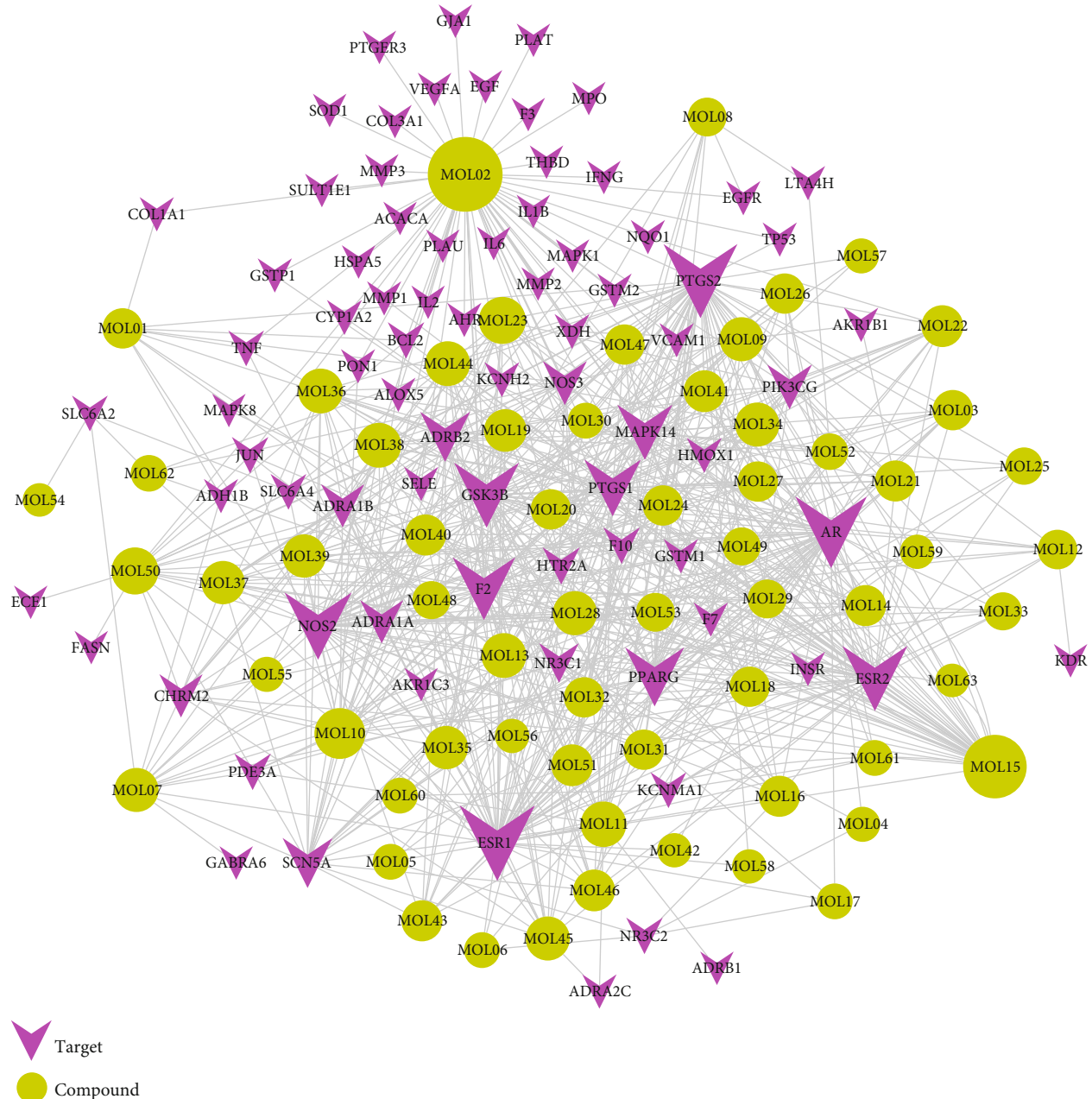


FIGURE 4: C-T network analysis. A compound node and a target node were connected if the protein was targeted by the corresponding compound. Node size was relative to its degree. The yellow circle represents the compounds, and the purple triangle represents the targets.

3.11. Effect of the QX1 Formula on Serum Cytokine Production. Cytokines have been thought to play an important role in the induction of cardiac dysfunction during sepsis. The production of 20 cytokines in serum of mice was determined by a multiplex assay after CLP or QX1 formula treatment (Figure 10). Compared with the sham group, the levels of eight cytokines (IFN- γ , IL-1 β , IL-3, IL-4, IL-6, IL-10, IL-17, and TNF- α) were significantly upregulated in the CLP group. Among them, IL-1 β , IL-3, IL-4, IL-6, and IL-10 increased in the CLP group were markedly reduced in both the QX1 Low and QX1 High groups. Compared with the CLP group, the levels of IL-17 and TNF- α were reduced in

the QX1 Low group and the level of IFN- γ was reduced in the QX1 High group.

4. Discussion

In this study, we demonstrated that the QX1 formula improved the survival outcome and ameliorated cardiac dysfunction in septic mice induced by CLP surgery. Based on the complex multicomponent property of the QX1 formula, a systems pharmacology approach was applied to explore the potential active components, targets, and networks. After *in silico* TCMSp-based prediction, we performed Western blot

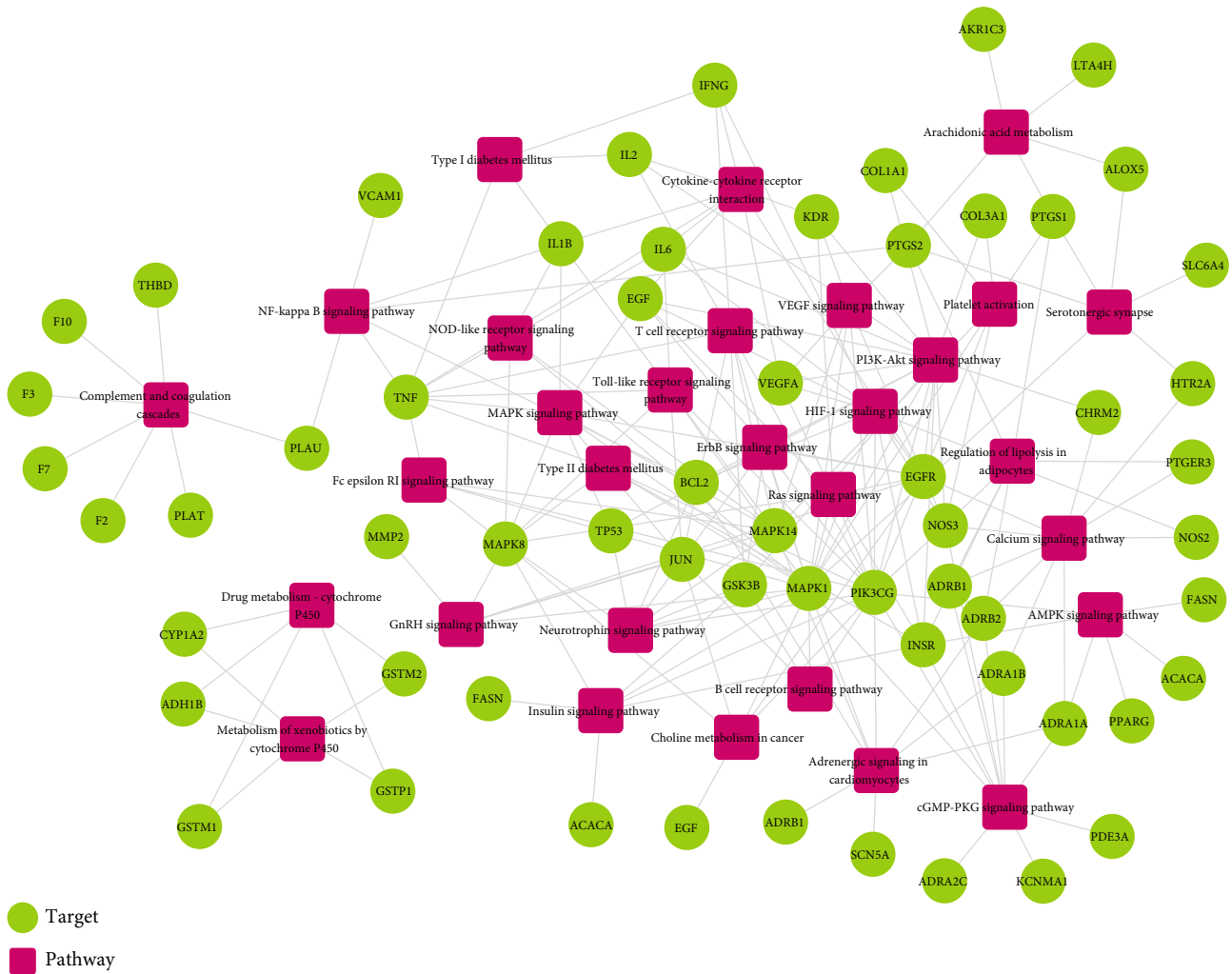


FIGURE 5: T-P network analysis. The T-P network was built by a target and a pathway if the pathway was lighted at the target. Node size was related to the degree. The green circle represents the target, and the red box represents the pathway.

and mouse cytokine array experiments to verify our predicted pathway and elucidated the preliminary mechanism. We found that QX1 formula treatment enhanced the activation the PI3K/AKT pathway and attenuated the activity of the calcium, MAPK, and TLR4/NF-κB pathway in the septic mice. To our knowledge, this is the first report to comprehensively elucidate the protective mechanism of the QX1 formula on sepsis-induced cardiac dysfunction.

Cardiac dysfunction is a common complication in patients with sepsis and dramatically increases mortality from 20% to as high as 70%–90% in patients with sepsis [18, 19]. CLP surgery in mice is the most frequently used experimental model and is considered the gold standard in sepsis research [20]. The position of cecal ligation in mice is the primary determinant of sepsis severity and mortality. Reduction of sepsis mortality is one of the most important indicators to evaluate the efficacy of drug therapy. The QX1 formula is an applicable TCM prescription for sepsis-related cardiac dysfunction and has been used in the clinical practice for more than 30 years. Our previous study showed that the high-dose QX1 formula significantly increased the

3-day survival rate in mice with severe sepsis from 22% to 40% [7]. In the present study, a CLP-induced moderate sepsis model was established and 60% of mice died during 7 days. Administration of low (5 g/kg) or high dose of QX1 (10 g/kg) improved the survival outcome in septic mice and led to an increase in the 7-day survival rate to 50% and 60%, respectively. Echocardiography is the most effective tool to evaluate the cardiac function of sepsis. The LVEF and LVFS are well-known powerful factors for predicting the mortality and outcome in heart failure patients [21, 22]. We found that QX1 formula treatment notably elevated LVEF and LVFS in septic mice. Moreover, QX1 formula treatment alleviated the sepsis-induced damage of cardiac histological and ultrastructure. The effects of the high-dose QX1 formula on the survival outcome, LVEF and LVFS, and cardiac morphological structure damage were comparable to those of TMZ treatment. Our results suggested that administration of the QX1 formula effectively improved the survival outcome and ameliorated sepsis-induced cardiac dysfunction.

Deeply studying the molecular mechanism of TCM is difficult due to its multicomponent property. Now, systems

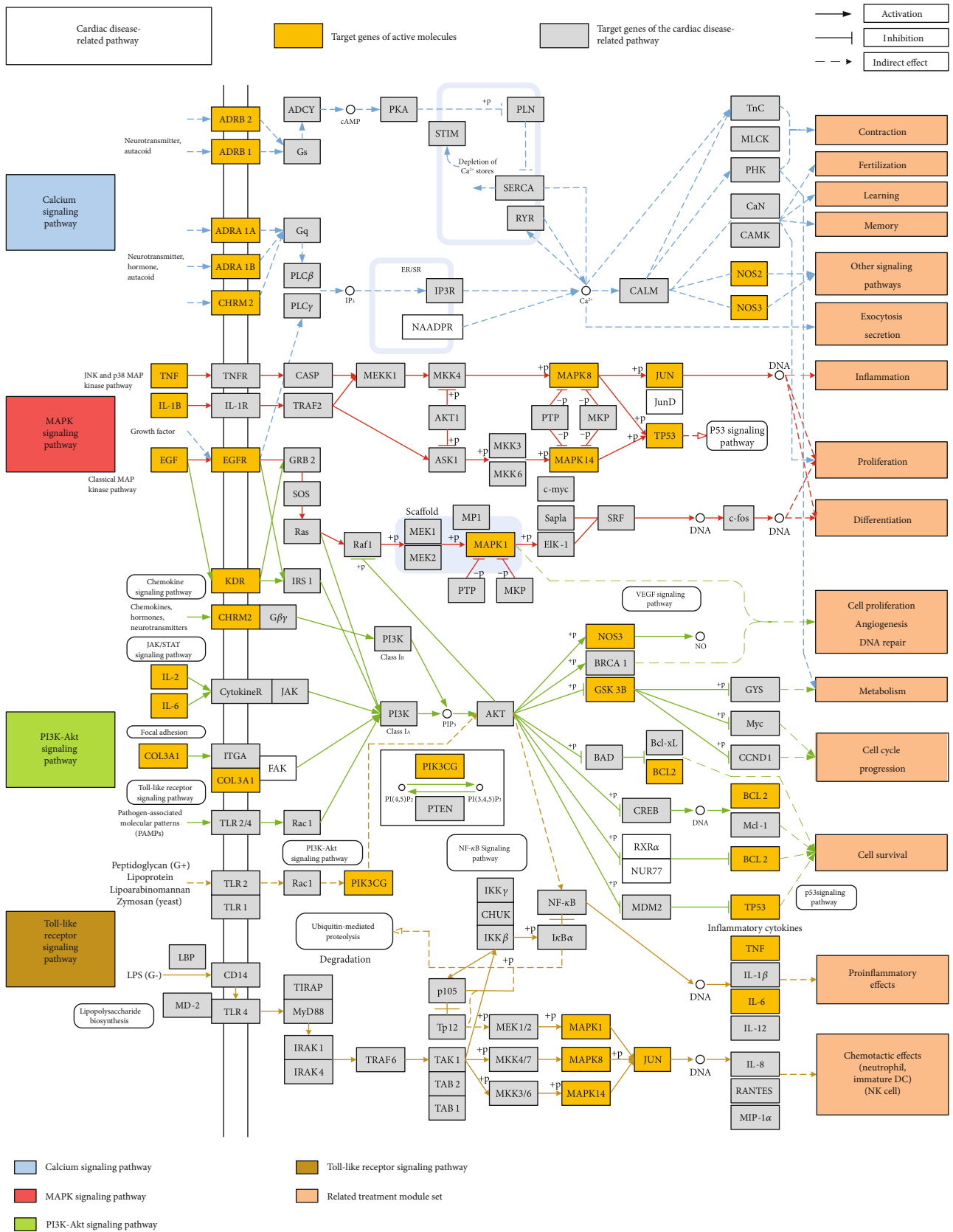


FIGURE 6: Distribution of target proteins of the QX1 formula on the integrated “cardiac disease-related pathway.” The cardiac disease-related pathway contained calcium, MAPK, PI3K/AKT, and Toll-like receptor signaling pathways. Arrows represent activation activity, T-arrows show inhibition activity, and segments represent indirect activation effect.

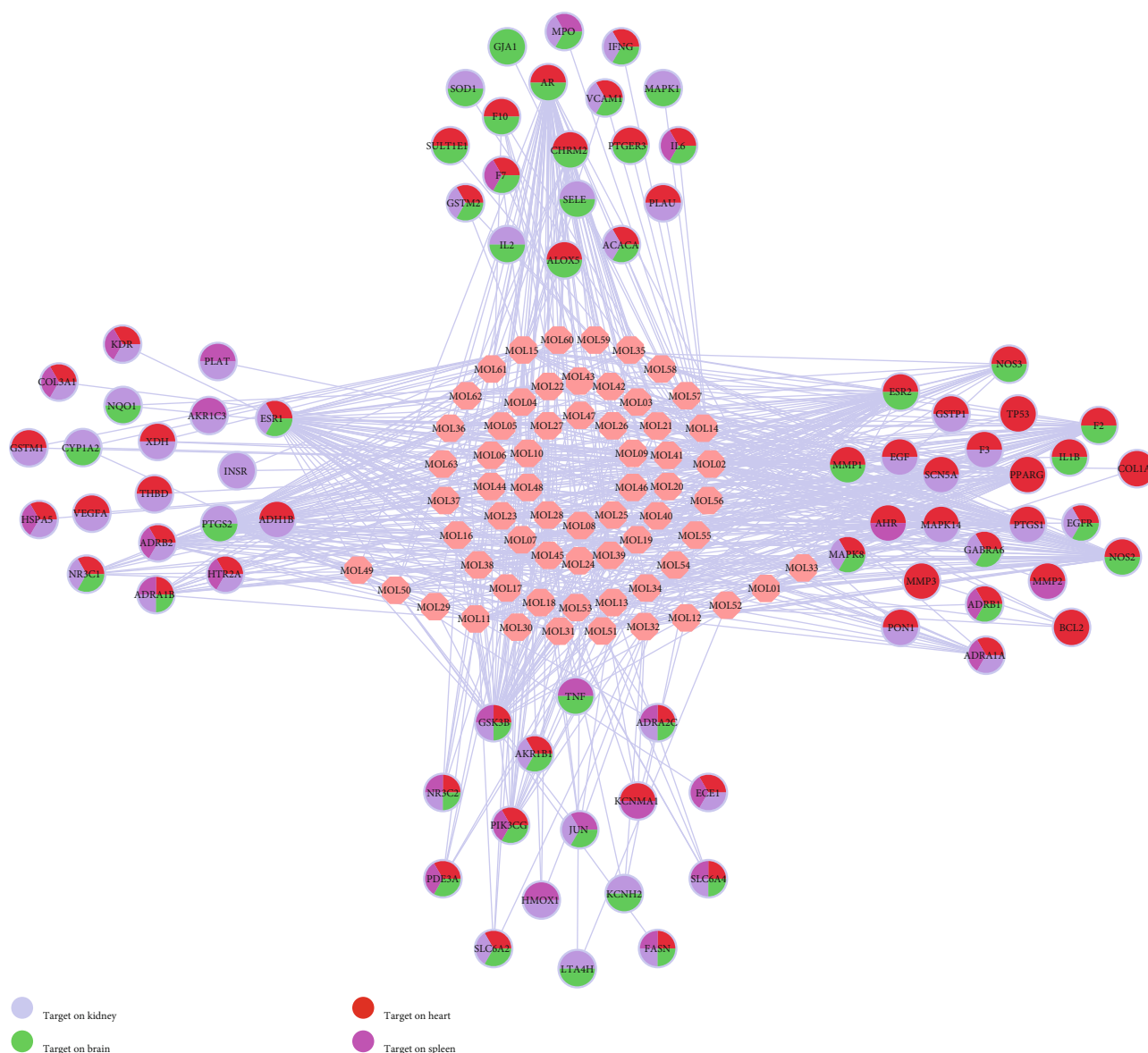


FIGURE 7: Tissue organ distribution of the target proteins of the QX1 formula. The pink node represents the compound molecule, and colored circles represent the target protein nodes and the organs where the target proteins are located.

pharmacology has become a promising approach to elucidate the mechanisms of multiple target components in TCM [23]. Using the ADME system, 63 QX1 potential active compounds were screened out in this study based on the standards of $OB \geq 28\%$, $DL \geq 0.18$, $HL \geq 4$, and Caco-2 cell permeability ≥ -0.4 . Among them, quercetin (MOL02), formononetin (MOL13), kaempferol (MOL15), taxifolin (MOL21), cryptotanshinone (MOL35), and tanshinone IIA (MOL50) are also identified and quantified using UPLC-MS/MS analysis in our previous study, which confirmed the reliability of systematic pharmacological screening of herbal active ingredients [7]. In the present study, these six active compounds were also detectable in rat plasma after treatment of QX1 decoction. QX1 formula treatment ameliorates myocardial tissue damage in mice suffering from sepsis partly by inhibiting endoplasmic reticulum- and mitochondria-related

apoptosis [7]. In this study, as predicted by a systems pharmacology approach, QX1 may play a therapeutic role in sepsis-induced cardiac dysfunction primarily by regulating calcium signaling, MAPK, PI3K/AKT, and TLR pathways. To further validate this prediction, we evaluated the effect of QX1 on the key protein expression in these pathways in septic mice using Western blot. QX1 formula treatment significantly inhibited the sepsis-induced activation of CaMKII, MAPK (P38, ERK1/2, and JNK), and TLR4/NF- κ B pathways and promoted the activation of AKT. This study proved the reliability of the systems pharmacology approach in exploring cardiac protective effect and the underlying mechanism of QX1.

Accumulating evidence has documented that calcium signaling plays a pivotal role in sepsis-induced cardiac dysfunction [24, 25]. CaMKII is a molecular switch that

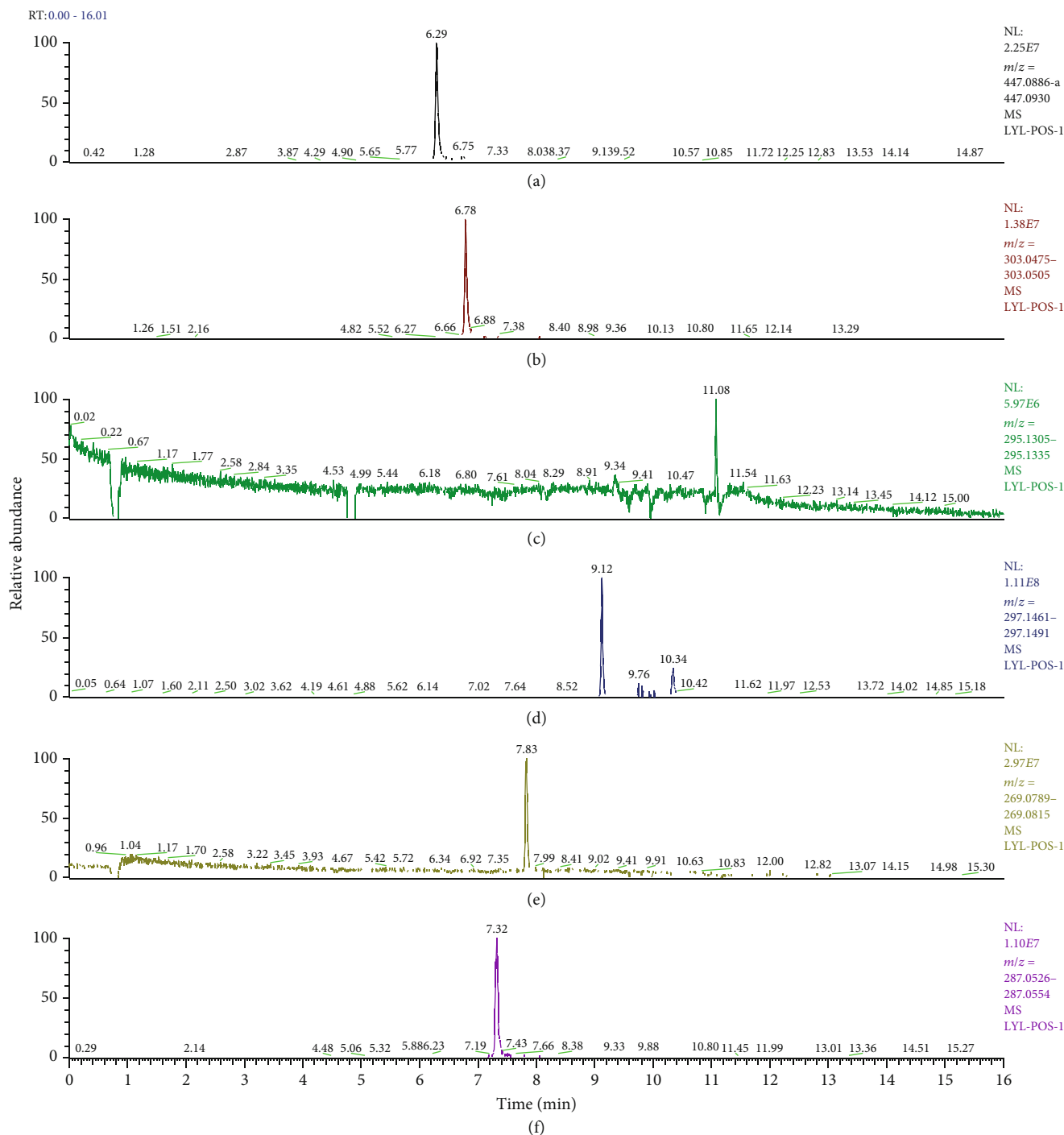


FIGURE 8: Chromatograms of the six main bioactive compounds in plasma at 30 min after oral administration of QX1: (a) taxifolin, (b) quercetin, (c) tanshinone IIA, (d) cryptotanshinone, (e) formononetin, and (f) kaempferol.

regulates myocardial Ca^{2+} signaling, and excessive CaMKII activation is detrimental to the integrity and function of the heart [26, 27]. The activity of CaMKII was significantly increased in septic mice [25]. In this study, QX1 treatment decreased the level of P-CaMKII. Cryptotanshinone (degree = 14) and tanshinone IIA (degree = 19), the primary bioactive compounds in Danshen, ameliorate hypoxia-induced damage of cardiomyocyte H9c2 cells by regulating intracellular NO, calcium, and mitochondrial ROS produc-

tion [24]. It was proposed that the bioactive compounds cryptotanshinone and tanshinone in the QX1 formula may alter Ca^{2+} handling to exert their cardiac protective effects.

The PI3K/AKT pathway is a classical pathway that regulates cell proliferation, survival, and cell homeostasis [28]. The previous study has shown that inhibition of PI3K increased the inflammatory and apoptotic processes and mortality in septic mice [29]. By contrast, the activation of the PI3K/AKT pathway improved cardiac dysfunction and

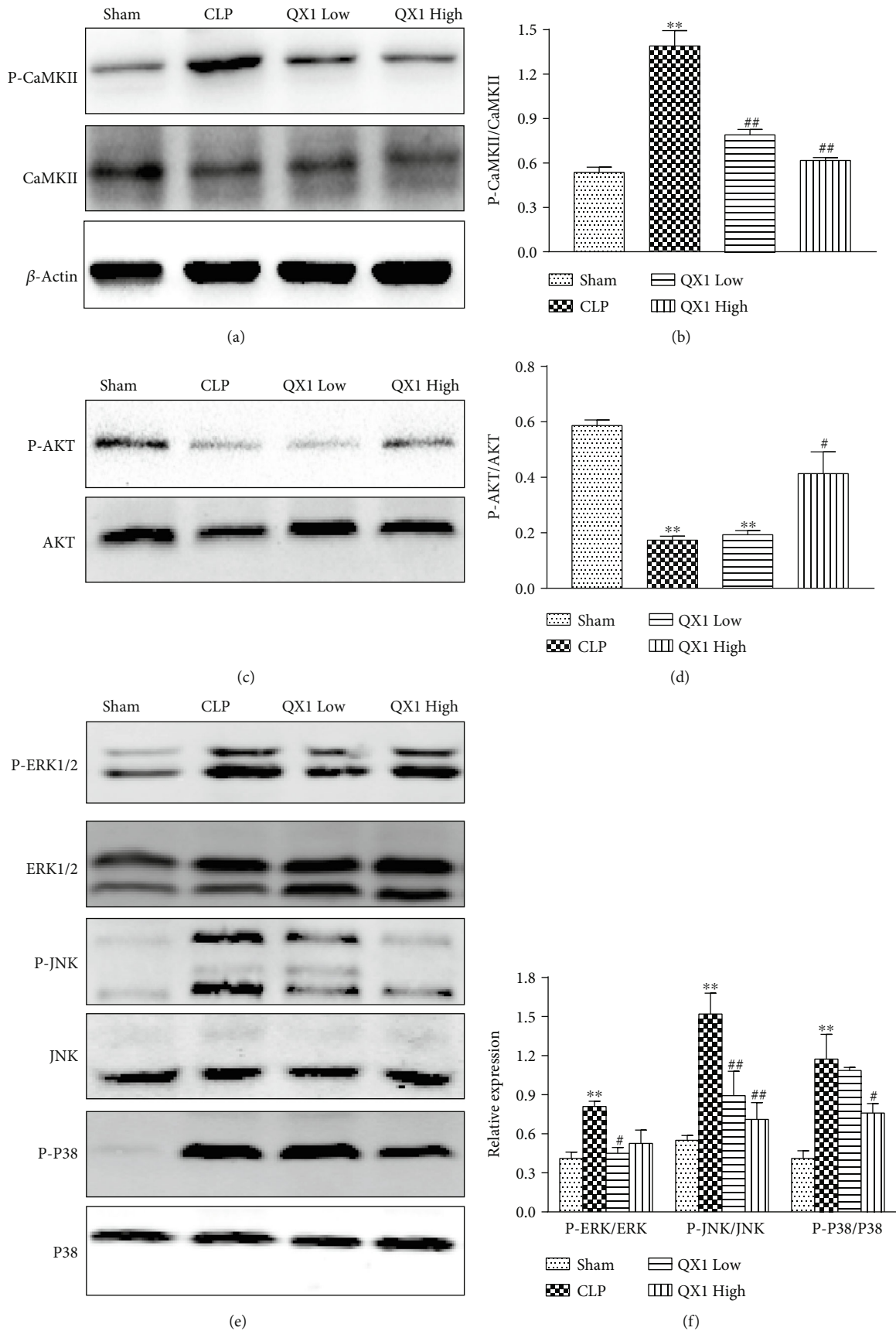


FIGURE 9: Continued.

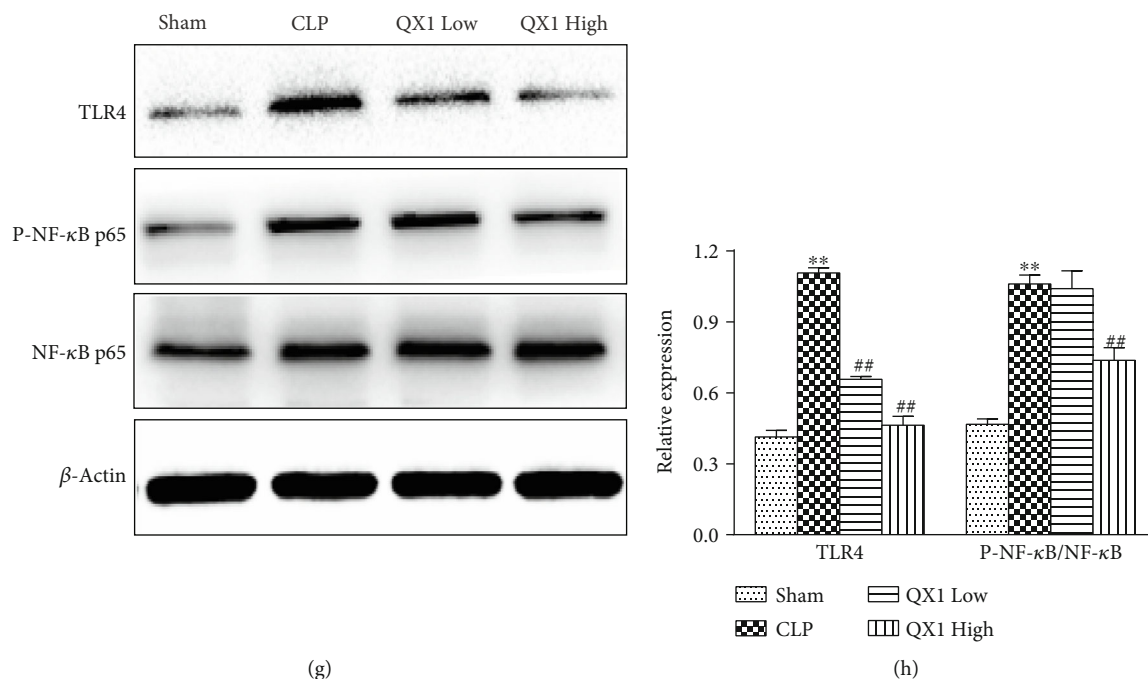


FIGURE 9: Effects of the QX1 formula on the sepsis-induced cardiac dysfunction pathway. (a, b) Western blot analysis of total CaMKII and P-CaMKII protein expression in heart tissues. (c, d) The expression levels of P-AKT and AKT proteins were determined in cardiac tissue. (e, f) Protein levels of ERK1/2, P-ERK1/2, P38, P-P38, JNK, and P-JNK were detected by Western blot. (g, h) Protein levels of TLR4 and NF- κ B were detected by Western blot. Data were presented as means \pm SD, and differences between means were compared using one-way ANOVA with Tukey's multiple comparison test. ** $P < 0.01$ compared to the sham group, # $P < 0.05$, ## $P < 0.01$ compared to the CLP group.

reduced sepsis mortality in an animal sepsis model [30, 31]. Formononetin (degree = 16), a methoxyisoflavone widely found in many herbs, has been shown to protect cardiomyocyte H9c2 cells from oxygen-glucose deprivation and reoxygenation injury via suppression of reactive oxygen species (ROS) formation by promoting AKT activation and GSK-3 β phosphorylation [32]. Quercetin, a natural flavonoid, is the key component of QX1 and displayed the highest number of target interactions (degree = 56). Besides, quercetin post-conditioning significantly alleviates cardiac ischemia/reperfusion injury in rats via activating the PI3K/AKT pathway [33]. Our study demonstrated that formononetin and quercetin in the QX1 formula may activate the PI3K/Akt pathway, which partially contributes to their curative effects.

MAPK, as the serine-threonine kinases, regulates several important cellular processes, including cell proliferation, inflammation, survival, stress response, and apoptosis [34]. A recent study revealed that inhibition of MAPK signaling pathways could alleviate sepsis-induced cardiac injury in AT1R-knockdown rats [35]. ERK1/2, JNK, and p38 are the three major subfamilies of MAPK signaling proteins. Taxifolin (degree = 11), an active flavonoid, was shown to exert a cardioprotective effect against cardiac ischemia/reperfusion injury by modulating oxidative stress and attenuating mitochondrial apoptosis [36]. Kaempferol (degree = 33), a dietary flavonoid, has been indicated to ameliorate myocardial ischemic injury by inhibiting the phosphorylation of JNK and p38 proteins and activation of ERK1/2 [37], which may be responsible for the inhibitory effect of the QX1 formula on the MAPK pathway in septic mice.

In sepsis, the activation of the MAPK pathway might result from aberrant upstream signaling, such as TLR4 [38]. TLR4 is one of the most studied members of the TLR family, which plays a pivotal role in the signal transduction of sepsis-induced inflammatory response. It has been reported that activation of TLR4 induces inflammation and aggravates cardiac dysfunction in severe sepsis, while knockout of the *TLR4* gene improves sepsis-induced cardiac dysfunction [39]. Therefore, TLR4 has been considered a potential therapeutic target for controlling inflammatory response and improving cardiac function [40]. The NF- κ B pathway, a typical inflammatory signaling pathway, can be activated by TLR4 and lead to the excessive release of proinflammatory cytokines leading to secondary sepsis myocardial injury [41]. In the present study, we found that the TLR4/NF- κ B signaling pathway was activated during sepsis. QX1 formula treatment significantly inhibited the activation of the TLR4/NF- κ B inflammatory signaling pathway. It was reported that in mice, quercetin protects mice from LPS-induced sepsis by inhibiting proinflammatory cytokine TNF- α and IL-1 β expression, NF- κ B activation, and apoptosis [42]. Quercetin in the QX1 formula may play an important role in preventing myocardial dysfunction via the TLR4/NF- κ B signaling pathway during sepsis.

An acute severe systemic inflammatory response known as "cytokine storm" is a key factor in the development and progression of septic cardiac dysfunction [43]. Both proinflammatory and opposing anti-inflammatory responses occur concomitantly in sepsis, and sepsis is regarded as an immunosuppressive disorder [44]. Analysis of cytokine

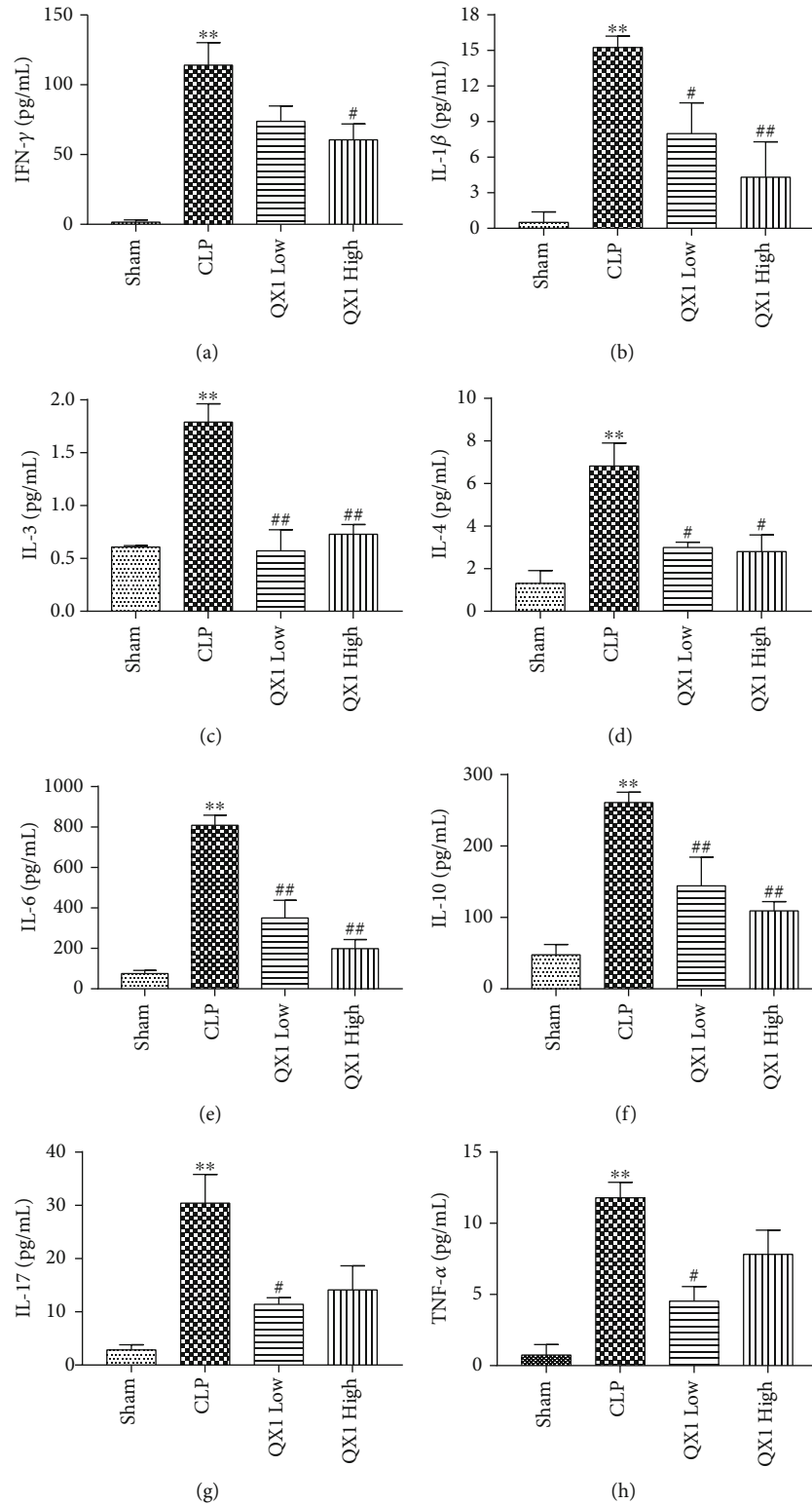


FIGURE 10: Effects of the QX1 formula on cytokine expression. The levels of (a) IFN- γ , (b) IL-1 β , (c) IL-3, (d) IL-4, (e) IL-6, (f) IL-10, (g) IL-17, and (h) TNF- α in serum were quantified by a mouse cytokine assay. Data were presented as means \pm SD, and differences between means were compared using one-way ANOVA with Tukey's multiple comparison test. ** $P < 0.01$ compared to the sham group. # $P < 0.05$, ## $P < 0.01$ compared to the CLP group.

profiles and mortality in 464 patients showed that a high ratio of IL-10 to TNF- α is associated with mortality in patients with community-acquired infection [44]. In this study, we observed that sepsis led to cytokine storm accompanied by the upregulated serum levels of IFN- γ , IL-1 β , IL-3, IL-4, IL-6, IL-10, IL-17, and TNF- α , whereas QX1 treatment decreased the production of typical Th1/Th2-associated proinflammatory cytokines (IFN- γ , IL-1 β , IL-3, IL-6, and TNF- α) and Th17-associated proinflammatory cytokines (IL-17). Our study also found that QX1 markedly downregulated the levels of typical Th2-associated anti-inflammatory cytokines (IL-4, IL-10). Elevated concentrations of TNF- α and IL-1 β are found in the serum of septic patients and are responsible for sepsis-related cardiac depression [45]. The IL-1 β level is also increased in LPS-treated mice and plays an important role in suppressing myocardial contractility [46]. TNF- α is a proinflammatory cytokine mainly expressed in the initial hyperinflammatory stage of sepsis and is responsible for myocardial diastolic and systolic dysfunction [47]. In sepsis, overexpression of TNF- α increases the level of NO by inducing the production of inducible nitric oxide synthase (iNOS), which leads to apoptosis of myocardial cells and heart failure [48]. Suppression of the systolic function of cardiomyocytes *in vitro* is associated with IL-6 production, and removal of IL-6 in the culture supernatant significantly improves the systolic function of cardiomyocytes [49]. IL-3 plays a critical role during sepsis. It was reported that the addition of a CD123 (IL-3 receptor alpha chain) antibody reduces mortality and alleviates organ dysfunction by restraining the JAK2-STAT5 signaling pathway and reduces serum cytokines in the development of early sepsis in a rat model induced by CLP [50]. IL-6 contributes to host defense against infections and tissue injuries; however, excessive levels of IL-6 lead to cytokine storm via inhibiting cardiac function but activating the coagulation pathway and vascular endothelial cells [51]. In the CLP-induced sepsis, calcium-sensing receptor activation promotes T cell apoptosis and the secretion of the proinflammatory cytokine TNF- α and the anti-inflammatory cytokine IL-4 probably through NF- κ B and partial ERK and JNK signal transduction pathways [52]. Our results suggested that the QX1 formula may constitute a novel therapeutic strategy for suppressing the activity of CaMKII, TLR4/NF- κ B, and MAPK pathways, but promoting the activation of AKT, thereby decreasing the release of downstream inflammatory cytokines and thus controlling cytokine storm and regulating immune balance in sepsis.

In conclusion, the QX1 formula improved cardiac dysfunction in sepsis mice by inhibiting calcium, MAPK, and TLR4 signaling pathways, activating PI3K/AKT pathways, and reducing the subsequent release of inflammation cytokines. This study demonstrated the multicomponent, multitarget, and multipathway characteristics of QX1, which provided a novel understanding of QX1 in the clinical application on cardiac dysfunction during sepsis.

Data Availability

The data used to support the findings of this study are available from the corresponding authors upon request.

Conflicts of Interest

The authors confirm that there are no conflicts of interest.

Acknowledgments

This work was supported by the National Natural Science Foundation of China (81803879), the Project funded by China Postdoctoral Science Foundation (2019M660724), the Beijing Administration of Traditional Chinese Medicine Project (JJ2018-52), the National Major Scientific and Technological Project (2017ZX10305501), and the Beijing Science and Technology Planning Project (Z201100005420009).

Supplementary Materials

Supplementary 1. Figure S1: chromatograms of the six main bioactive compounds in rat plasma. (A) Blank plasma. (B) Blank rat plasma spiked with the six main bioactive compounds: (a) taxifolin, (b) quercetin, (c) tanshinone IIA, (d) cryptotanshinone, (e) formononetin, and (f) kaempferol.

Supplementary 2. Table S1: the potential targets for the 63 bioactive compounds in the QX1 formula.

Supplementary 3. Table S2: the degree of protein targets corresponding to potential compounds in the QX1 formula.

Supplementary 4. Table S3: the information of the target-pathway network in the QX1 formula.

References

- [1] M. Singer, C. S. Deutschman, C. W. Seymour et al., "The third international consensus definitions for sepsis and septic shock (Sepsis-3)," *Journal of the American Medical Association*, vol. 315, no. 8, pp. 801–810, 2016.
- [2] H. C. Prescott and D. C. Angus, "Enhancing recovery from sepsis: a review," *Journal of the American Medical Association*, vol. 319, no. 1, pp. 62–75, 2018.
- [3] Z. Zheng, H. Ma, X. Zhang et al., "Enhanced glycolytic metabolism contributes to cardiac dysfunction in polymicrobial sepsis," *The Journal of Infectious Diseases*, vol. 215, no. 9, pp. 1396–1406, 2017.
- [4] A. Arfaras-Melainis, E. Polyzogopoulou, F. Triposkiadis et al., "Heart failure and sepsis: practical recommendations for the optimal management," *Heart Failure Reviews*, vol. 25, no. 2, pp. 183–194, 2020.
- [5] Y. C. Liu, M. M. Yu, S. T. Shou, and Y. F. Chai, "Sepsis-induced cardiomyopathy: mechanisms and treatments," *Frontiers in Immunology*, vol. 8, p. 1021, 2017.
- [6] W. Jiang, W. Li, X. Hu, R. Hu, B. Li, and L. Lan, "CTRP1 prevents sepsis-induced cardiomyopathy via Sirt1-dependent pathways," *Free Radical Biology & Medicine*, vol. 152, pp. 810–820, 2020.
- [7] X. Xu, Q. Liu, S. He et al., "Qiang-Xin 1 formula prevents sepsis-induced apoptosis in murine cardiomyocytes by suppressing endoplasmic reticulum- and mitochondria-associated pathways," *Frontiers in Pharmacology*, vol. 9, p. 818, 2018.
- [8] W. Zhang, Y. Huai, Z. Miao, A. Qian, and Y. Wang, "Systems pharmacology for investigation of the mechanisms of action of

- traditional Chinese medicine in drug discovery,” *Frontiers in Pharmacology*, vol. 10, p. 743, 2019.
- [9] W. J. Lv, C. Liu, Y. F. Li et al., “Systems pharmacology and microbiome dissection of Shen Ling Bai Zhu San reveal multi-scale treatment strategy for IBD,” *Oxidative Medicine and Cellular Longevity*, vol. 2019, Article ID 8194804, 30 pages, 2019.
- [10] X. Su, Y. Li, M. Jiang et al., “Systems pharmacology uncover the mechanism of anti-non-small cell lung cancer for Hedyotis diffusa Willd,” *Biomedicine & Pharmacotherapy*, vol. 109, pp. 969–984, 2019.
- [11] G. Yu, Z. Luo, Y. Zhou et al., “Uncovering the pharmacological mechanism of *Carthamus tinctorius* L. on cardiovascular disease by a systems pharmacology approach,” *Biomedicine & Pharmacotherapy*, vol. 117, article 109094, 2019.
- [12] D. Rittirsch, M. S. Huber-Lang, M. A. Flierl, and P. A. Ward, “Immunodesign of experimental sepsis by cecal ligation and puncture,” *Nature Protocols*, vol. 4, no. 1, pp. 31–36, 2009.
- [13] J. Ru, P. Li, J. Wang et al., “TCMSP: a database of systems pharmacology for drug discovery from herbal medicines,” *Journal of Cheminformatics*, vol. 6, no. 1, p. 13, 2014.
- [14] H. Liu, J. Wang, W. Zhou, Y. Wang, and L. Yang, “Systems approaches and polypharmacology for drug discovery from herbal medicines: an example using licorice,” *Journal of Ethnopharmacology*, vol. 146, no. 3, pp. 773–793, 2013.
- [15] C. Zheng, Z. Guo, C. Huang et al., “Large-scale direct targeting for drug repositioning and discovery,” *Scientific Reports*, vol. 5, no. 1, p. 11970, 2015.
- [16] S. He, F. Liu, L. Xu et al., “Protective effects of ferulic acid against heat stress-induced intestinal epithelial barrier dysfunction in vitro and in vivo,” *PLoS One*, vol. 11, article e145236, 2016.
- [17] S. Z. Xie, B. Liu, H. Y. Ye et al., “Dendrobium huoshanense polysaccharide regionally regulates intestinal mucosal barrier function and intestinal microbiota in mice,” *Carbohydrate Polymers*, vol. 206, pp. 149–162, 2019.
- [18] J. N. Pulido, B. Afessa, M. Masaki et al., “Clinical spectrum, frequency, and significance of myocardial dysfunction in severe sepsis and septic shock,” *Mayo Clinic Proceedings*, vol. 87, no. 7, pp. 620–628, 2012.
- [19] C. Fleischmann, A. Scherag, N. K. Adhikari et al., “Assessment of global incidence and mortality of hospital-treated sepsis. Current estimates and limitations,” *American Journal of Respiratory and Critical Care Medicine*, vol. 193, no. 3, pp. 259–272, 2016.
- [20] L. Dejager, I. Pinheiro, E. Dejonckheere, and C. Libert, “Cecal ligation and puncture: the gold standard model for polymicrobial sepsis?,” *Trends in Microbiology*, vol. 19, no. 4, pp. 198–208, 2011.
- [21] D. Aoyama, S. Miyazaki, K. Hasegawa et al., “Preprocedural troponin T levels predict the improvement in the left ventricular ejection fraction after catheter ablation of atrial fibrillation/flutter,” *Journal of the American Heart Association*, vol. 9, article e15126, 2020.
- [22] Y. P. Sun, C. P. Wei, S. C. Ma et al., “Effect of carvedilol on serum heart-type fatty acid-binding protein, brain natriuretic peptide, and cardiac function in patients with chronic heart failure,” *Journal of Cardiovascular Pharmacology*, vol. 65, no. 5, pp. 480–484, 2015.
- [23] W. Y. Lee, C. Y. Lee, Y. S. Kim, and C. E. Kim, “The methodological trends of traditional herbal medicine employing network pharmacology,” *Biomolecules*, vol. 9, no. 8, p. 362, 2019.
- [24] H. J. Jin and C. G. Li, “Tanshinone IIA and cryptotanshinone prevent mitochondrial dysfunction in hypoxia-induced H9c2 cells: association to mitochondrial ROS, intracellular nitric oxide, and calcium levels,” *Evidence-based Complementary and Alternative Medicine*, vol. 2013, Article ID 610694, 11 pages, 2013.
- [25] M. Sepulveda, L. A. Gonano, M. Viotti et al., “Calcium/calmodulin protein kinase II-dependent ryanodine receptor phosphorylation mediates cardiac contractile dysfunction associated with sepsis,” *Critical Care Medicine*, vol. 45, no. 4, pp. e399–e408, 2017.
- [26] M.-l. A. Joiner, O. M. Koval, J. Li et al., “CaMKII determines mitochondrial stress responses in heart,” *Nature*, vol. 491, no. 7423, pp. 269–273, 2012.
- [27] J. Beckendorf, M. van den Hoogenhof, and J. Backs, “Physiological and unappreciated roles of CaMKII in the heart,” *Basic Research in Cardiology*, vol. 113, no. 4, p. 29, 2018.
- [28] L. C. Cantley, “The phosphoinositide 3-kinase pathway,” *Science*, vol. 296, no. 5573, pp. 1655–1657, 2002.
- [29] D. L. Williams, C. Li, T. Ha et al., “Modulation of the phosphoinositide 3-kinase pathway alters innate resistance to polymicrobial sepsis,” *Journal of Immunology*, vol. 172, pp. 449–456, 2003.
- [30] R. An, L. Zhao, C. Xi et al., “Melatonin attenuates sepsis-induced cardiac dysfunction via a PI3K/Akt-dependent mechanism,” *Basic Research in Cardiology*, vol. 111, no. 1, p. 8, 2016.
- [31] C. Li, F. Hua, T. Ha et al., “Activation of myocardial phosphoinositide-3-kinase p110 α ameliorates cardiac dysfunction and improves survival in polymicrobial sepsis,” *PLoS One*, vol. 7, no. 9, article e44712, 2012.
- [32] Y. Cheng, Z. Xia, Y. Han, and J. Rong, “Plant Natural Product Formononetin Protects Rat Cardiomyocyte H9c2 Cells against Oxygen Glucose Deprivation and Reoxygenation via Inhibiting ROS Formation and Promoting GSK-3 β Phosphorylation,” *Oxidative Medicine and Cellular Longevity*, vol. 2016, Article ID 2060874, 11 pages, 2016.
- [33] Y. Wang, Z. Z. Zhang, Y. Wu, J. J. Ke, X. H. He, and Y. L. Wang, “Quercetin postconditioning attenuates myocardial ischemia/reperfusion injury in rats through the PI3K/Akt pathway,” *Brazilian Journal of Medical and Biological Research*, vol. 46, no. 10, pp. 861–867, 2013.
- [34] S. He, X. Hou, X. Xu et al., “Quantitative proteomic analysis reveals heat stress-induced injury in rat small intestine via activation of the MAPK and NF- κ B signaling pathways,” *Molecular BioSystems*, vol. 11, no. 3, pp. 826–834, 2015.
- [35] T. Zhang, Y. C. Yin, X. Ji et al., “AT1R knockdown confers cardioprotection against sepsis-induced myocardial injury by inhibiting the MAPK signaling pathway in rats,” *Journal of Cellular Biochemistry*, vol. 121, pp. 25–42, 2019.
- [36] Z. Tang, C. Yang, B. Zuo et al., “Taxifolin protects rat against myocardial ischemia/reperfusion injury by modulating the mitochondrial apoptosis pathway,” *PeerJ*, vol. 7, article e6383, 2019.
- [37] K. Suchal, S. Malik, N. Gamad et al., “Kaempferol attenuates myocardial ischemic injury via inhibition of MAPK signaling pathway in experimental model of myocardial ischemia-reperfusion injury,” *Oxidative Medicine and Cellular Longevity*, vol. 2016, Article ID 7580731, 10 pages, 2016.
- [38] R. Yuan, L. Huang, L. J. Du et al., “Dihydro-tanshinone exhibits an anti-inflammatory effect in vitro and in vivo through

- blocking TLR4 dimerization,” *Pharmacological Research*, vol. 142, pp. 102–114, 2019.
- [39] D. Zhou, Y. Zhu, M. Z. Ouyang et al., “Knockout of Toll-like receptor 4 improves survival and cardiac function in a murine model of severe sepsis,” *Molecular Medicine Reports*, vol. 17, no. 4, pp. 5368–5375, 2018.
- [40] V. K. Topkara, S. Evans, W. Zhang et al., “Therapeutic targeting of innate immunity in the failing heart,” *Journal of Molecular and Cellular Cardiology*, vol. 51, no. 4, pp. 594–599, 2011.
- [41] X. Xu, S. Rui, C. Chen et al., “Protective effects of astragalus polysaccharide nanoparticles on septic cardiac dysfunction through inhibition of TLR4/NF- κ B signaling pathway,” *International Journal of Biological Macromolecules*, vol. 153, pp. 977–985, 2020.
- [42] X. Wei, X. Meng, Y. Yuan, F. Shen, C. Li, and J. Yang, “Quercetin exerts cardiovascular protective effects in LPS-induced dysfunction in vivo by regulating inflammatory cytokine expression, NF- κ B phosphorylation, and caspase activity,” *Molecular and Cellular Biochemistry*, vol. 446, no. 1–2, pp. 43–52, 2018.
- [43] J. Chen, J. E. Kieswich, F. Chiazza et al., “IkappaB kinase inhibitor attenuates sepsis-induced cardiac dysfunction in CKD,” *Journal of the American Society of Nephrology*, vol. 28, pp. 94–105, 2016.
- [44] R. S. Hotchkiss, G. Monneret, and D. Payen, “Immunosuppression in sepsis: a novel understanding of the disorder and a new therapeutic approach,” *The Lancet Infectious Diseases*, vol. 13, no. 3, pp. 260–268, 2013.
- [45] A. Kumar, V. Thota, L. Dee, J. Olson, E. Uretz, and J. E. Parrillo, “Tumor necrosis factor alpha and interleukin 1beta are responsible for in vitro myocardial cell depression induced by human septic shock serum,” *The Journal of Experimental Medicine*, vol. 183, no. 3, pp. 949–958, 1996.
- [46] B. Sun, J. Xiao, X. B. Sun, and Y. Wu, “Notoginsenoside R1 attenuates cardiac dysfunction in endotoxemic mice: an insight into oestrogen receptor activation and PI3K/Akt signalling,” *British Journal of Pharmacology*, vol. 168, no. 7, pp. 1758–1770, 2013.
- [47] A. Kumar, A. Kumar, B. Paladugu, J. Mensing, and J. E. Parrillo, “Transforming growth factor-beta1 blocks in vitro cardiac myocyte depression induced by tumor necrosis factor-alpha, interleukin-1beta, and human septic shock serum,” *Critical Care Medicine*, vol. 35, no. 2, pp. 358–364, 2007.
- [48] A. B. Levine, D. Punihaole, and T. B. Levine, “Characterization of the role of nitric oxide and its clinical applications,” *Cardiology*, vol. 122, no. 1, pp. 55–68, 2012.
- [49] N. Pathan, J. L. Franklin, H. Eleftherohorinou et al., “Myocardial depressant effects of interleukin 6 in meningococcal sepsis are regulated by p38 mitogen-activated protein kinase,” *Critical Care Medicine*, vol. 39, no. 7, pp. 1692–1711, 2011.
- [50] J. Hu, Z. Tang, J. Xu et al., “The inhibitor of interleukin-3 receptor protects against sepsis in a rat model of cecal ligation and puncture,” *Molecular Immunology*, vol. 109, pp. 71–80, 2019.
- [51] T. Tanaka, M. Narazaki, and T. Kishimoto, “Immunotherapeutic implications of IL-6 blockade for cytokine storm,” *Immunotherapy*, vol. 8, no. 8, pp. 959–970, 2016.
- [52] C. L. Wu, Q. Y. Wu, J. J. Du et al., “Calcium-sensing receptor in the T lymphocyte enhanced the apoptosis and cytokine secretion in sepsis,” *Molecular Immunology*, vol. 63, no. 2, pp. 337–342, 2015.